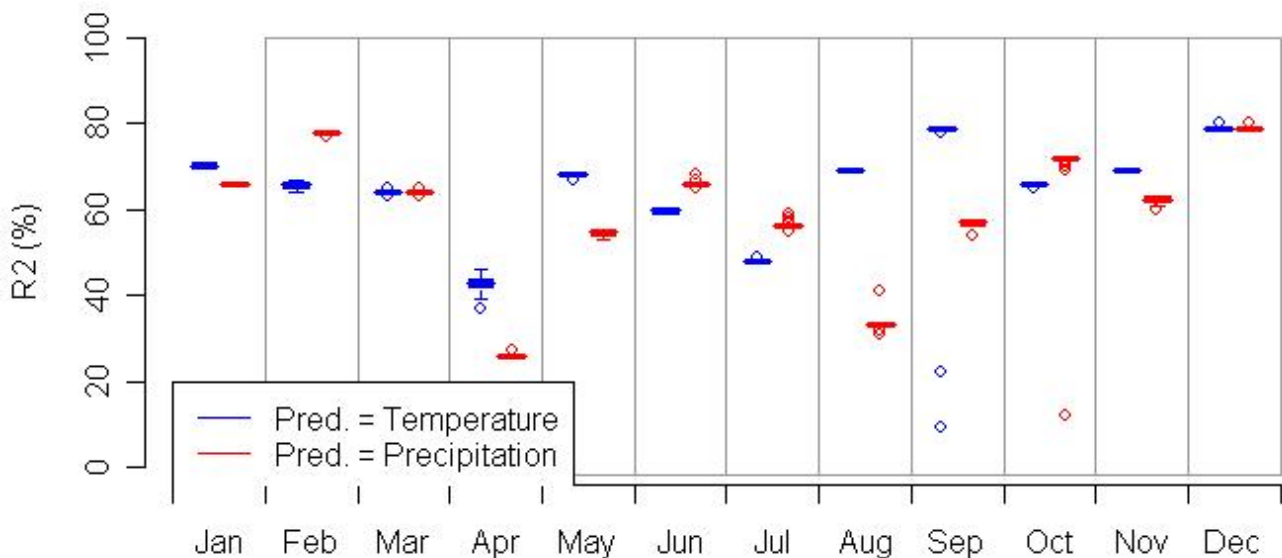




Empirically downscaling of runoff in Norway; Is it feasible?

Torill Engen-Skaugen, Rasmus Benestad and Lars A. Roald

Results from ESD of runoff for Røykenes catchment



R^2 from the regression between the observational part of the common EOFs of ERA40/GCMs and observed runoff is presented in a boxplot for Røykenes. 68 GCMs with temperature as predictor (blue) and 67 GCMs with precipitation as predictor (red) are used.

Title Empirically downscaling of runoff in Norway. Is it feasible?	Date 19.12.2007
Section Climate	Report no. no. 15.07
Author(s) Rasmus Benestad ¹ , Torill Engen-Skaugen ¹ and Lars A. Roald ² ¹ Norwegian Meteorological Institute, ² Norwegian Water Resources and Energy Directorate	Classification <input checked="" type="checkbox"/> Free <input type="checkbox"/> Restricted
	ISSN 1503-8025
	e-ISSN 1503-8025
Client(s) EBL Norwegian Electricity Industry Association	Client's reference MKU-1.8_06
Abstract <p>River runoff for seven catchments in Norway was used as predictands in an Empirical-Statistical Downscaling (ESD) analysis, taking ERA40 precipitation and temperature as predictors. The ESD was applied to the Intergovernmental Panel on climate Change (IPCC 2007) multi-model dataset (MMD ; also known as 'CMIP3') from the fourth assessment report (AR4) global climate model (GCM) ensemble. The tool <i>clim.pact</i> was used to carry out the calculations, using a common EOF based framework and linear multiple regression as a basis for the empirical-statistical model.</p> <p>The ESD was made for 38 (temperature) and 34 (precipitation) GCM runs with SRES emission scenario A1b (IPCC, 2001) and 30 (temperature) and 33 (precipitation) GCM control runs with different GCMs ('MMD' in IPCC AR4).</p> <p>The strength of the regression (coefficient of determination, also referred to as the R^2-statistics, from the regression analysis) suggests weak relationship between the predictors and the predictands, but this is dependent on season and location. The R^2-statistics were considered good for autumn, winter and spring, both when using precipitation and temperature as predictors for catchments dominated by rainfall floods throughout the year. These are typically small to medium sized catchments at the western coast of Norway. The two predictors lead to opposite trends projected for the future, thus effect will depend on which has the stronger effect. A method that combines the predictors may be further developed to obtain a more comprehensive scenario.</p>	
Keywords Empirical downscaling, river runoff, climate change	
Disciplinary signature <hr/> Inger Hanssen-Bauer	Responsible signature <hr/> Eirik J. Førland

Postal address	Office	Telephone	Telefax	e-mail: met@met.no	Bank account	Swift code
P.O.Box 43, Blindern NO-0313 OSLO Norway	Niels Henrik Abelsvei 40	+47 22 96 30 00	+47 22 96 30 50	Internet: met.no	7694 05 00628	DNBANOKK

1 Introduction

The hydrological regime in catchments or regions is described by river runoff. Cold winter climate where winter precipitation falls as snow leads to low winter runoff and marked spring flood during snowmelt. This is characteristic for eastern and inland parts of Norway. The runoff is also affected by the winter climate, where mild conditions with less snow are associated with more frequent winter floods. Such conditions are typical for southern and coastal parts of the country. The hydrological regime reflects the size of the catchments; the larger the catchments, the larger river runoff amounts. The runoff is also a function of the amounts of rainfall typical for the season. In larger catchments, the rainfall will be transported further than in small catchments, giving a more delayed and convoluted response. Thus, response time depends on the size, topography and saturation of the catchments.

The saturation is dependent of the ground conditions (soil/rock), the thickness of the soil layer (infiltration) and rainfall amounts. The rainfall is dependent of weather types (the situation of the circulation in the weather system). E.g. when the weather circulation reaches Norway from the south or south-west, the largest rainfall amounts and the largest frequency of days with precipitation is experienced in western parts (Tveito et al., 2005).

River runoff is traditionally modelled with rainfall-runoff models, e.g. HBV (Bergström, 1995; Sælthun, 1996), where time series of temperature and precipitation are used as input. The model is calibrated with observations. The models are used in e.g. flood forecasting and hydropower production. The rainfall-runoff models are commonly used in climate change predictions as well (Beldring et al., 2003).

Daily mean temperature and precipitation sums are in Roald et al. (2006) interpolated from Regional Climate Models (RCMs), dynamically downscaled, and used as input in rainfall-runoff models. Difficulties due to spatial resolution, systematic errors as well as limitations in descriptions of physical processes, lead to a description of precipitation and temperature that is not representative locally. The precipitation and temperature was therefore empirically adjusted to be applicable in hydrological modelling (Engen-Skaugen, 2007). Daily runoff series were established for 34 Norwegian catchments for the control period 1961-1990 and for the scenario period 2071-2100 for the SRES A2 (high) and SRES B2 (moderate) emission scenarios. The changes were calculated for annual and seasonal means as well as extremes. The projected changes show seasonal shifts, which agrees regionally for the winter, spring and summer compared to trends in observed time series, but not for the autumn (Hisdal et al., 2007).

The aim of the present report is to establish whether there exist good statistical relations between large scale atmospheric circulation and runoff that can be used in Empirical-Statistical Downscaling (ESD) methods (Benestad, 2004, 2005). Large scale fields of mean monthly temperature and monthly precipitation sums are used as predictors. The motivation for this is the close physical link between weather circulation, rainfall and river levels. Temperature was also used as predictor in a parallel analysis, as spring-time river runoff also may depend on the snow-melt, due to high temperatures. If such relations is found it is thought to be useful in describing uncertainties of the scenarios obtained with dynamical downscaling (e.g. Beldring et al., 2003).

Roald (2008) has compared daily rainfall data with daily circulation indices focussed on Germany and Great Britain (Gerstengarbe and Werner, 2005, Hulme and Barrow, 1997), and related this to rainfall floods for a large number of Norwegian catchments. The study shows that a high percentage of these events are linked to a small number of related circulation types in each catchment. There is a well-defined regional pattern in the dominant circulation classes over Norway as well as local differences reflecting the exposure of each catchment.

River runoff for seven catchments in Norway; Atnasjø, Austenå, Dalsbøvatn, Høggås Bru, Nautsundvatn, Øvrevatn, and Røykenes, were used as predictands in an ESD analysis, taking ERA40 (Simmons and Gibson, 2000; Bengtsson et al. 2004) precipitation and temperature as predictors. The ESD was applied to the Meehl et al. (2007) MMD Global Climate Models (GCMs) ensemble. The implementation was similar to the work documented in Benestad (2005) for each GCM implemented, and performed for monthly mean values. The tool *clim.pact* (Benestad, 2004) was used to carry out the calculations, using a common EOF

based framework (Benestad, 2001) and a step-wise linear multiple regression as a basis for the empirical-statistical model.

The observed river runoff from the selected catchments is described hydrologically in Section 2.1. ESD with precipitation as predictor was made for 34 GCM runs with SRES emission scenario A1b (IPCC, 2000) and 33 GCM control runs with different GCMs ('MMD' in IPCC AR4). The same method was performed with temperature as predictor for 38 GCM runs with SRES emission scenario A1b (IPCC, 2000) and 30 GCM control runs with different GCMs ('MMD' in IPCC AR4) (Section 2.2). The ESD method is presented in section 3. Results from the analyses are presented in Section 4, a discussion with concluding remarks are given in Section 5.

2 Data

2.1 Historical observations of runoff

ESD methods are performed on time series of historical river runoff from seven catchments in Norway (Figure 2.1). The selected stations represent different regions of the country, which is reflected in the stations hydrographs (Figure 2.2).

The eastern, interior regions of the country are characterised by a marked spring flood due to snow melting and large runoff during autumn. Winter floods are more common in coastal catchments along the south coast, but spring floods caused by snowmelt are also common in the larger rivers draining from the mountains. The southern region is also affected by summer or early autumn rainstorms. The western parts experience rather large runoff throughout the year, especially during autumn, winter and spring due to the influence of coastal climate; less snow and warmer winters. The northernmost area in Finnmark is characterised by cold winter climate. The snow accumulates all through the winter, and the snow melts simultaneously over the entire catchment because of a gentle topography. The resulting spring flood occurs concentrated in May or June, and can result in higher discharge than in other larger basins in southern Norway because of the short duration of the flood.

Requirements to be fulfilled for the time series of observations to be basis for empirical downscaling are:

1. The observations have to cover the ERA40 time period (1958-2002).
2. The time series have to be homogeneous,
3. The catchments should be sufficiently large.
4. The catchments should represent different hydrological regimes of the country.

The selected stations with their catchment size and runoff amounts are shown in Table 2.1. The location is shown in Figure 2.1. The catchments cover a range of different regions and the catchments properties documented in the National Norwegian Hydrological Database HYDRA II..

Øvrevatn is a large catchment (~526 km²) in Northern Norway (Table 2.1 and Figure 2.1). It is an elongated catchment from the Swedish boarder to the coast, a region that experience large amounts of annual precipitation (~1000 mm) (Førland, 1993). The catchment is dominated by cold, inland climate with large spring or summer floods due to snowmelt (Figures 2.2 left and 2.6e). The range in altitudes is quite high. The snowmelt flood has therefore long duration compared to the less steep basins further north. Although snowmelt floods occur every year, the largest flood event was caused by rainfall in early October 1959 which caused floods in the northern part of Nordland and the southern part of Troms. The circulation type was southerly to south-easterly during the event, which resulted in up to 142 mm rainfall at Alsvåg in Vesterålen and around 80 mm at several stations in inner Troms. Late summer or autumn floods caused by rainfall occur in many years, but they are usually smaller than the spring flood

Atnasjø is a large catchment (~463 km²) in the eastern part of the country (Table 2.1 and Figure 2.1). The basin includes part of the alpine Rondane area. The catchment is in a high mountain region in the leeward side of the east-west water divide. The dominant wind directions are usually from west or southwest, the annual precipitation amounts in this region (~700-1000 mm) is therefore smaller compared to catchments

further west. This is reflected in the hydrograph (Figure 2.2 right). The dominant spring flood season extends normally from May to June, although the flood may occur later in some years (Figure 2.6f). The largest floods are all spring floods. The 1995-flood was the largest observed since the start of observations in 1916. This flood was caused by snowmelt combined with rainfall. The area is, however, affected by occasional summer rainstorms, which can be quite intensive. A rainstorm 24th July 1940 resulted in 116 mm rainfall at Atnasjø. The storm caused extreme damages in the Gaula basin further to the north. Another local summer rainstorm in Rondane caused the flood level to raise several meters, inundating a sediment sampling station in 1996. The high intensive rainfall events in this region are most frequently linked to the northwest type circulation patterns caused by weather systems penetrating from the Trondheimsfjord region. Weather systems from southeast can also cause very heavy precipitation such as under Storofsen in 1789 (Østmo, 1985).

Røykenes is a smaller catchment near the west coast (~50 km²) (Table 2.1 and Figure 2.1). The altitude ranges from 53 to 960 m.a.s.l. The lake and bog percentages are low, the forest and bare rock percentages are 52.16 and 31.66 % respectively. It is therefore a fast responding catchment (Table 2.1). The seasonal runoff is highly influenced by the mild winters and heavy rainfall from west. The hydrograph is characterised by flooding throughout the year, especially during autumn and winter (Figure 2.3 left and Figure 2.6 a). The largest floods have occurred in the late autumn and are linked to westerly circulation types with anticyclones over the European mainland and/or over Great Britain.

Austena is a middle sized catchment (277 km²) in the southern part of the country (Table 2.1 and Figure 2.1). The catchment is situated in the upper part of Tovdalselv. The lake percentage is 11.9 %, and 61.87 % of the catchment is covered by forests. The altitudes ranges from 228 to 1146 m.a.s.l.. The seasonal runoff is characterised by a well-defined snowmelt period from April to May. Most of the largest floods occurs, however, in the summer and autumn, and is caused by convective rainfall (Figure 2.3 right and Figure 2.6d). Around 50-60 % of the larger rainfall events are linked to weather systems from southwest to northwest, often with anti-cyclonic circulation over Great Britain or the northern European Mainland (Roald, 2008).

Dalsbøvatn is a small catchment (25.6 km²) at the extreme west coast (Figure 2.1). It is similar to Røykenes, but with even more maritime climate. The altitude ranges from 47 to 528 m.a.s.l. The lake percentage is fairly high (10.1%), but 66.48 % comprises of bare rocks, making it a fast responding catchment (Table 2.1). The region is influenced by mild winter climate with little or no snow cover in most years. The catchment is exposed to wind directions between south-west and north-west. Most large floods occur in the autumn or winter (Figure 2.4 left and Figure 2.6b). The largest flood occurred 8th September 1966, and was caused by the remnant of tropical hurricane Faith, which caused severe flooding in several locations further to the south in West Norway.

Høggås Bru is situated in the Central Norway (Figure 2.1). The catchment is large (495 km²) and extends inland from the Trondheimsfjord. The altitude ranges from 97 to 1247 m.a.s.l. The basin has a low lake percentage (2.38), but as much as 26.18 % comprises of bogs (Table 2.1). This causes the catchment to react slowly. It is characterised by a distinct spring flood as well, and autumn rainfall floods are common (Figure 2.4 right and Figure 2.6g). Around 60 % of all large rainfall events are linked to anti-cyclones over Great Britain or the northern European Mainland with westerly wind further north (Roald, 2008).

Nautsundvatn is a middle sized catchment (~220 km²) at the west coast (Table 2.1, Figure 2.1). The catchment is situated in the maximum precipitation zone in Sunnfjord. The maximum daily rainfall exceeds 100 mm in many years, and was as high as 208 mm 26th November 1940, which caused the largest flood observed since the start of observations in 1909. The dominant rainfall and flood season is in the autumn and winter (Figure 2.5 and Figure 2.6 c). Snowmelt contributes to some of the winter and early spring floods, but rainfall is the predominant cause of floods. The months from May to July have usually few floods. Around 50 % of all heavy rainfall events occur at westerly circulation types. The response of the catchment is slow though.

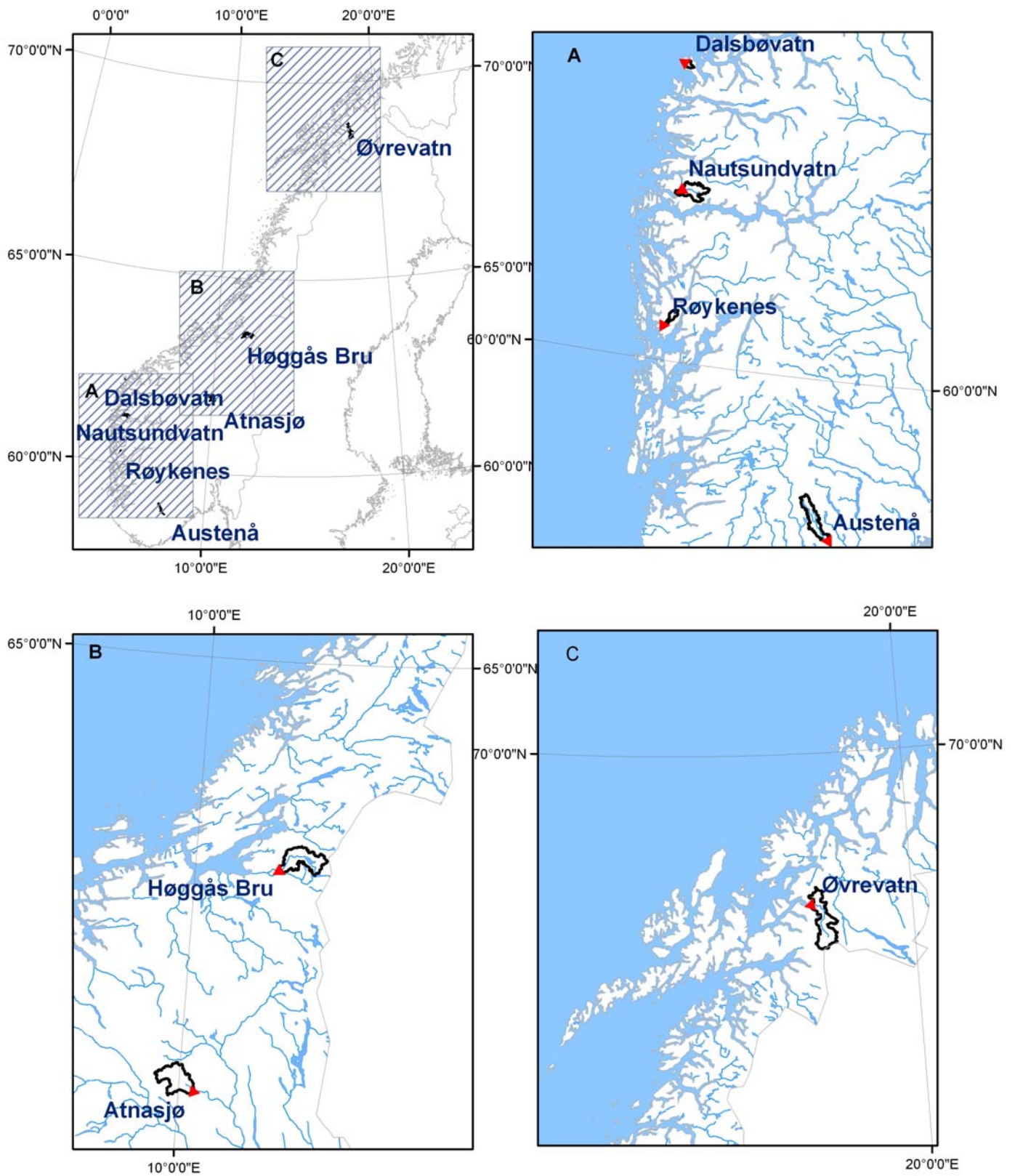


Figure 2.1 Locations of the runoff stations used and their catchments.

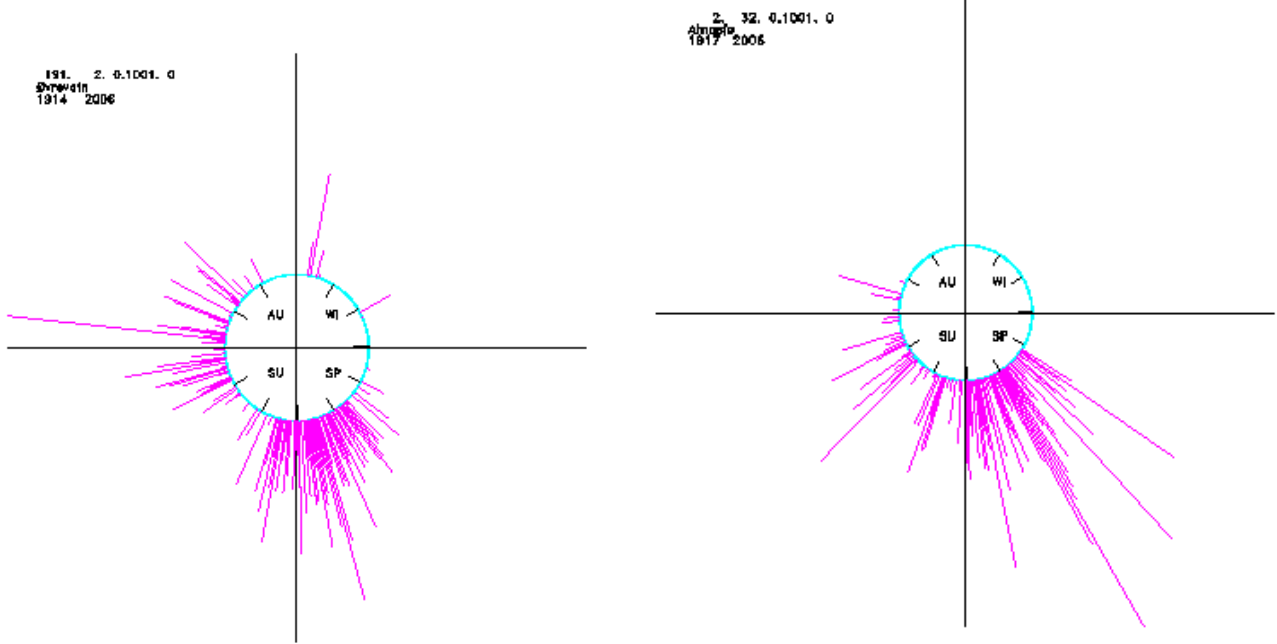


Figure 2.2 Relative magnitude and seasonal distribution of the floods selected by the Peak-Over Threshold Method for Øvrevatn (left) and Atnasjø (right)

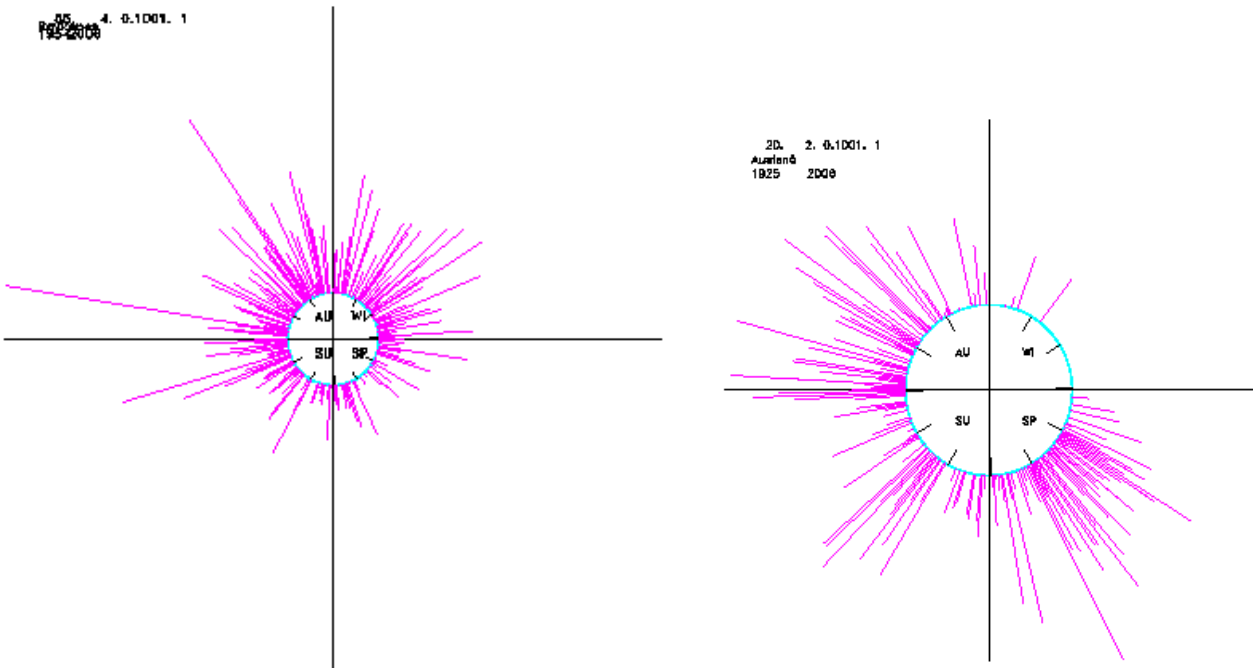


Figure 2.3 Relative magnitude and seasonal distribution of the floods selected by the Peak-Over Threshold Method for Røykenes (left) and Austenå (right).

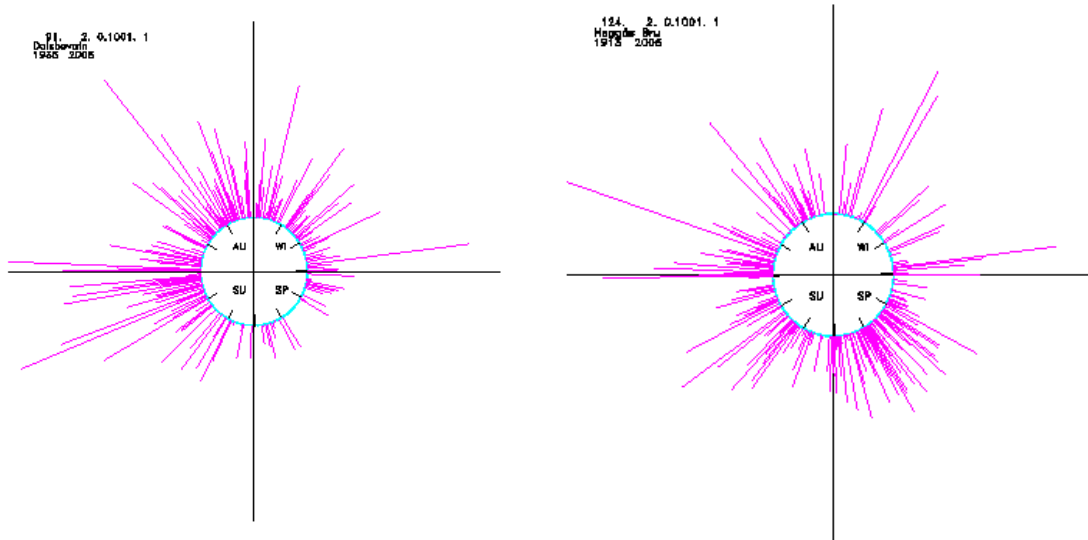


Figure 2.4 Relative magnitude and seasonal distribution of the floods selected by the Peak-Over Threshold Method for Dalsbøvatn (left) and Høggås Bru (right).

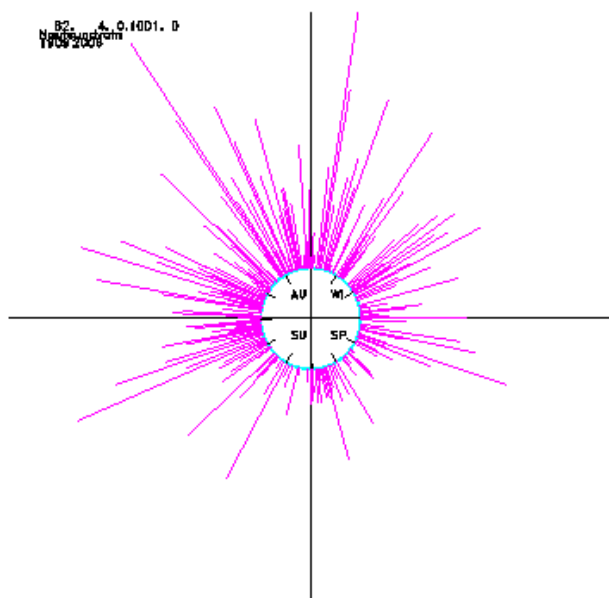


Figure 2.5 Relative magnitude and seasonal distribution of the floods selected by the Peak-Over Threshold Method for Nautsundvatn

Table 2.1 Characterisation of the runoff station and the corresponding catchments.

Station Number	Station Name	Catchments size [km ²]	Mean annual runoff (m ³ /s)r	Specific runoff (1961-90) (l/s km ²)
191.2.0.1001.0	Øvrevatn	525.69	677.20	40.83
55.4.0.1001.1	Røykenes	49.89	158.36	100.61
2.32.0.1001.0	Atnasjø	462.88	323.17	22.13
20.2.0.1001.1	Austenå	276.46	319.36	36.61
91.2.0.1001.1	Dalsbøvatn	25.57	51.37	63.68
124.2.0.1001.1	Høggås bru	495.12	652.16	41.75
82.4.0.1001.0	Nautsundvatn	218.96	666.38	96.46

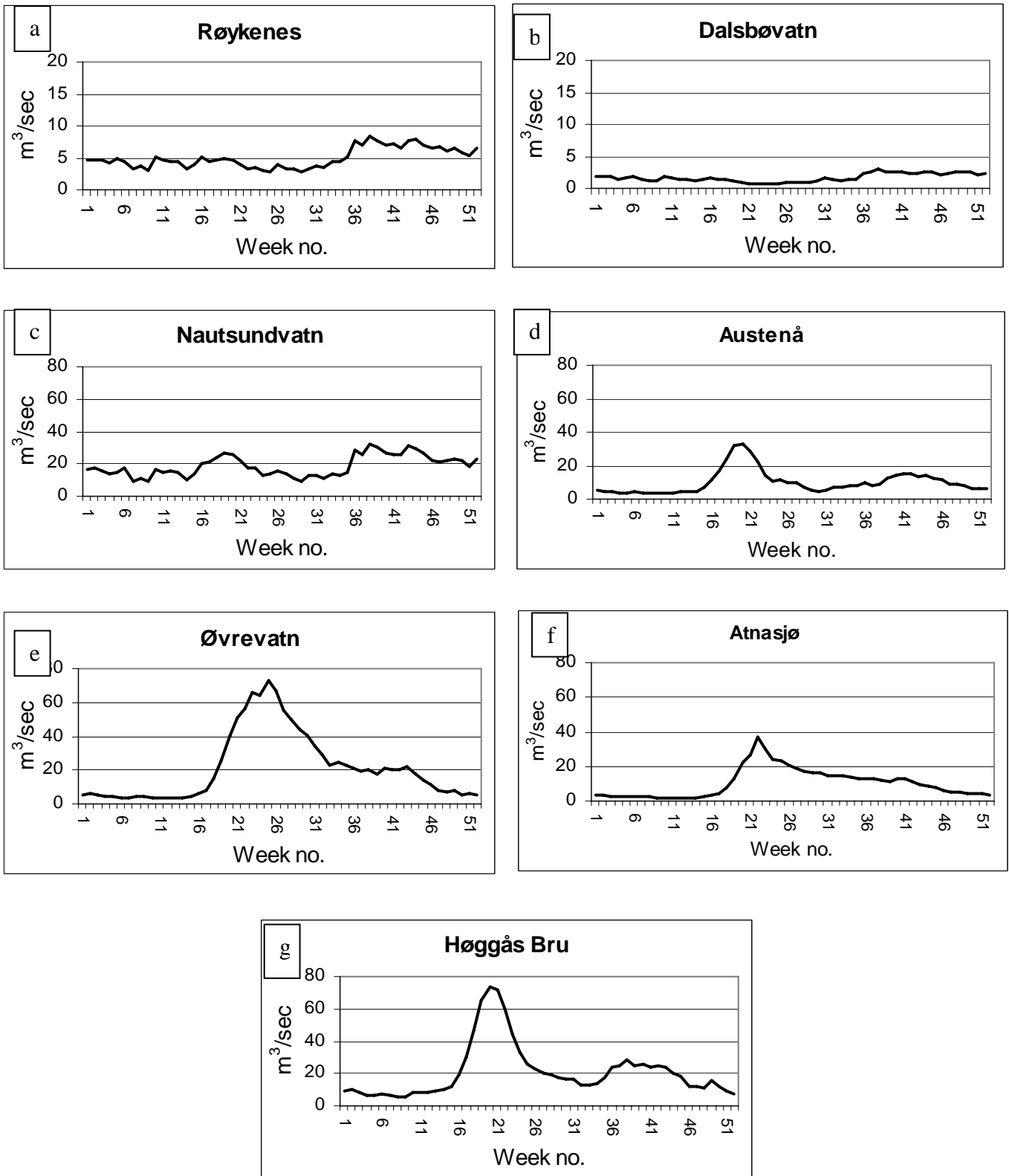


Figure 2.6 Hydrographs of the 7 selected catchments (Figure 2.1). The graphs show mean weekly runoff for the normal period 1961-1990

2.2 Global climate scenarios

The multi-model ensemble of global climate scenario runs made with a range of different GCMs, used here and reported in IPCC AR4 (Meehl et al., 2007), are freely available from Program for Climate Model Diagnosis and Intercomparison (PCMDI; <https://esg.llnl.gov:8443/index.jsp>). This model ensemble includes both simulations for the 20th century (c20) and scenario runs for the 21th century following the Special Report Emission Scenarios (SRES) emission scenario A1b (SRES A1b) (IPCC, 2000). Some of the GCMs have been used to make several parallel runs, differing by using different initial conditions (starting point). Table 2.2 provides an overview of the various runs downscaled in this study, a complete list of the exact runs is listed in Appendix A. The list of different runs is more complete at the PCMDI, and the ones used here is limited to the results that were available at the time of the analysis (the results were made available continuously as they were ready).

Table 2.2 Simulations from 14 different GCMs for the 20th and 21th century (A1b) (Meehl et al., 2007) is used. Empirical downscaling of runoff is performed with temperature (101) and precipitation (601) as predictors, 68 and 67 runs respectively.

Predictor:	101	101	601	601
Emission scenario:	20th Century	sres a1b	20th Century	sres a1b
Global climate modell	No of runs	No of runs	No of runs	No of runs
BCC.cm1	2	0	2	0
BCCR.bcm2.0	1	1	1	1
CCCMA.CGCM3.1	1	1	1	1
CNRM.cm3	1	1	1	1
CSIRO.mk3.0	1	0	1	1
GFDL.cm2.0	1	1	1	1
GFDL.cm2.1	3	1	3	1
GISS.aom	1	2	2	2
GISS.modell_e.h	5	3	4	3
GISS.modell_e.r	0	5	0	2
INMCN3.0	1	1	1	1
IPSL.cm4	1	1	1	1
MIROC3.2.hires	0	1	1	0
MIROC3.2.medres	0	2	0	2
MIUB.echo.g	0	2	0	2
MPI.ECHAM5	3	3	3	2
MRI.cgcm2.3.2a	0	5	0	5
NCAR.cesm3.0	4	3	6	3
NCAR.pcm1	3	3	3	3
UKMO.hadcm3	2	1	2	1
UKMO.hadgem1	0	1	0	1

3 Empirical statistical downscaling method (ESD)

River runoff was used as predictand in a Empirical-Statistical Downscaling (ESD) analysis, taking gridded ERA40 (Simmons and Gibson, 2000; Bengtsson et al. 2004) precipitation or temperature over a larger region as predictors. The implementation was similar to the work documented in Benestad (2005) for each GCM implemented, and performed for monthly mean values. The ESD was applied to the IPCC AR4 (Meehl et al., 2007) MMD GCM ensemble for both the 20th century and the 21st century simulations separately, and the tool *clim.pact* (Benestad, 2004) was used to carry out the calculations, using a common empirical orthogonal function (EOF) based framework (Benestad, 2001) and linear multiple regression as a basis for the empirical-statistical model.

The common EOF framework combined large-scale gridded temperature or precipitation anomalies estimated from the ERA40 re-analysis with corresponding anomalies from a simulation performed by a GCM (interpolated onto the same grid as the former), and an ordinary EOF analysis is applied to this combined data set. The principal components (PCs) describing the temporal variations of the different modes (predominant spatial temperature or precipitation pattern) then represent exactly the same spatial structures for GCMs and the ERA40. The step-wise regression analysis uses the part of the PCs describing the ERA40 data together with the predictand (run-off series) to calibrate the model. This calibration returns R^2 -statistics, describing how well the run-off can be reproduced with the statistical model if the ERA40 data is used as predictor. The part of the PCs representing the GCMs was used for prediction (scenarios).

Because the various GCMs may differ in their ability to provide an exact representation of the spatio-temporal structure of the temperature or precipitation modes, the common EOFs may differ somewhat from GCM to GCM. Thus the R^2 -statistics may vary with the GCM, although the variation in the R^2 -statistics should be small for realistic GCMs (large deviations in the R^2 -statistics may be an indicator of model problems).

The *clim.pact* tool makes predictions based on the calibration data (here ERA40) as well as the GCM (here either 20th century or the 21st century). However, the ESD-results derived from ERA40 are *not* independent and only serves as a visual check of the quality of the statistical downscaling model. The downscaling for the 20th century, on the other hand, provides independent data which can be used in the validation against the actual observations. This validation will test whether the ESD-model is good (here the R^2 -statistic is also a measure of skill).

4 Results

Predictions for runoff are established based on statistical relations between the predictand (observed runoff) and the predictors (temperature and precipitation from the ERA40 dataset respectively) (Section 3). The statistical relations are used to obtain the runoff predictions from a set of GCMs (Section 2.2) to 7 catchments in Norway; Øvrevatn, Atnasjø, Røykenes, Austenå, Dalsbøvatn, Høggås bru, Nautsundvatn (Section 2.1). The results are presented in section 4.1-4.7 respectively.

4.1 Øvrevatn

An indication for how well the empirically downscaled runoff represents the observed runoff series is the coefficient of determination R^2 . A boxplot of R^2 from the regression between the observational part of the common EOFs of ERA40/GCMs and observed runoff is presented in Figure 4.1.1. The open circle symbols show some outliers representing a few cases where the models failed to provide a good representation of the given location. Here the GCMs probably differed from the ERA40 data in terms of the representation of the surrounding large-scale predictor structure or the algorithm may have failed to select a good predictor domain. However, such a failure is the exception rather than the rule, as the R^2 scores tend to be much more similar for the great majority of GCMs. The spread of the downscaled runoff with precipitation and temperature as predictor for Øvrevatn are presented in Figures 4.1.2 and 4.1.4 respectively. Mean seasonal change in runoff are presented in Figures 4.1.3 and 4.1.5 with precipitation and temperature as predictors respectively.

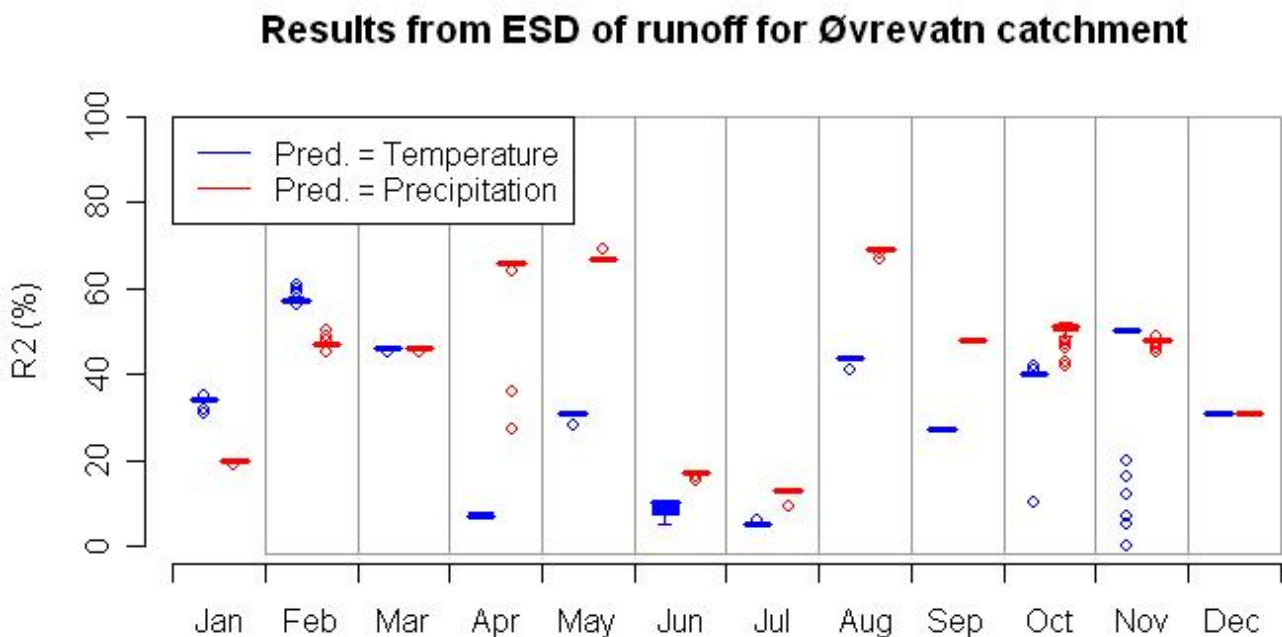


Figure 4.1.1 R^2 from the regression between the observational part of the common EOFs of ERA40/GCMs and observed runoff is presented in a boxplot. 68 GCMs with temperature as predictor (blue) and 67 GCMs with precipitation as predictor (red) are used.

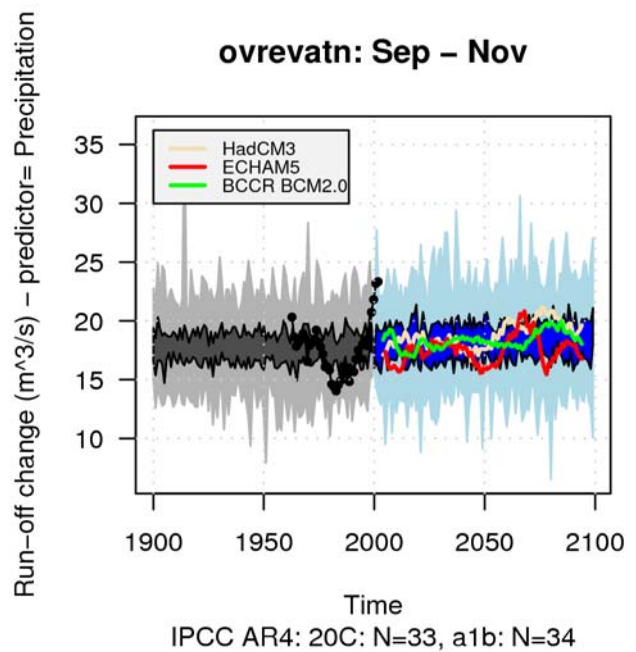
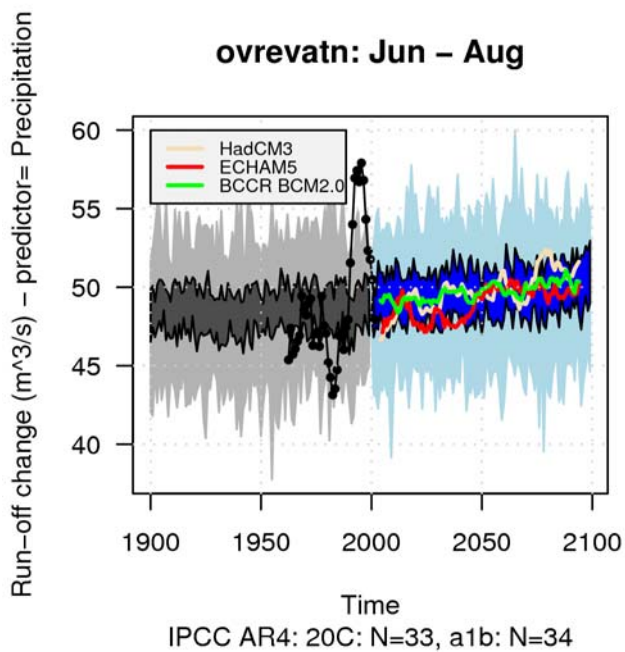
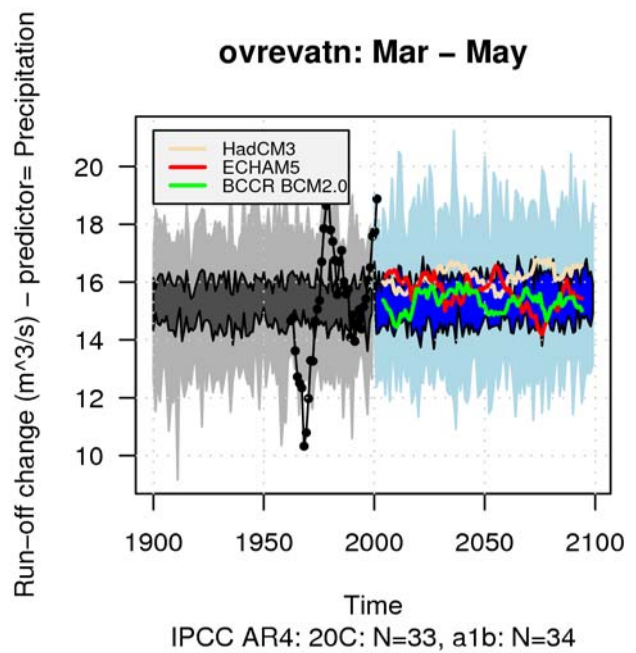
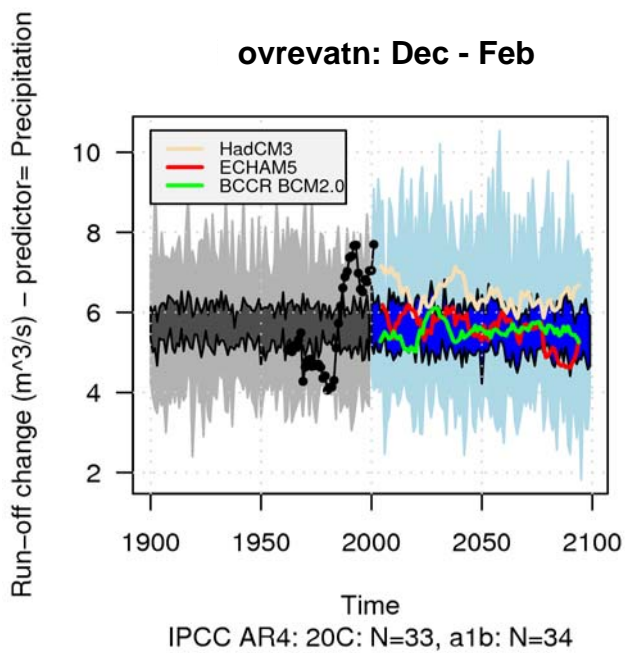
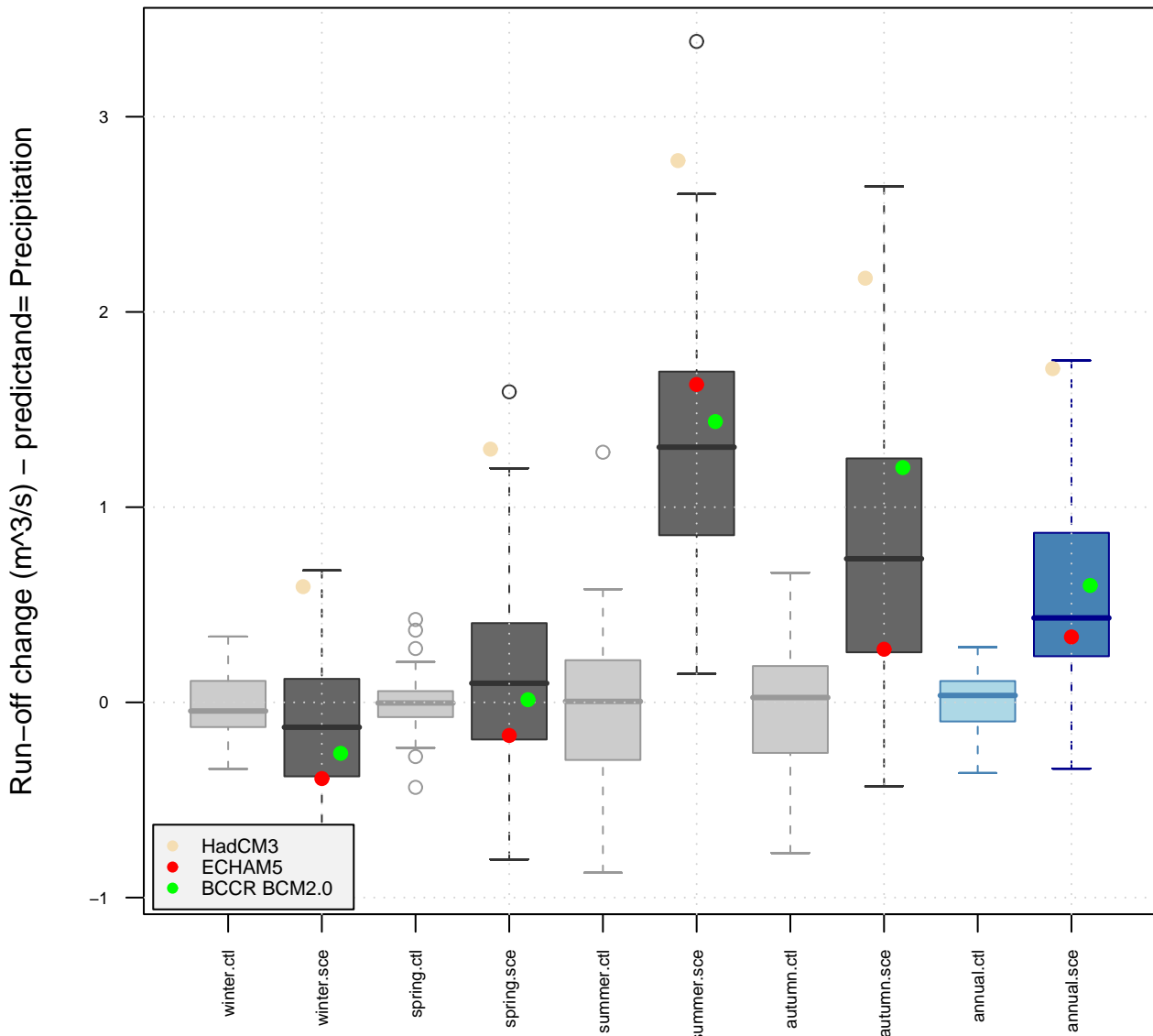


Figure 4.1.2 The figure shows the spread of the evolution of empirically downscaled runoff with precipitation as a predictor from the 33 GCMs used for the historic period 1958 -2002 and the 34 GCMs for the future period 2000-2100 following the SRES A1b emission scenario. Scenarios are established for four seasons; winter (upper left), spring (upper right), summer (lower left) and autumn (lower right). The historic period represents the control runs. Observed runoff is drawn as a black curve. Three selected GCMs are presented in the figure, HadCM3, ECHAM5 and BCCR.

ovrevatn



2070—2099 scenario w.r.t. 1961—1990N sce=34 N 20c=33

Figure 4.1.3 The figure shows box plot of the change in runoff obtained by empirically downscaled runoff with precipitation as a predictor from the 33 GCMs used for the historic period 1961-1990 (light grey) (light blue is annual mean) and the 34 GCMs for the future period 2070-2099 following the SRES A1b emission scenario (dark grey) (dark blue is annual mean). Results from three models; HadCM3 (off white), ECHAM5 (red) and BCCR BCM2.0 (green) are specified in the figure. Scenarios are established annually and for four seasons. The boxes mark the 25 and 75 percentiles, and the whiskers extend up to 1.5 times the inter-quantile range (IQR). Data beyond 1.5 IQR from the box are marked as outliers.

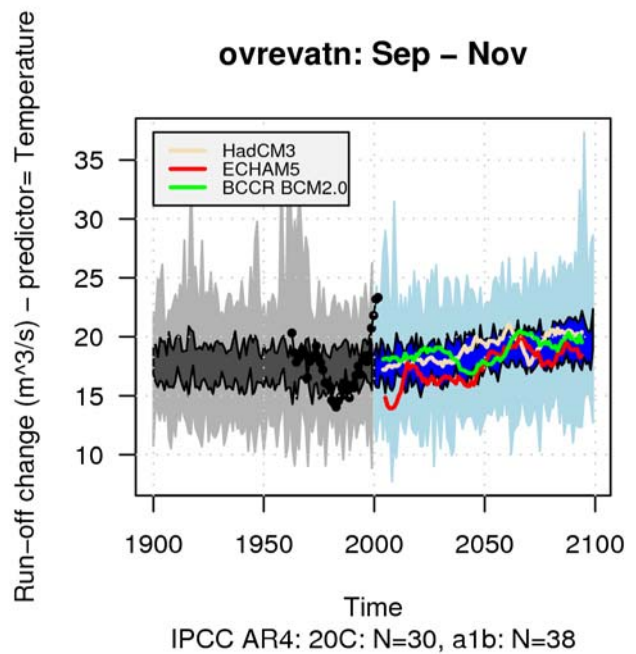
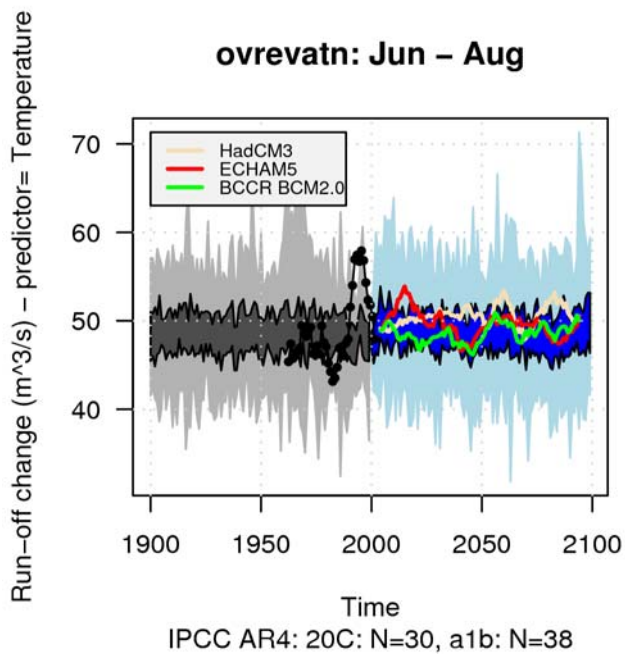
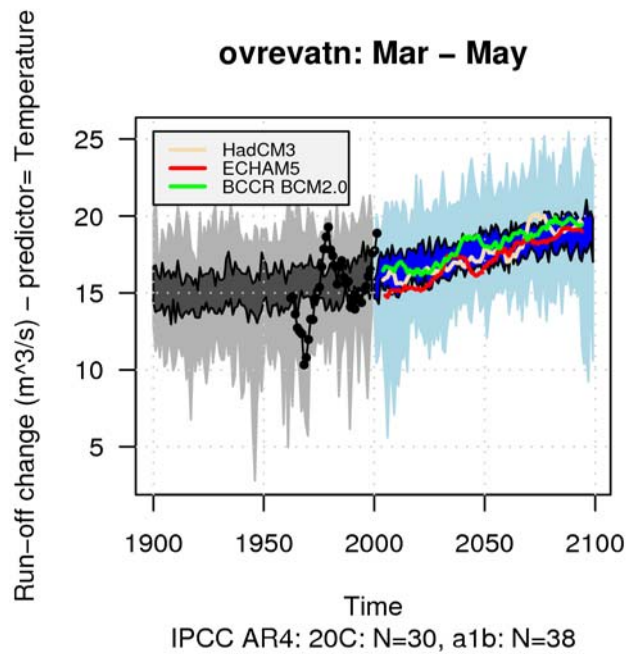
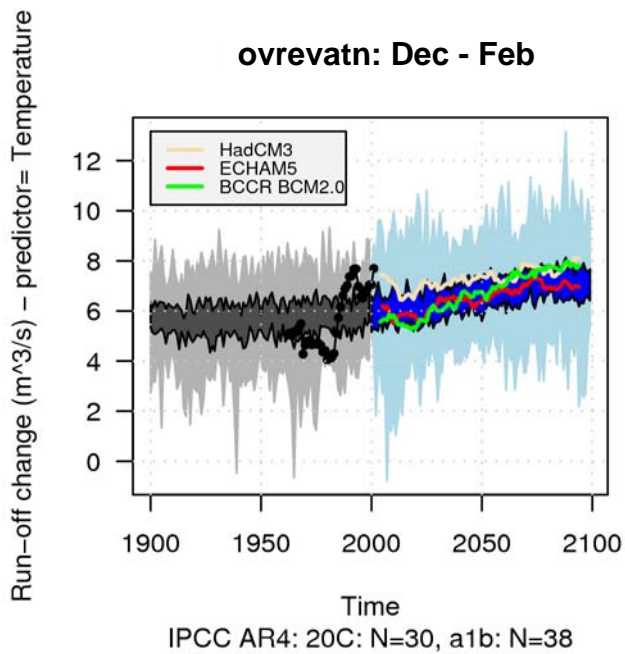
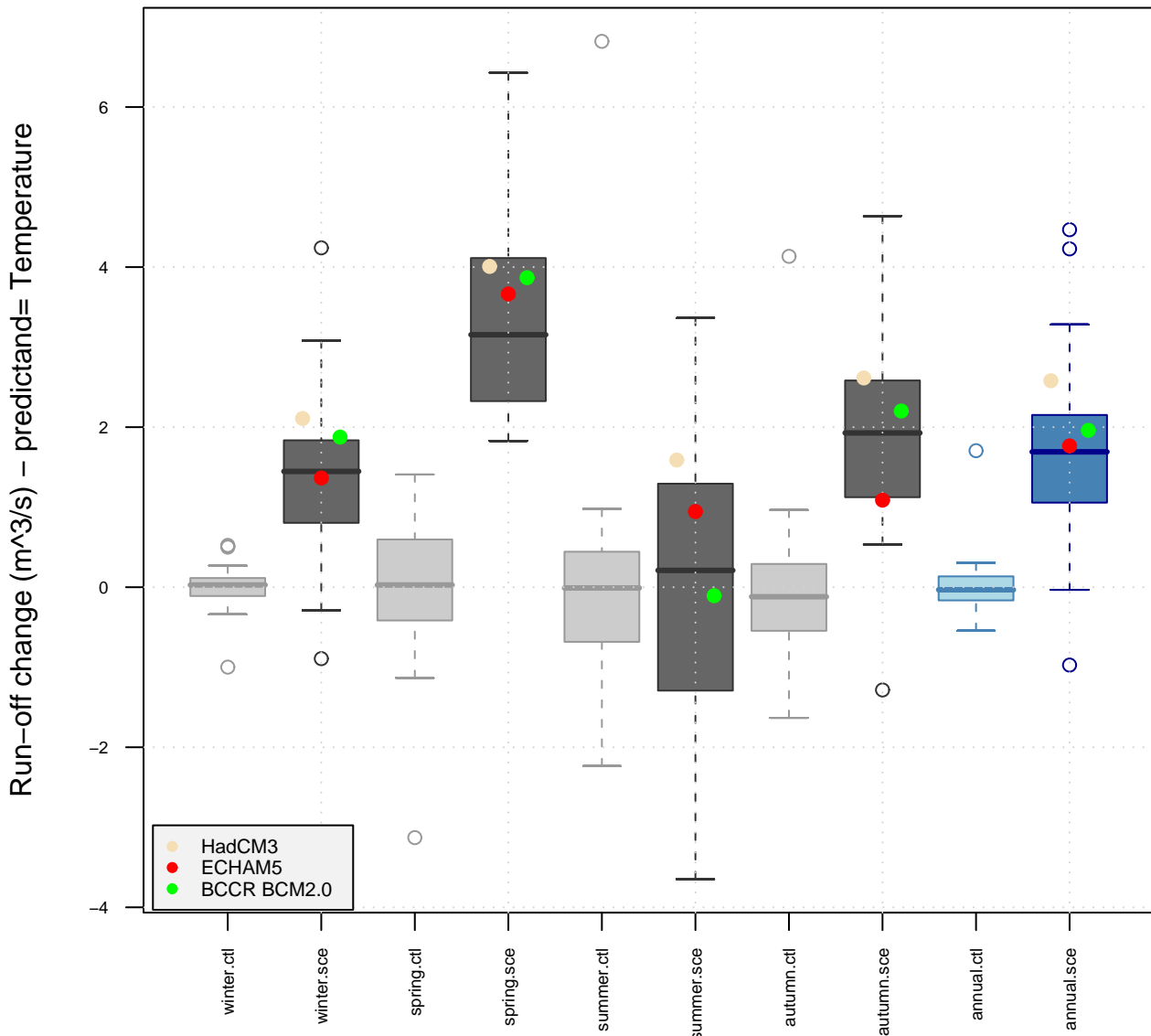


Figure 4.1.4 The figure shows the spread of the evolution of empirically downscaled runoff with temperature as a predictor from the 30 GCMs used for the historic period 1958 -2002 and the 38 GCMs for the future period 2000-2100 following the SRES A1b emission scenario. Scenarios are established for four seasons; winter (upper left), spring (upper right), summer (lower left) and autumn (lower right). The historic period represents the control runs. Observed runoff is drawn as a black curve. Three selected GCMs are presented in the figure, HadCM3, ECHAM5 and BCCR.

ovrevatn



2070--2099 scenario w.r.t. 1961--1990N sce=38 N 20c=30

Figure 4.1.5 The figure shows box plot of the change in runoff obtained by empirically downscaled runoff with precipitation as a predictor from the 33 GCMs used for the historic period 1961-1990 (light grey) (light blue is annual mean) and the 34 GCMs for the future period 2070-2099 following the SRES A1b emission scenario (dark grey) (dark blue is annual mean). Results from three models; HadCM3 (off white), ECHAM5 (red) and BCCR BCM2.0 (green) are specified in the figure. Scenarios are established annually and for four seasons. The boxes mark the 25 and 75 percentiles, and the whiskers extend up to 1.5 times the inter-quartile range (IQR). Data beyond 1.5 IQR from the box are marked as outliers.

4.2 Atnasjø

An indication for how well the empirically downscaled runoff represents the observed runoff series is the coefficient of determination R^2 . A boxplot of R^2 from the regression between the observational part of the common EOFs of ERA40/GCMs and observed runoff is presented in Figure 4.2.1. The spread of the downscaled runoff with precipitation and temperature as predictor for Øvrevatn are presented in Figures 4.2.2 and 4.2.4 respectively. Figure 4.2.2(a) shows much too weak variability for the 20th century simulations during winter, and thus indicates likely errors in the analysis for this particular location, and season. Furthermore, the three marker scenarios also exhibit weak amplitudes, but have different constant values. Thus, the appearance of large spread in the future is misleading as the R^2 values show low scores for February and December, and the different ensemble member vary in the mean level. This shortcoming is even more apparent in Figure 4.2.4., which is also seen in the difference in the R^2 values for the temperature and precipitation predictors in Figure 4.2.1. Mean seasonal change in runoff are presented in Figures 4.2.3 and 4.2.5 with precipitation and temperature as predictors respectively.

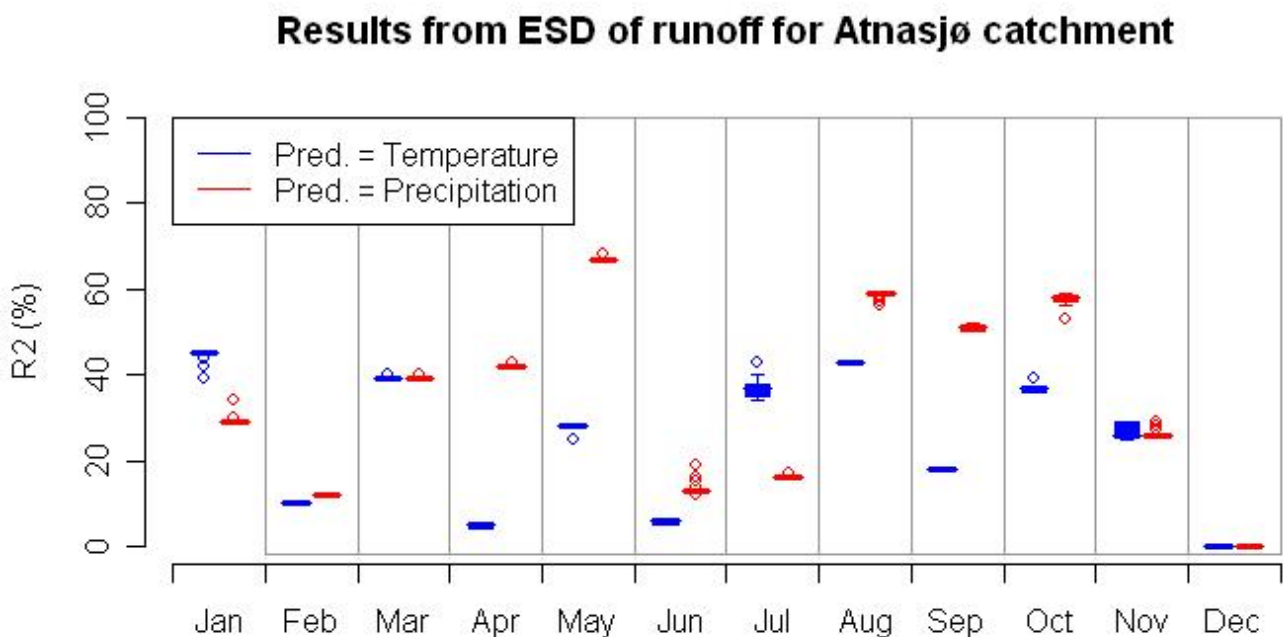


Figure 4.2.1 R^2 from the regression between the observational part of the common EOFs of ERA40/GCMs and observed runoff is presented in a boxplot. 68 GCMs with temperature as predictor (blue) and 67 GCMs with precipitation as predictor (red) are used.

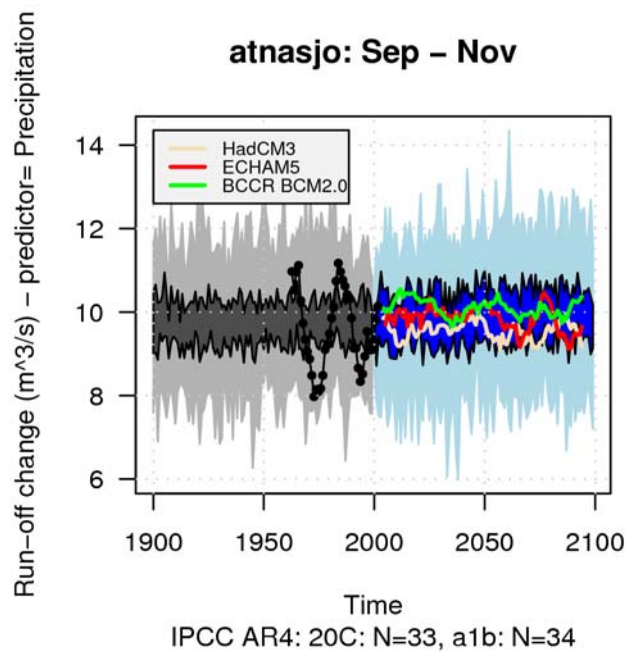
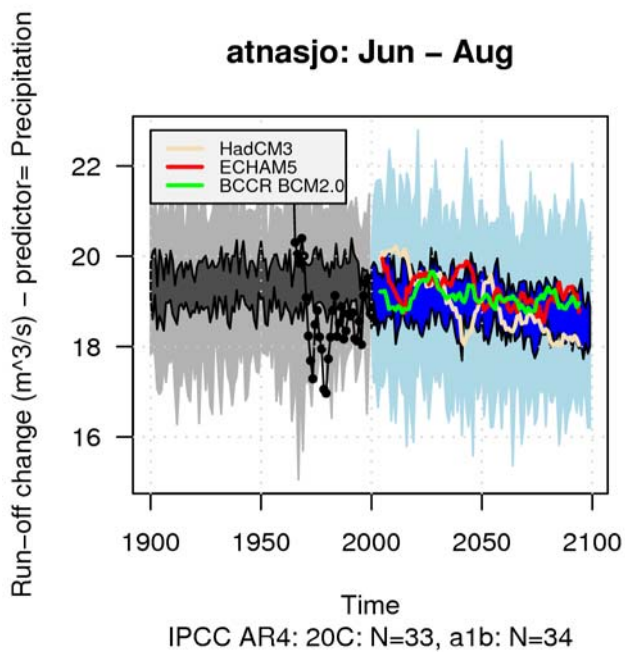
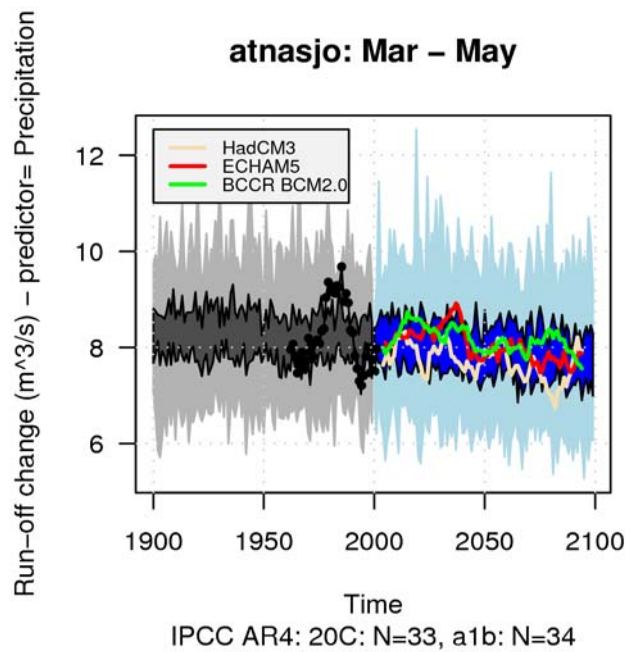
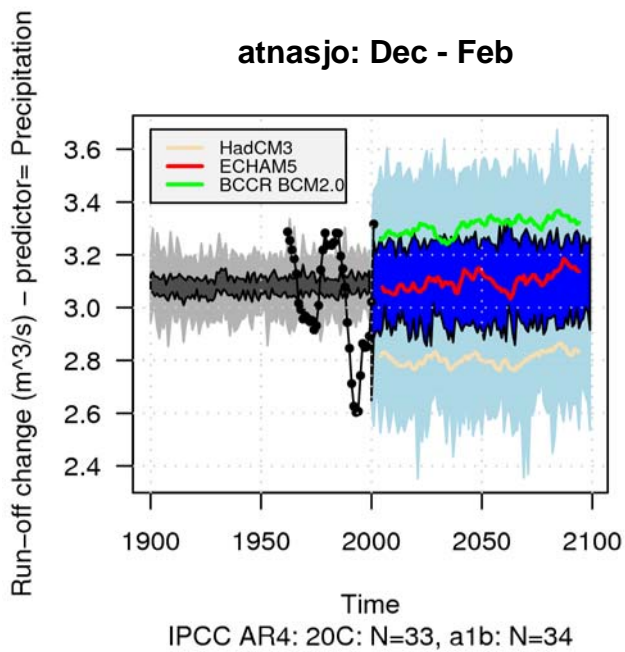
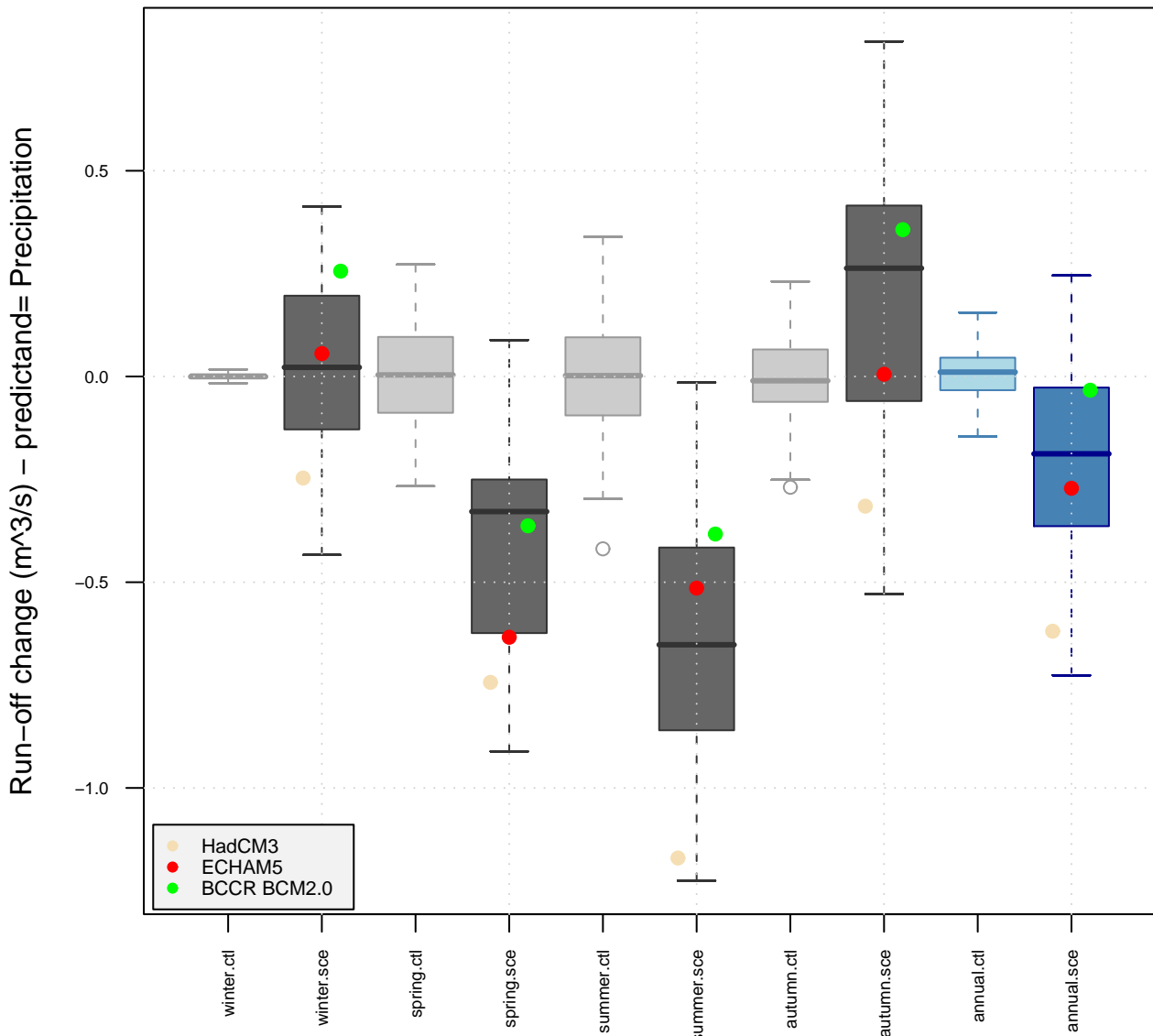


Figure 4.2.2 The figure shows the spread of the evolution of empirically downscaled runoff with precipitation as a predictor from the 33 GCMs used for the historic period 1958 -2002 and the 34 GCMs for the future period 2000-2100 following the SRES A1b emission scenario. Scenarios are established for four seasons; winter (upper left), spring (upper right), summer (lower left) and autumn (lower right). The historic period represents the control runs. Observed runoff is drawn as a black curve. Three selected GCMs are presented in the figure, HadCM3, ECHAM5 and BCCR.

atnasjo



2070--2099 scenario w.r.t. 1961--1990N sce=34 N 20c=33

Figure 4.2.3 The figure shows box plot of the change in runoff obtained by empirically downscaled runoff with precipitation as a predictor from the 33 GCMs used for the historic period 1961-1990 (light grey) (light blue is annual mean) and the 34 GCMs for the future period 2070-2099 following the SRES A1b emission scenario (dark grey) (dark blue is annual mean). Results from three models; HadCM3 (off white), ECHAM5 (red) and BCCR BCM2.0 (green) are specified in the figure. Scenarios are established annually and for four seasons. The boxes mark the 25 and 75 percentiles, and the whiskers extend up to 1.5 times the inter-quartile range (IQR). Data beyond 1.5 IQR from the box are marked as outliers.

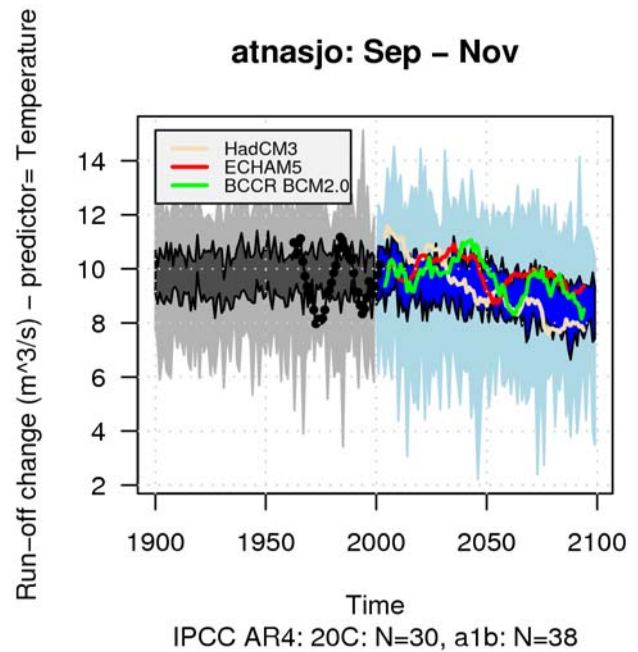
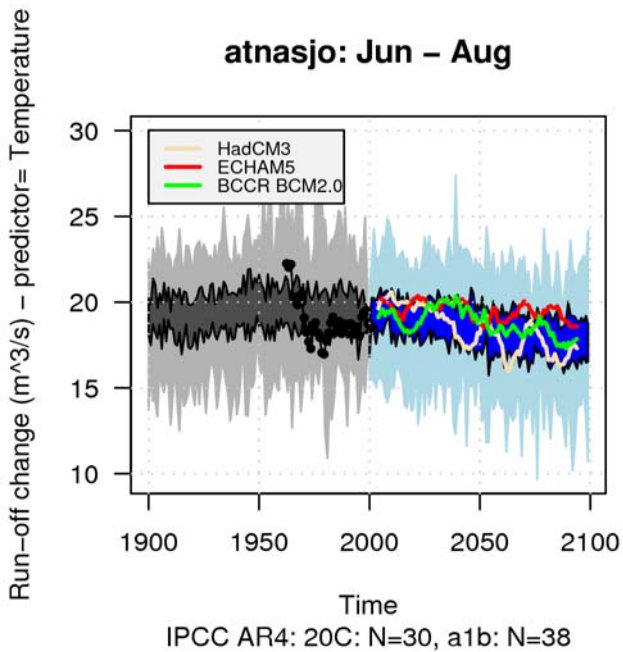
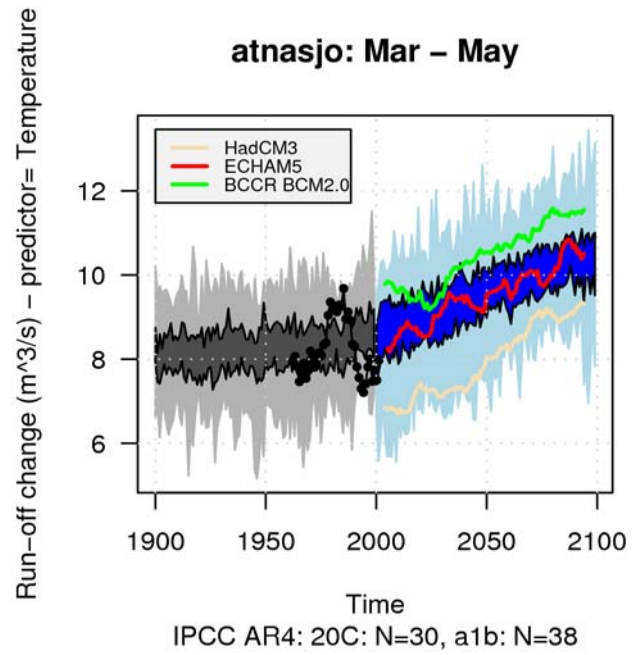
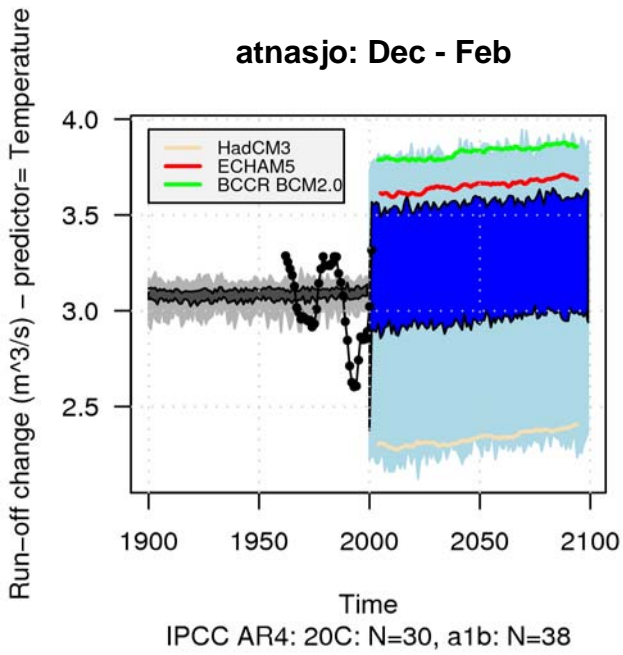
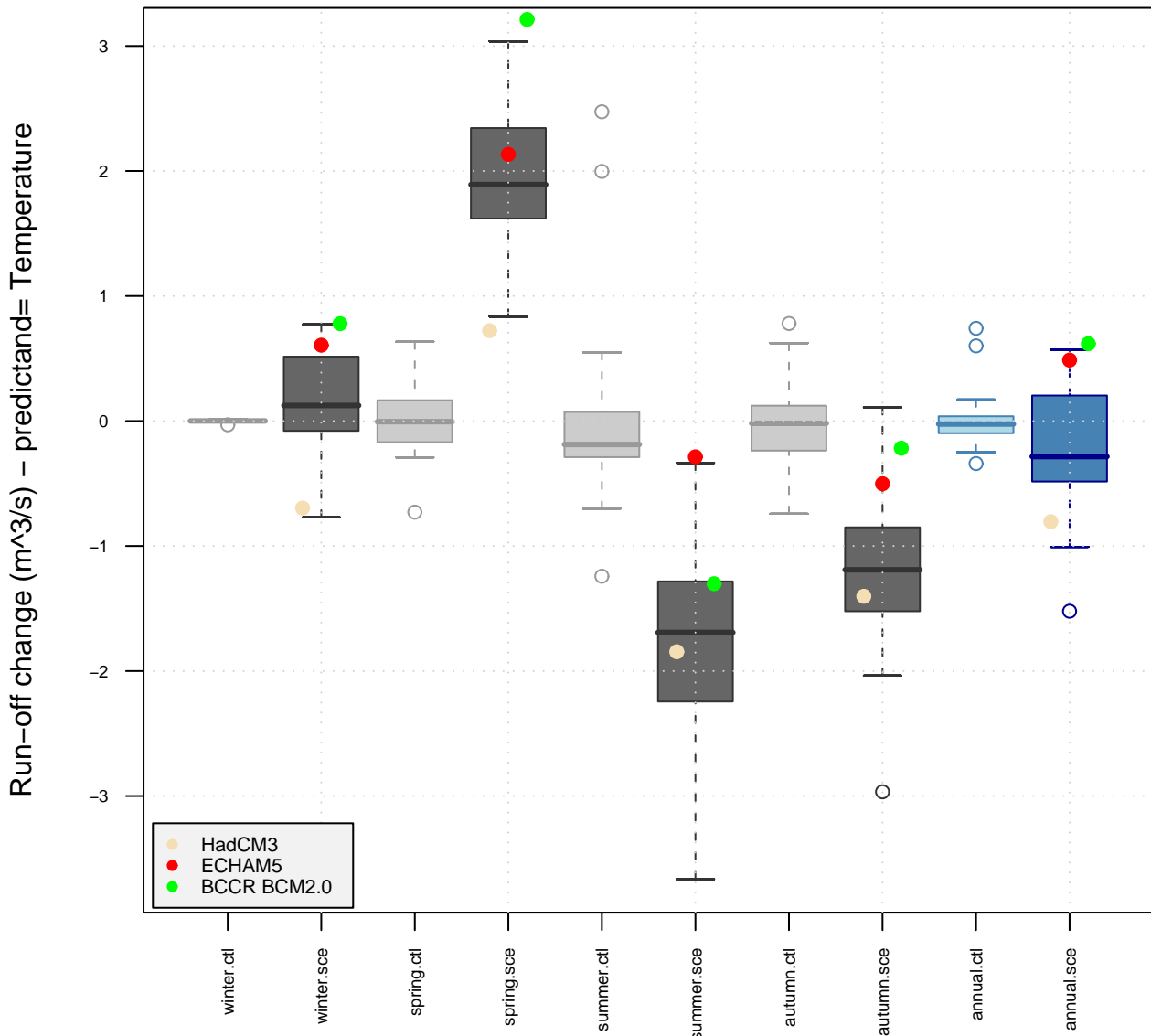


Figure 4.2.4 The figure shows the spread of the evolution of empirically downscaled runoff with temperature as a predictor from the 30 GCMs used for the historic period 1958 -2002 and the 38 GCMs for the future period 2000-2100 following the SRES A1b emission scenario. Scenarios are established for four seasons; winter (upper left), spring (upper right), summer (lower left) and autumn (lower right). The historic period represents the control runs. Observed runoff is drawn as a black curve. Three selected GCMs are presented in the figure, HadCM3, ECHAM5 and BCCR.

atnasjo



2070--2099 scenario w.r.t. 1961--1990N sce=38 N 20c=30

Figure 4.2.5 The figure shows box plot of the change in runoff obtained by empirically downscaled runoff with precipitation as a predictor from the 33 GCMs used for the historic period 1961-1990 (light grey) (light blue is annual mean) and the 34 GCMs for the future period 2070-2099 following the SRES A1b emission scenario (dark grey) (dark blue is annual mean). Results from three models; HadCM3 (off white), ECHAM5 (red) and BCCR BCM2.0 (green) are specified in the figure. Scenarios are established annually and for four seasons. The boxes mark the 25 and 75 percentiles, and the whiskers extend up to 1.5 times the inter-quantile range (IQR). Data beyond 1.5 IQR from the box are marked as outliers.

4.3 Røykenes

An indication for how well the empirically downscaled runoff represents the observed runoff series is the coefficient of determination R^2 . A boxplot of R^2 from the regression between the observational part of the common EOFs of ERA40/GCMs and observed runoff is presented in Figure 4.3.1. The spread of the downscaled runoff with precipitation and temperature as predictor for Øvrevatn are presented in Figures 4.3.2 and 4.3.4 respectively. Mean seasonal change in runoff are presented in Figures 4.3.3 and 4.3.5 with precipitation and temperature as predictors respectively.

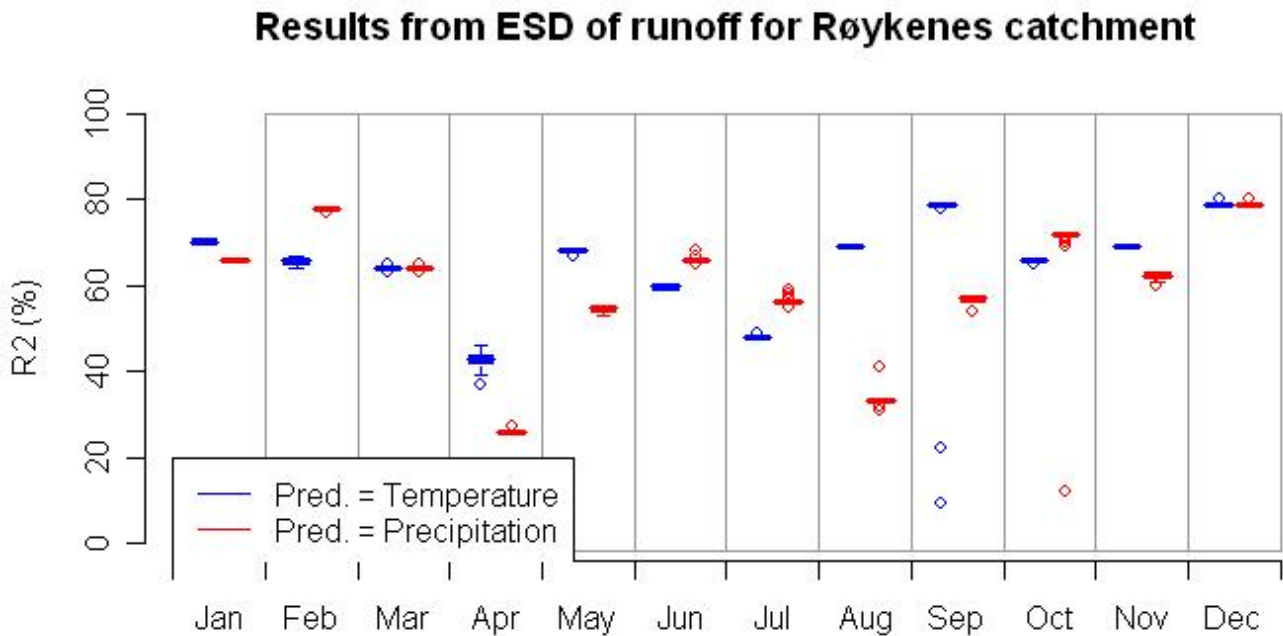


Figure 4.3.1 R^2 from the regression between the observational part of the common EOFs of ERA40/GCMs and observed runoff is presented in a boxplot. 68 GCMs with temperature as predictor (blue) and 67 GCMs with precipitation as predictor (red) are used.

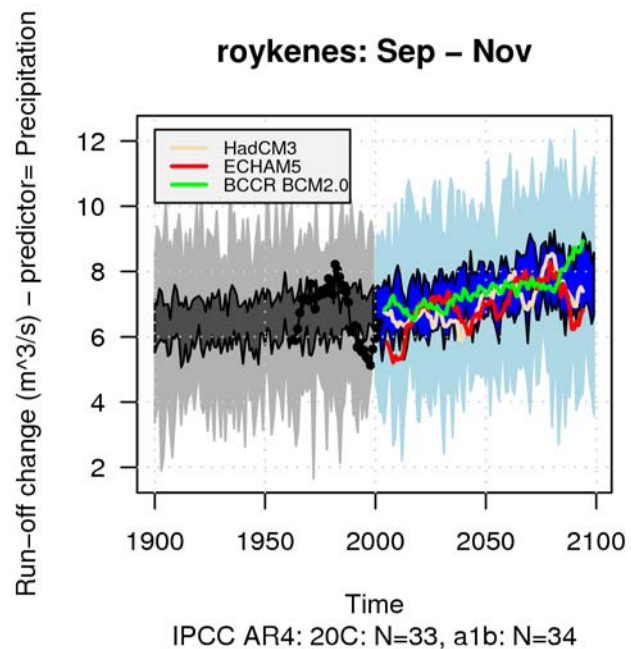
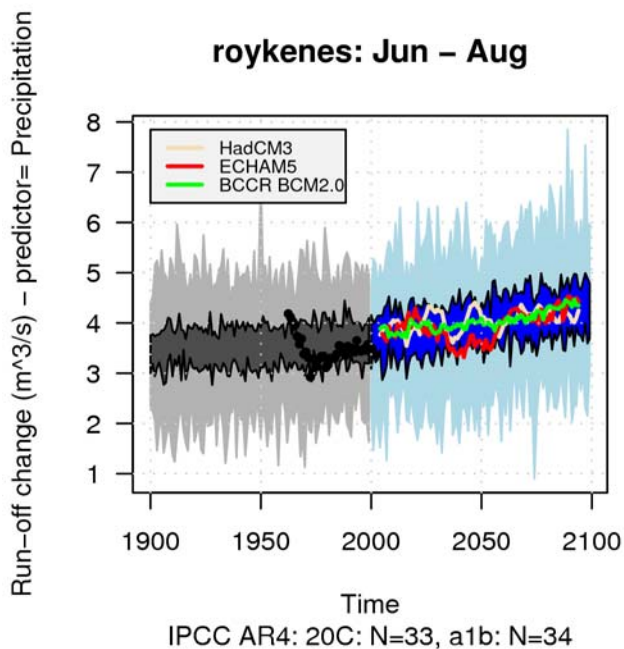
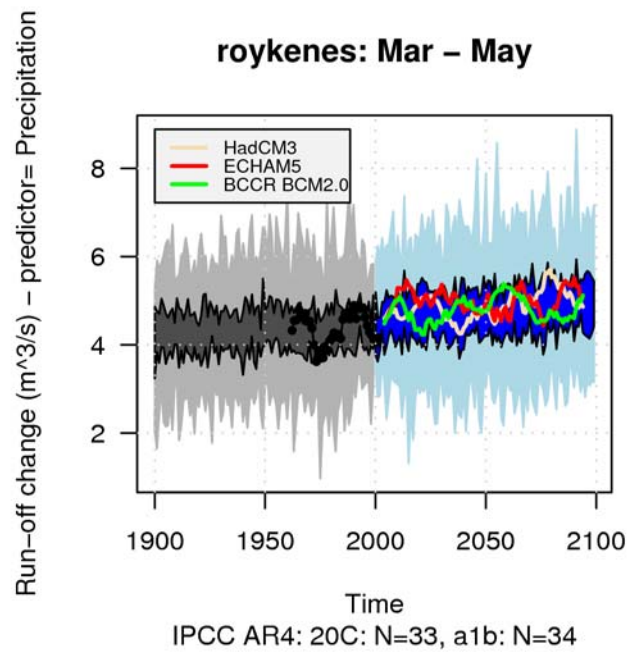
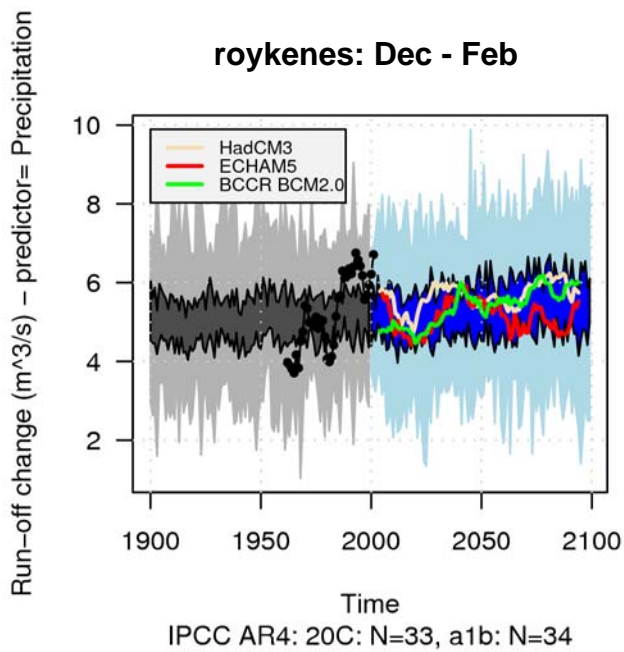
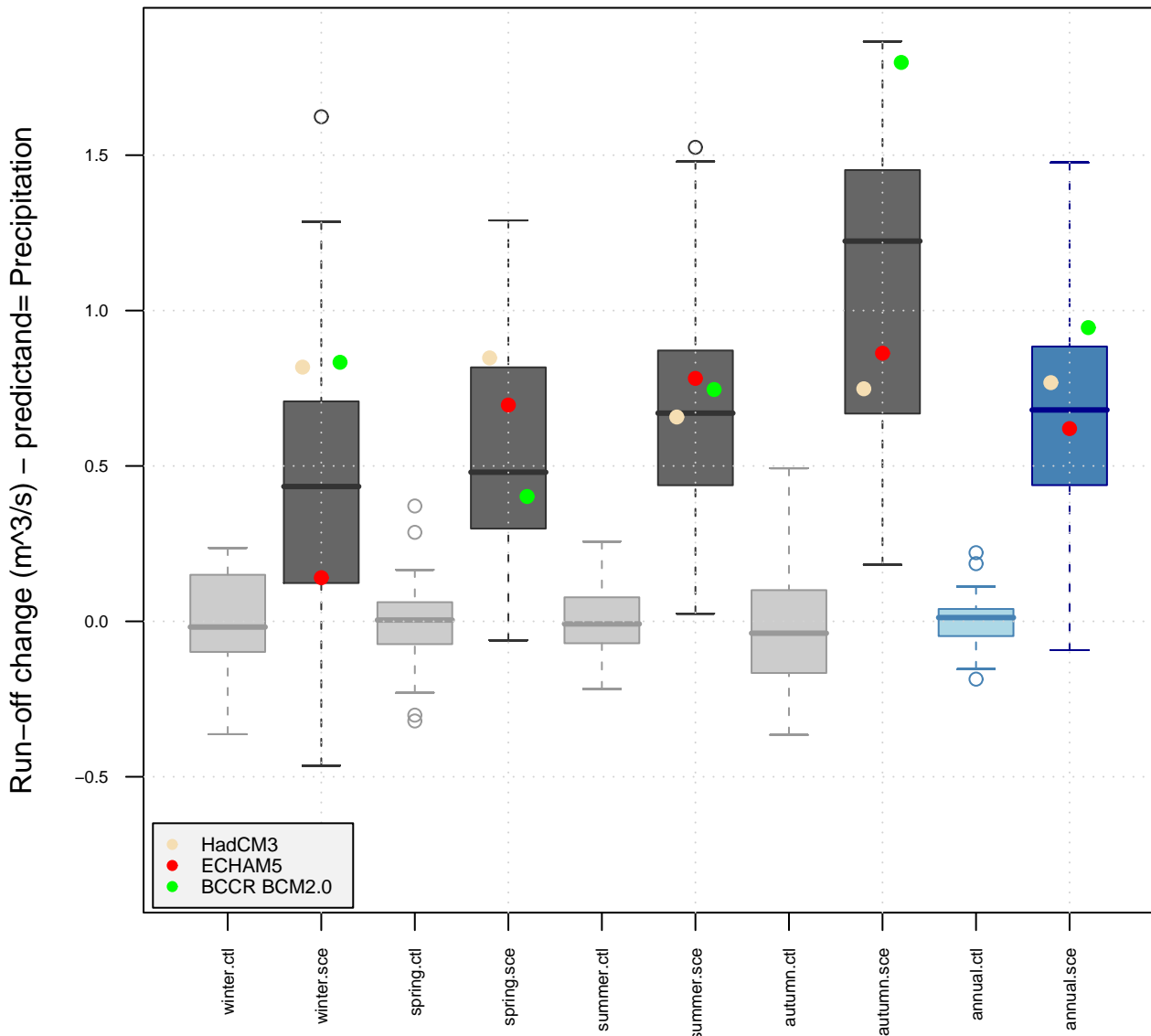


Figure 4.3.2 The figure shows the spread of the evolution of empirically downscaled runoff with precipitation as a predictor from the 33 GCMs used for the historic period 1958 -2002 and the 34 GCMs for the future period 2000-2100 following the SRES A1b emission scenario. Scenarios are established for four seasons; winter (upper left), spring (upper right), summer (lower left) and autumn (lower right). The historic period represents the control runs. Observed runoff is drawn as a black curve. Three selected GCMs are presented in the figure, HadCM3, ECHAM5 and BCCR.

roykenes



2070--2099 scenario w.r.t. 1961--1990N sce=34 N 20c=33

Figure 4.3.3 The figure shows box plot of the change in runoff obtained by empirically downscaled runoff with precipitation as a predictor from the 33 GCMs used for the historic period 1961-1990 (light grey) (light blue is annual mean) and the 34 GCMs for the future period 2070-2099 following the SRES A1b emission scenario (dark grey) (dark blue is annual mean). Results from three models; HadCM3 (off white), ECHAM5 (red) and BCCR BCM2.0 (green) are specified in the figure. Scenarios are established annually and for four seasons. The boxes mark the 25 and 75 percentiles, and the whiskers extend up to 1.5 times the inter-quantile range (IQR). Data beyond 1.5 IQR from the box are marked as outliers.

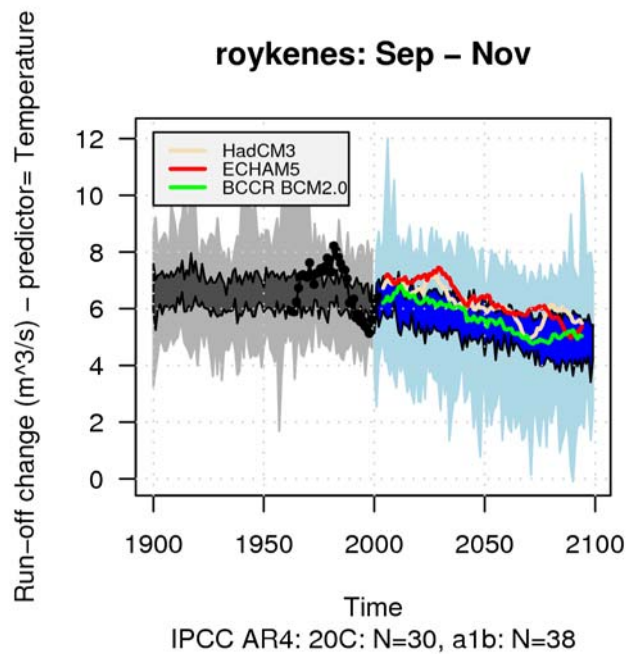
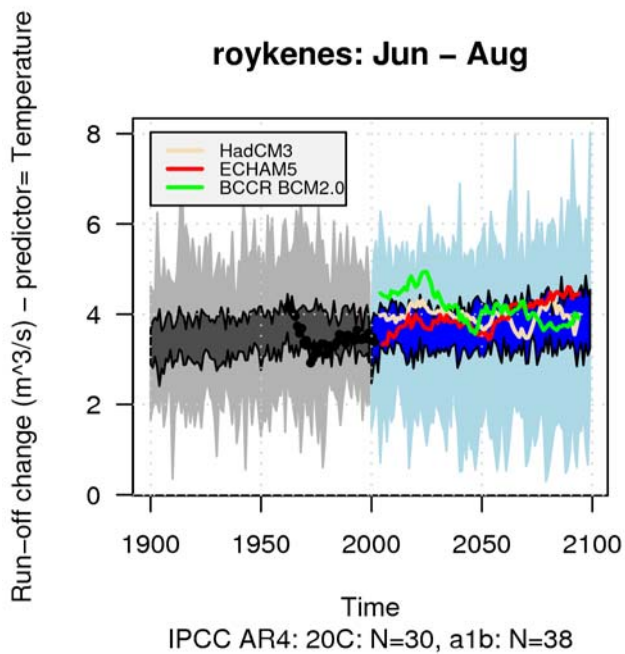
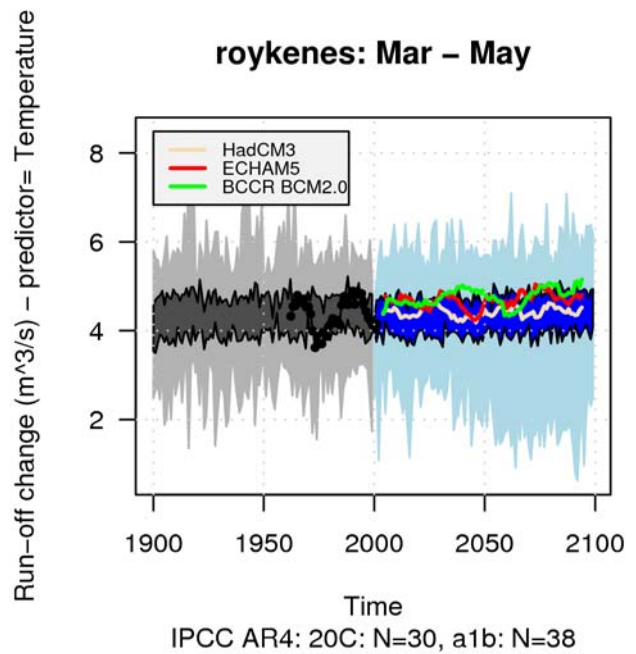
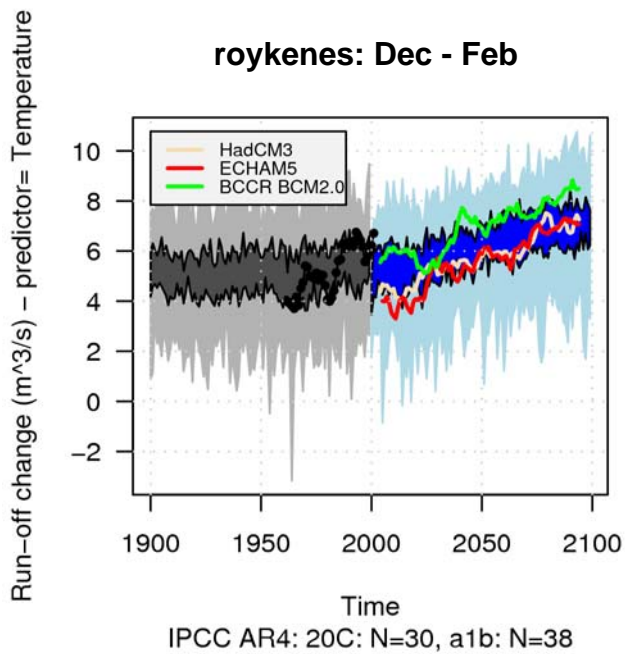
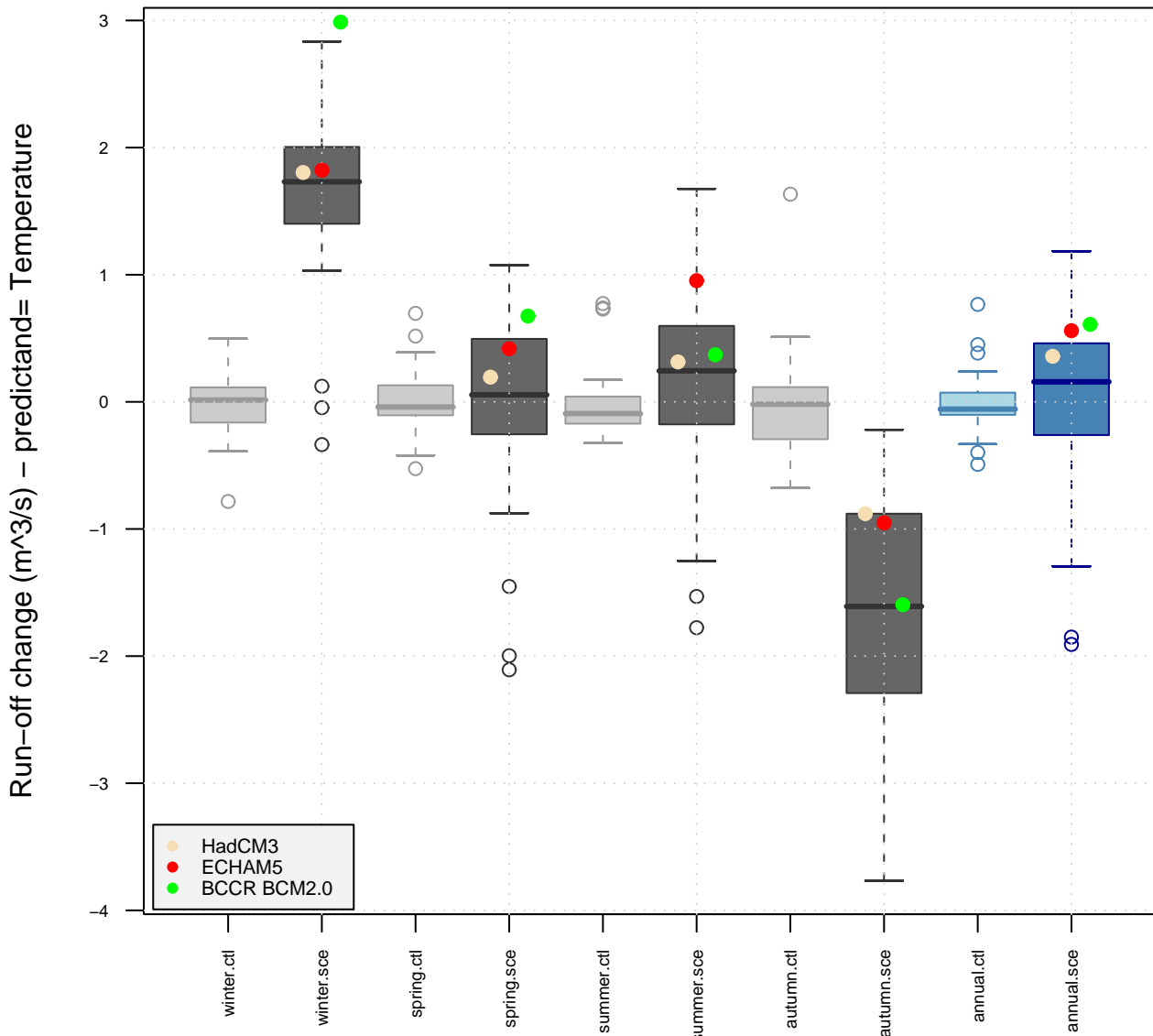


Figure 4.3.4 The figure shows the spread of the evolution of empirically downscaled runoff with temperature as a predictor from the 30 GCMs used for the historic period 1958 -2002 and the 38 GCMs for the future period 2000-2100 following the SRES A1b emission scenario. Scenarios are established for four seasons; winter (upper left), spring (upper right), summer (lower left) and autumn (lower right). The historic period represents the control runs. Observed runoff is drawn as a black curve. Three selected GCMs are presented in the figure, HadCM3, ECHAM5 and BCCR.

roykenes



2070--2099 scenario w.r.t. 1961--1990N sce=38 N 20c=30

Figure 4.3.5 The figure shows box plot of the change in runoff obtained by empirically downscaled runoff with precipitation as a predictor from the 33 GCMs used for the historic period 1961-1990 (light grey) (light blue is annual mean) and the 34 GCMs for the future period 2070-2099 following the SRES A1b emission scenario (dark grey) (dark blue is annual mean). Results from three models; HadCM3 (off white), ECHAM5 (red) and BCCR BCM2.0 (green) are specified in the figure. Scenarios are established annually and for four seasons. The boxes mark the 25 and 75 percentiles, and the whiskers extend up to 1.5 times the inter-quantile range (IQR). Data beyond 1.5 IQR from the box are marked as outliers.

4.4 Austenå

An indication for how well the empirically downscaled runoff represents the observed runoff series is the coefficient of determination R^2 . A boxplot of R^2 from the regression between the observational part of the common EOFs of ERA40/GCMs and observed runoff is presented in Figure 4.4.1 The spread of the downscaled runoff with precipitation and temperature as predictor for Øvrevatn are presented in Figures 4.4.2 and 4.4.4 respectively. Mean seasonal change in runoff are presented in Figures 4.4.3 and 4.4.5 with precipitation and temperature as predictors respectively.

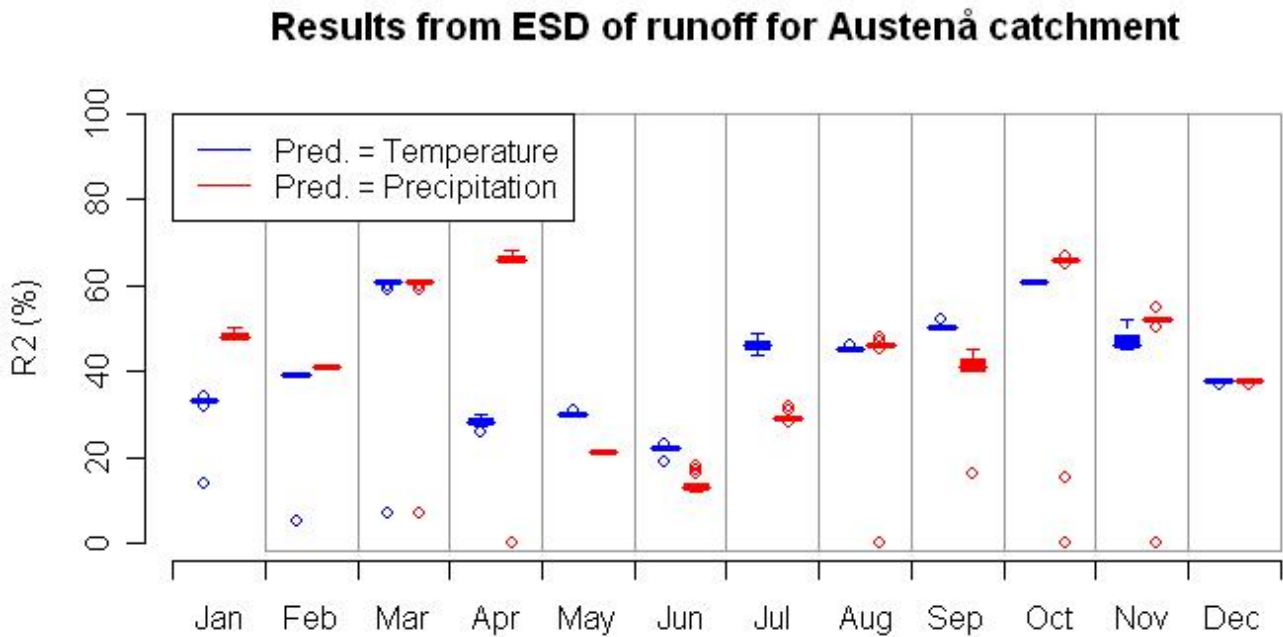


Figure 4.4.1 R^2 from the regression between the observational part of the common EOFs of ERA40/GCMs and observed runoff is presented in a boxplot. 68 GCMs with temperature as predictor (blue) and 67 GCMs with precipitation as predictor (red) are used.

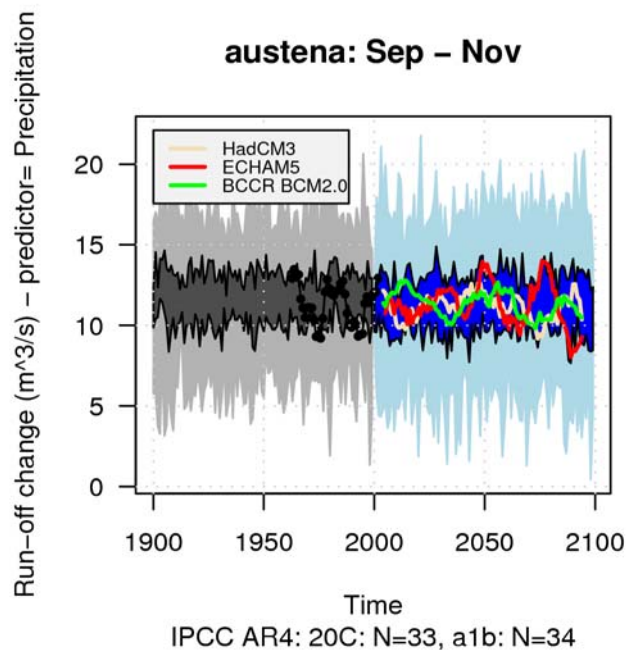
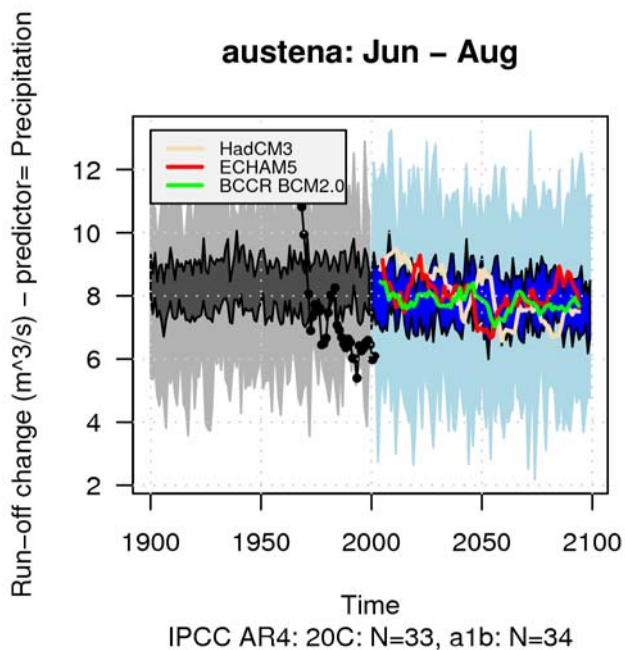
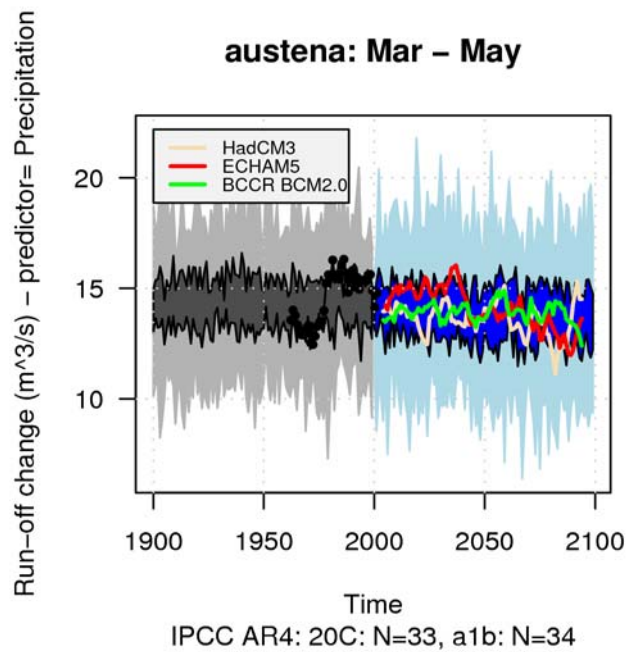
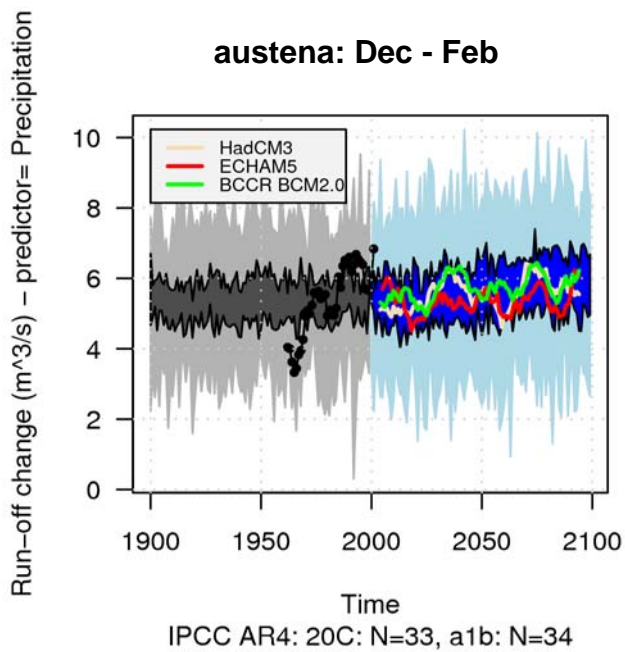
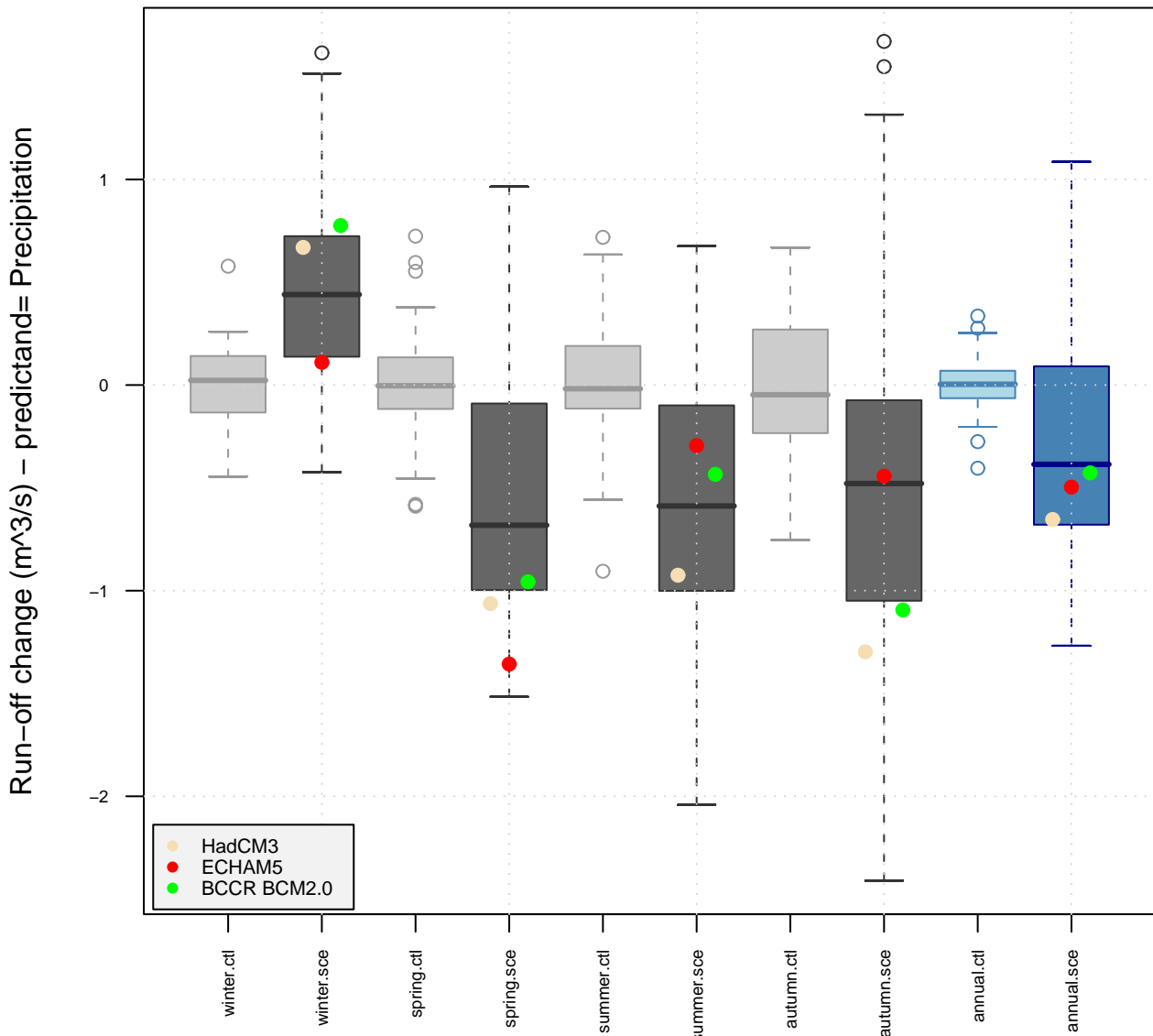


Figure 4.4.2 The figure shows the spread of the evolution of empirically downscaled runoff with precipitation as a predictor from the 33 GCMs used for the historic period 1958 -2002 and the 34 GCMs for the future period 2000-2100 following the SRES A1b emission scenario. Scenarios are established for four seasons; winter (upper left), spring (upper right), summer (lower left) and autumn (lower right). The historic period represents the control runs. Observed runoff is drawn as a black curve. Three selected GCMs are presented in the figure, HadCM3, ECHAM5 and BCCR.

austena



2070--2099 scenario w.r.t. 1961--1990N sce=34 N 20c=33

Figure 4.4.3 The figure shows box plot of the change in runoff obtained by empirically downscaled runoff with precipitation as a predictor from the 33 GCMs used for the historic period 1961-1990 (light grey) (light blue is annual mean) and the 34 GCMs for the future period 2070-2099 following the SRES A1b emission scenario (dark grey) (dark blue is annual mean). Results from three models; HadCM3 (off white), ECHAM5 (red) and BCCR BCM2.0 (green) are specified in the figure. Scenarios are established annually and for four seasons. The boxes mark the 25 and 75 percentiles, and the whiskers extend up to 1.5 times the inter-quartile range (IQR). Data beyond 1.5 IQR from the box are marked as outliers.

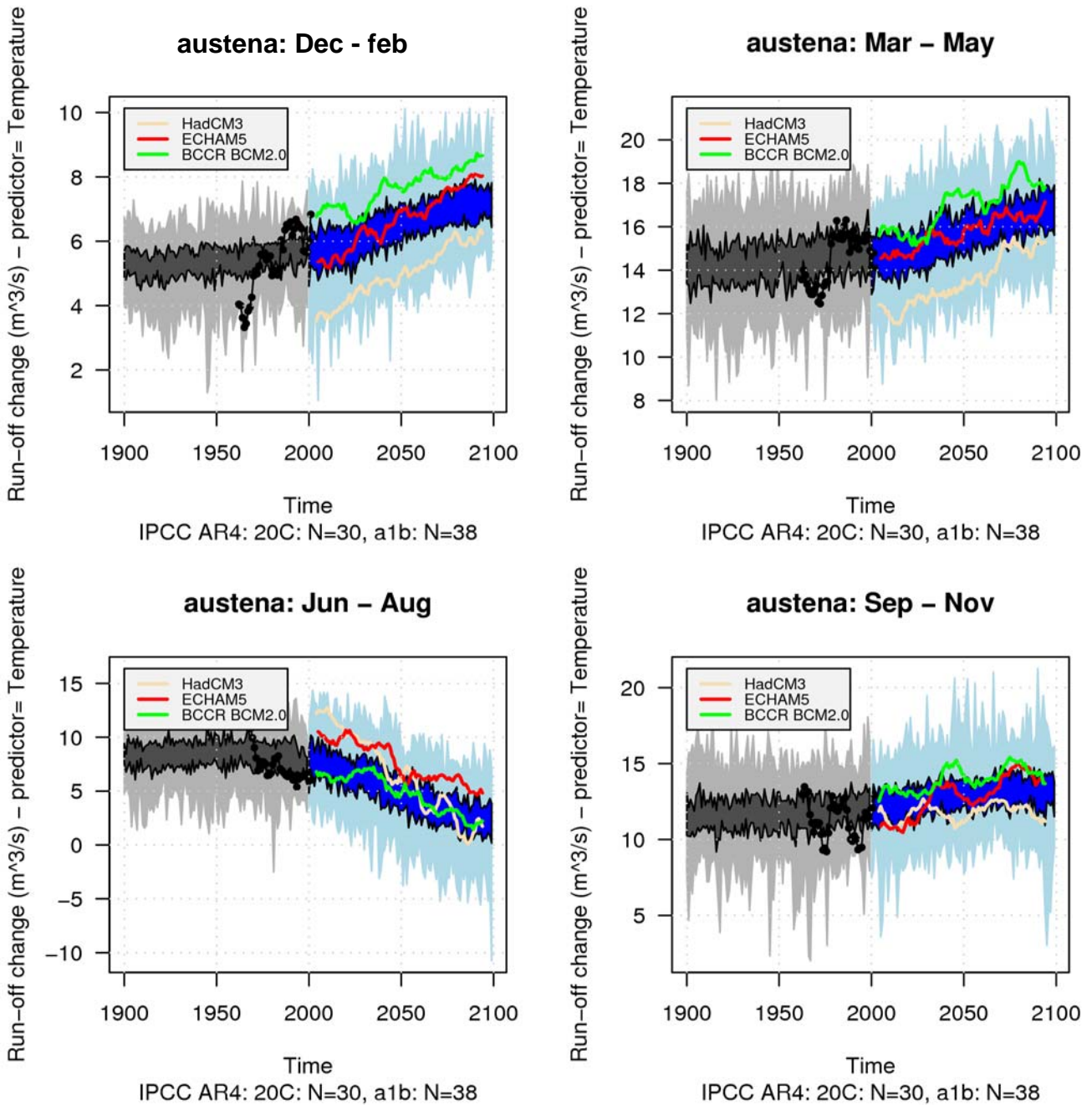
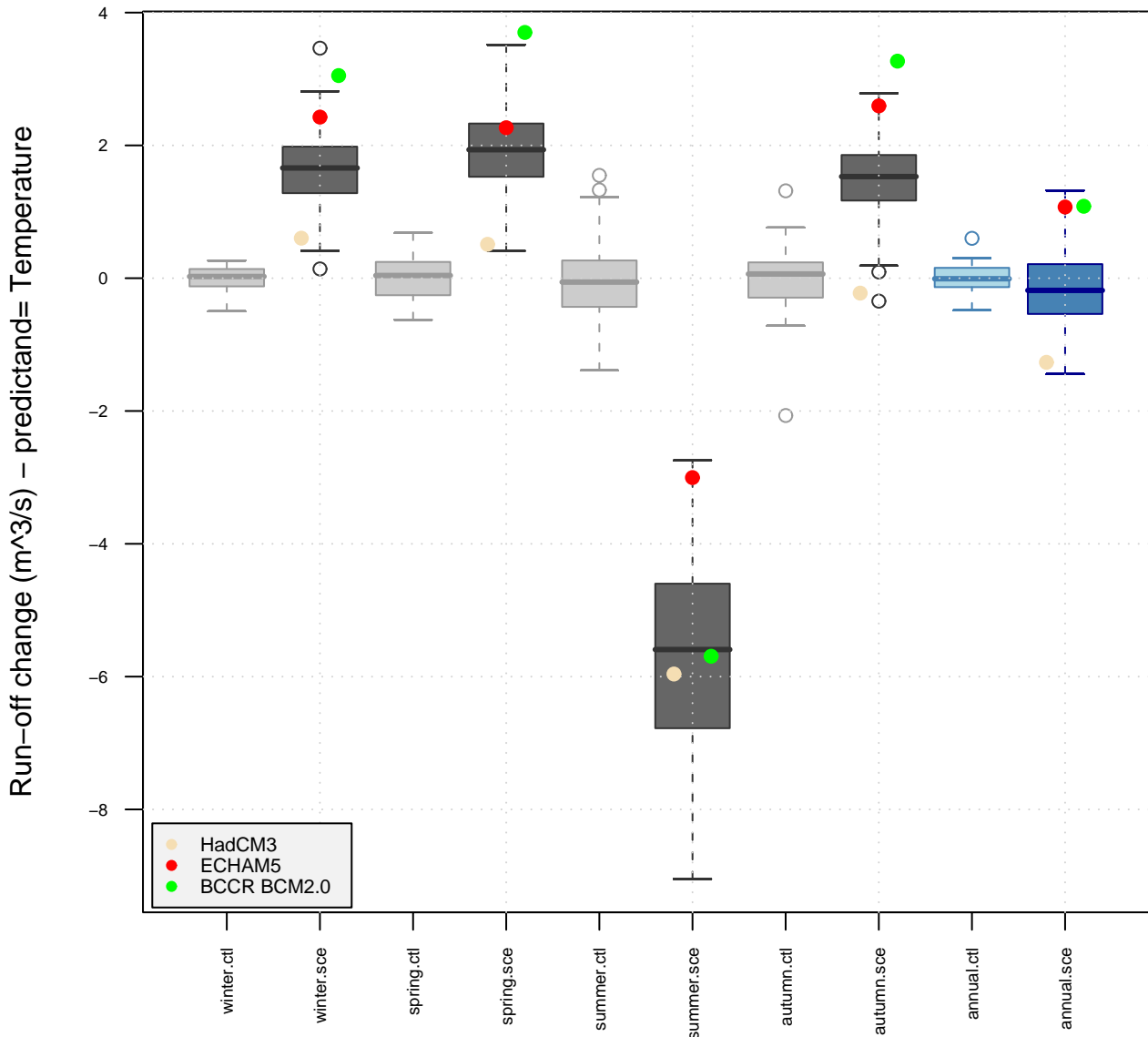


Figure 4.4.4 The figure shows the spread of the evolution of empirically downscaled runoff with temperature as a predictor from the 30 GCMs used for the historic period 1958 -2002 and the 38 GCMs for the future period 2000-2100 following the SRES A1b emission scenario. Scenarios are established for four seasons; winter (upper left), spring (upper right), summer (lower left) and autumn (lower right). The historic period represents the control runs. Observed runoff is drawn as a black curve. Three selected GCMs are presented in the figure, HadCM3, ECHAM5 and BCCR.

austena



2070--2099 scenario w.r.t. 1961--1990N sce=38 N 20c=30

Figure 4.4.5 The figure shows box plot of the change in runoff obtained by empirically downscaled runoff with precipitation as a predictor from the 33 GCMs used for the historic period 1961-1990 (light grey) (light blue is annual mean) and the 34 GCMs for the future period 2070-2099 following the SRES A1b emission scenario (dark grey) (dark blue is annual mean). Results from three models; HadCM3 (off white), ECHAM5 (red) and BCCR BCM2.0 (green) are specified in the figure. Scenarios are established annually and for four seasons. The boxes mark the 25 and 75 percentiles, and the whiskers extend up to 1.5 times the inter-quartile range (IQR). Data beyond 1.5 IQR from the box are marked as outliers.

4.5 Dalsbøvatn

An indication for how well the empirically downscaled runoff represents the observed runoff series is the coefficient of determination R^2 . A boxplot of R^2 from the regression between the observational part of the common EOFs of ERA40/GCMs and observed runoff is presented in Figure 4.5.1 The spread of the downscaled runoff with precipitation and temperature as predictor for Øvrevatn are presented in Figures 4.5.2 and 4.5.4 respectively. Mean seasonal change in runoff are presented in Figures 4.5.3 and 4.5.5 with precipitation and temperature as predictors respectively.

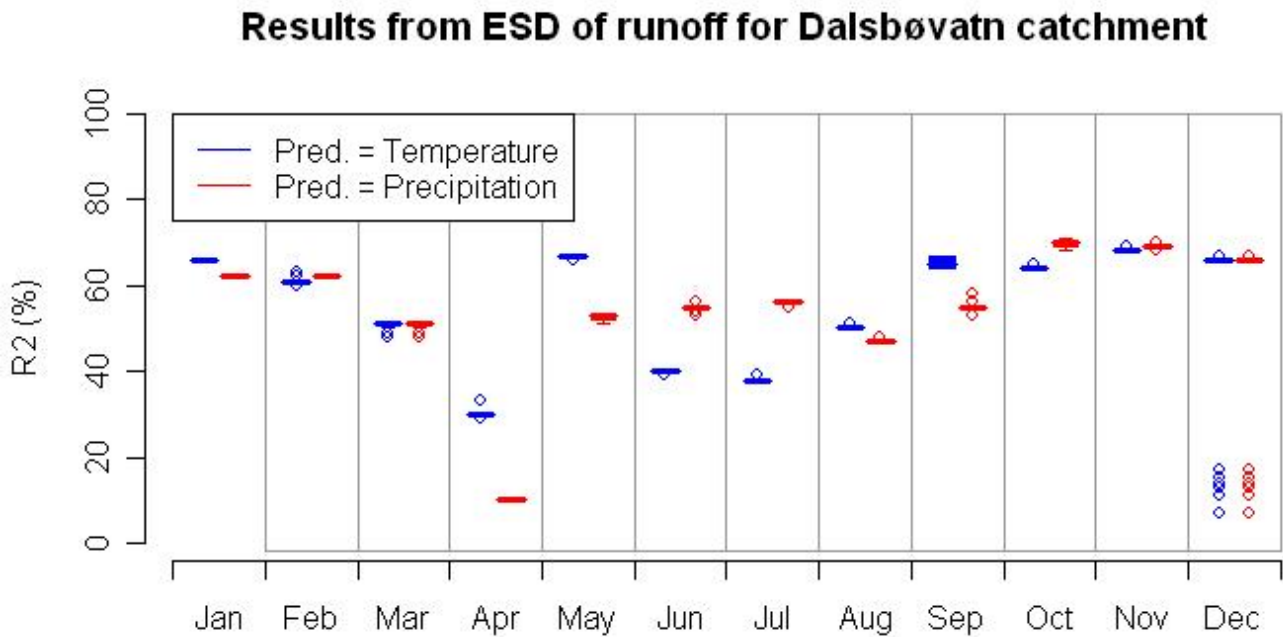


Figure 4.5.1 R^2 from the regression between the observational part of the common EOFs of ERA40/GCMs and observed runoff is presented in a boxplot. 68 GCMs with temperature as predictor (blue) and 67 GCMs with precipitation as predictor (red) are used.

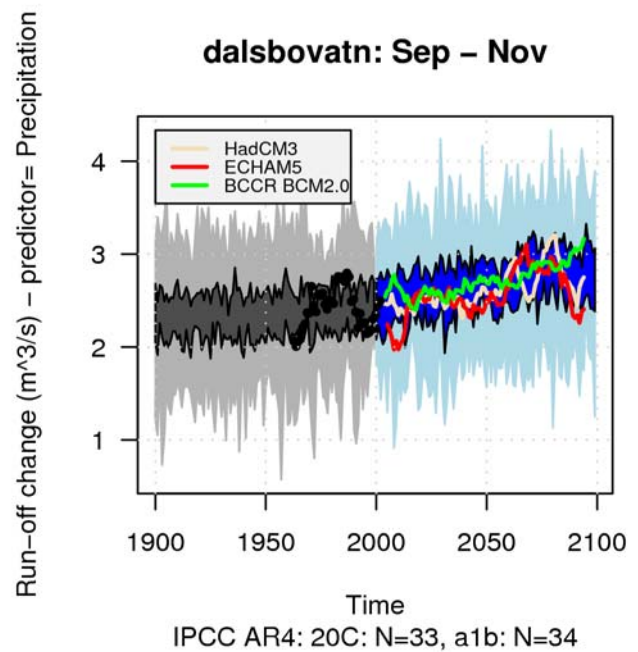
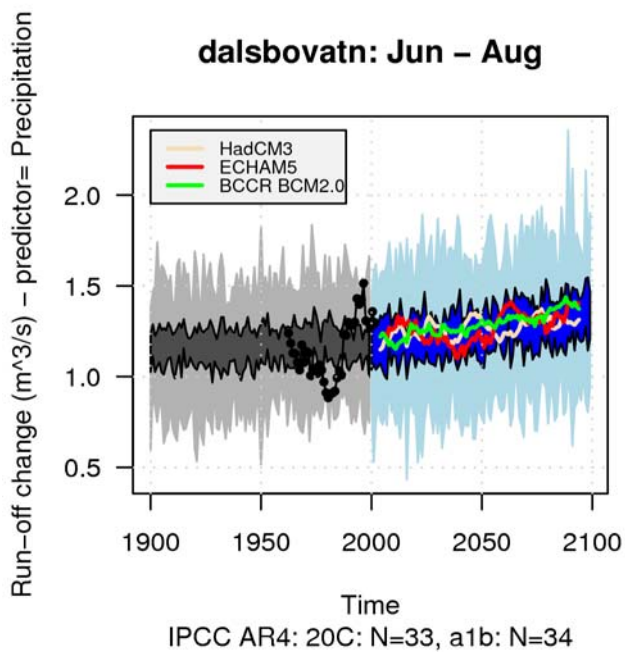
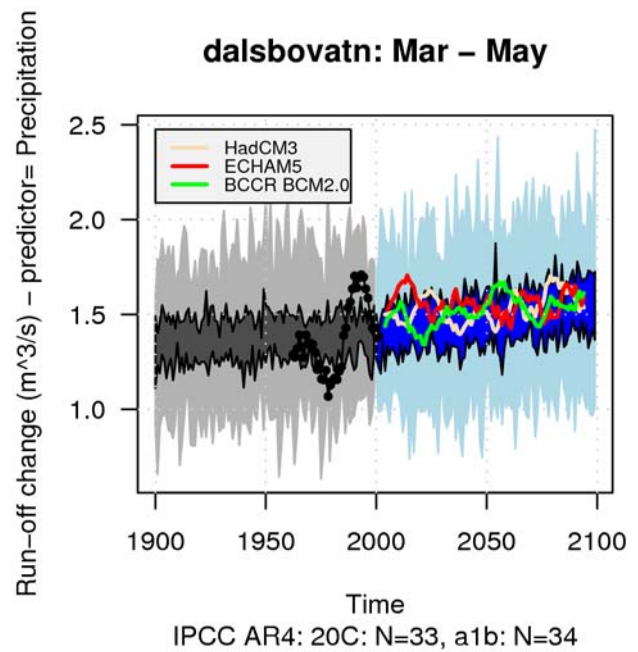
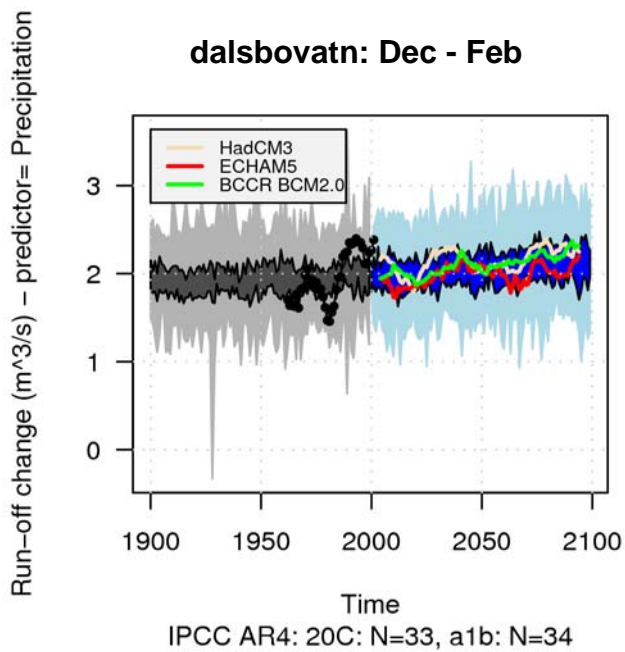
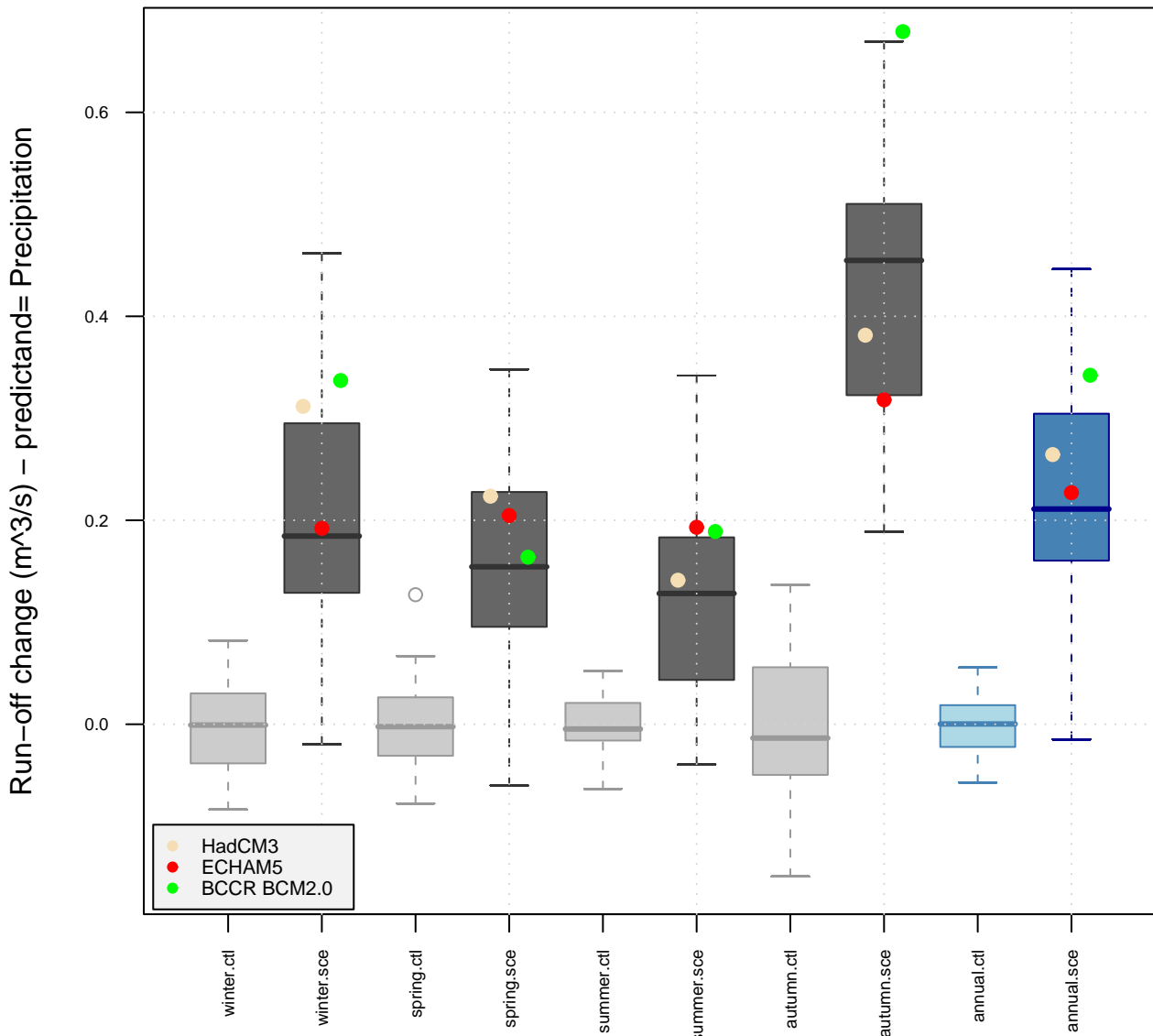


Figure 4.5.2 The figure shows the spread of the evolution of empirically downscaled runoff with precipitation as a predictor from the 33 GCMs used for the historic period 1958 -2002 and the 34 GCMs for the future period 2000-2100 following the SRES A1b emission scenario. Scenarios are established for four seasons; winter (upper left), spring (upper right), summer (lower left) and autumn (lower right). The historic period represents the control runs. Observed runoff is drawn as a black curve. Three selected GCMs are presented in the figure, HadCM3, ECHAM5 and BCCR.

dalsbovatn



2070--2099 scenario w.r.t. 1961--1990N sce=34 N 20c=33

Figure 4.5.3 The figure shows box plot of the change in runoff obtained by empirically downscaled runoff with precipitation as a predictor from the 33 GCMs used for the historic period 1961-1990 (light grey) (light blue is annual mean) and the 34 GCMs for the future period 2070-2099 following the SRES A1b emission scenario (dark grey) (dark blue is annual mean). Results from three models; HadCM3 (off white), ECHAM5 (red) and BCCR BCM2.0 (green) are specified in the figure. Scenarios are established annually and for four seasons. The boxes mark the 25 and 75 percentiles, and the whiskers extend up to 1.5 times the inter-quartile range (IQR). Data beyond 1.5 IQR from the box are marked as outliers.

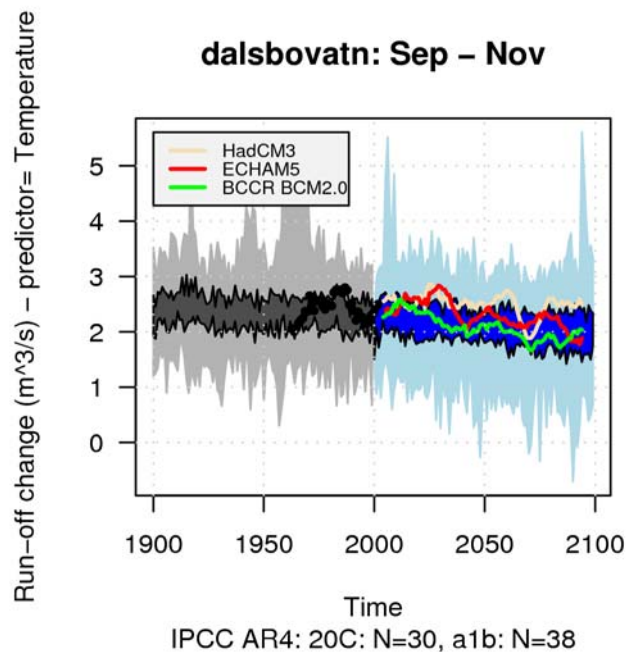
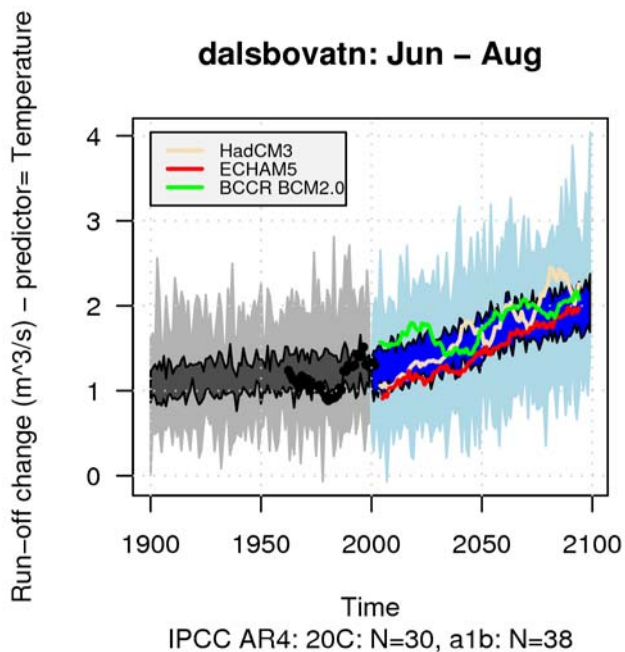
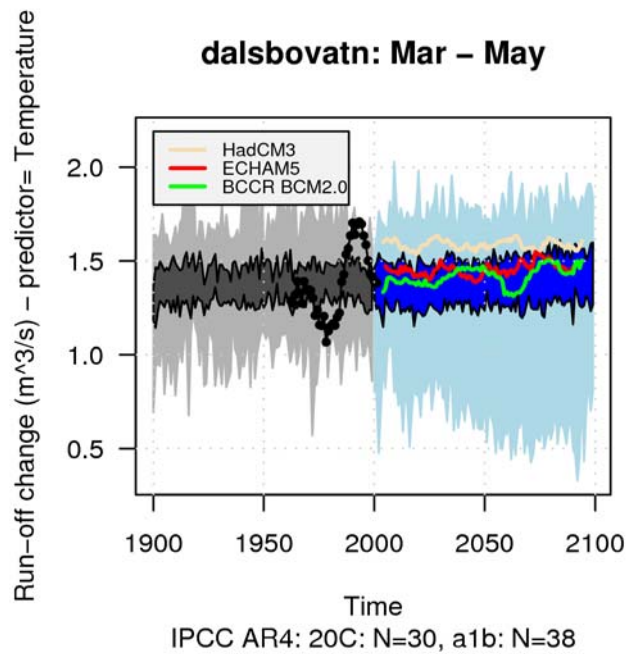
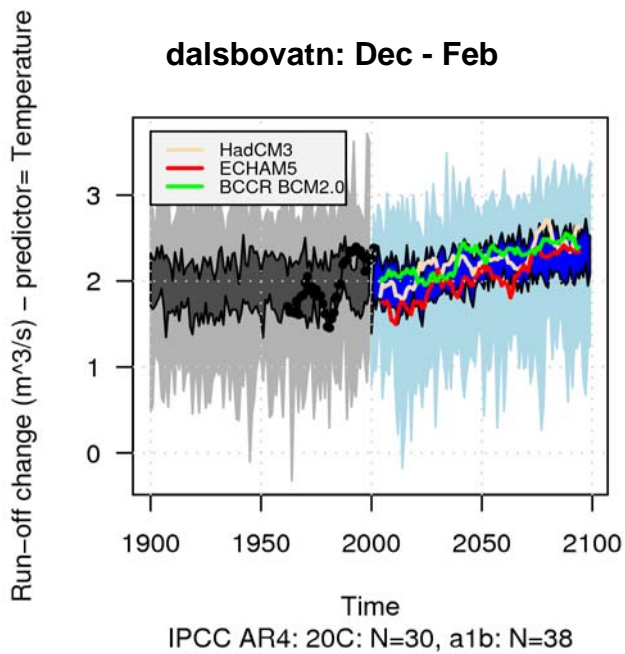
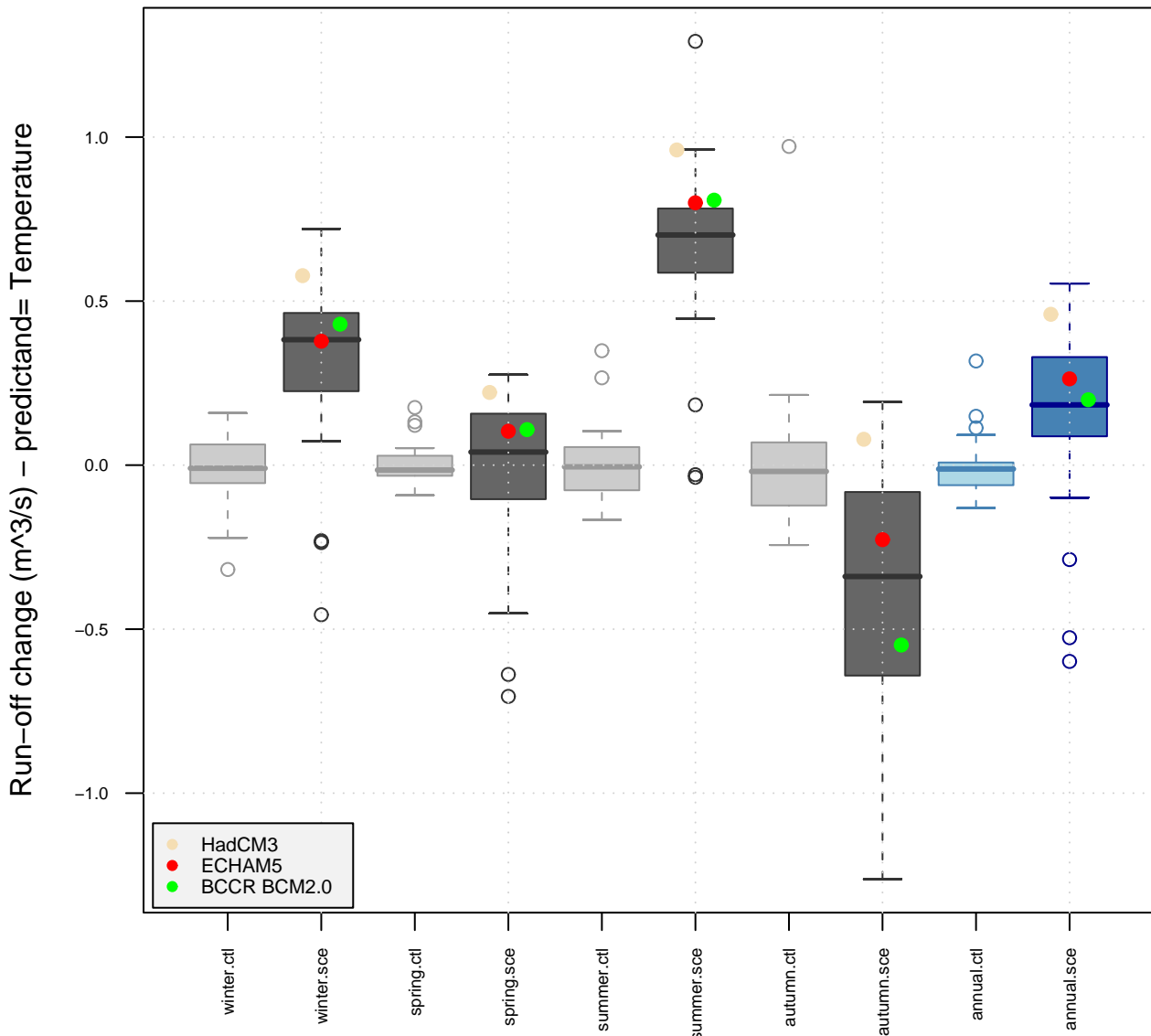


Figure 4.5.4 The figure shows the spread of the evolution of empirically downscaled runoff with temperature as a predictor from the 30 GCMs used for the historic period 1958 -2002 and the 38 GCMs for the future period 2000-2100 following the SRES A1b emission scenario. Scenarios are established for four seasons; winter (upper left), spring (upper right), summer (lower left) and autumn (lower right). The historic period represents the control runs. Observed runoff is drawn as a black curve. Three selected GCMs are presented in the figure, HadCM3, ECHAM5 and BCCR.

dalsbovatn



2070--2099 scenario w.r.t. 1961--1990N sce=38 N 20c=30

Figure 4.5.5 The figure shows box plot of the change in runoff obtained by empirically downscaled runoff with precipitation as a predictor from the 33 GCMs used for the historic period 1961-1990 (light grey) (light blue is annual mean) and the 34 GCMs for the future period 2070-2099 following the SRES A1b emission scenario (dark grey) (dark blue is annual mean). Results from three models; HadCM3 (off white), ECHAM5 (red) and BCCR BCM2.0 (green) are specified in the figure. Scenarios are established annually and for four seasons. The boxes mark the 25 and 75 percentiles, and the whiskers extend up to 1.5 times the inter-quantile range (IQR). Data beyond 1.5 IQR from the box are marked as outliers.

4.6 Høggås bru

An indication for how well the empirically downscaled runoff represents the observed runoff series is the coefficient of determination R^2 . A boxplot of R^2 from the regression between the observational part of the common EOFs of ERA40/GCMs and observed runoff is presented in Figure 4.6.1 The spread of the downscaled runoff with precipitation and temperature as predictor for Øvrevatn are presented in Figures 4.6.2 and 4.6.4 respectively. Mean seasonal change in runoff are presented in Figures 4.6.3 and 4.6.5 with precipitation and temperature as predictors respectively.

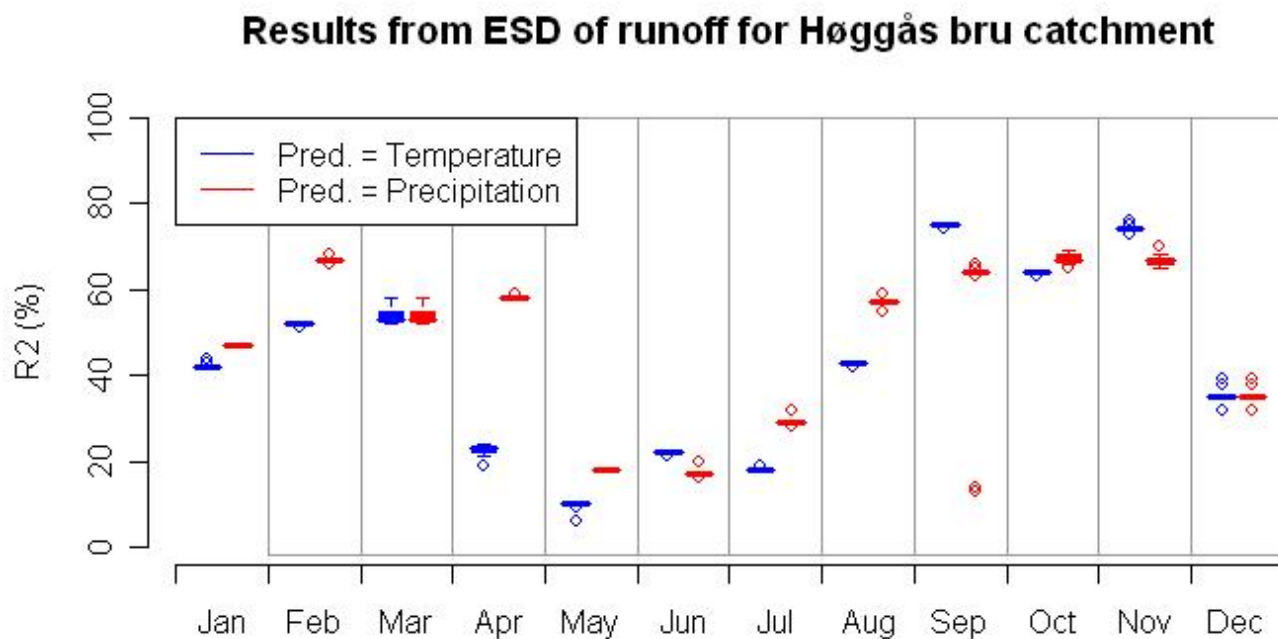


Figure 4.6.1 R^2 from the regression between the observational part of the common EOFs of ERA40/GCMs and observed runoff is presented in a boxplot. 68 GCMs with temperature as predictor (blue) and 67 GCMs with precipitation as predictor (red) are used.

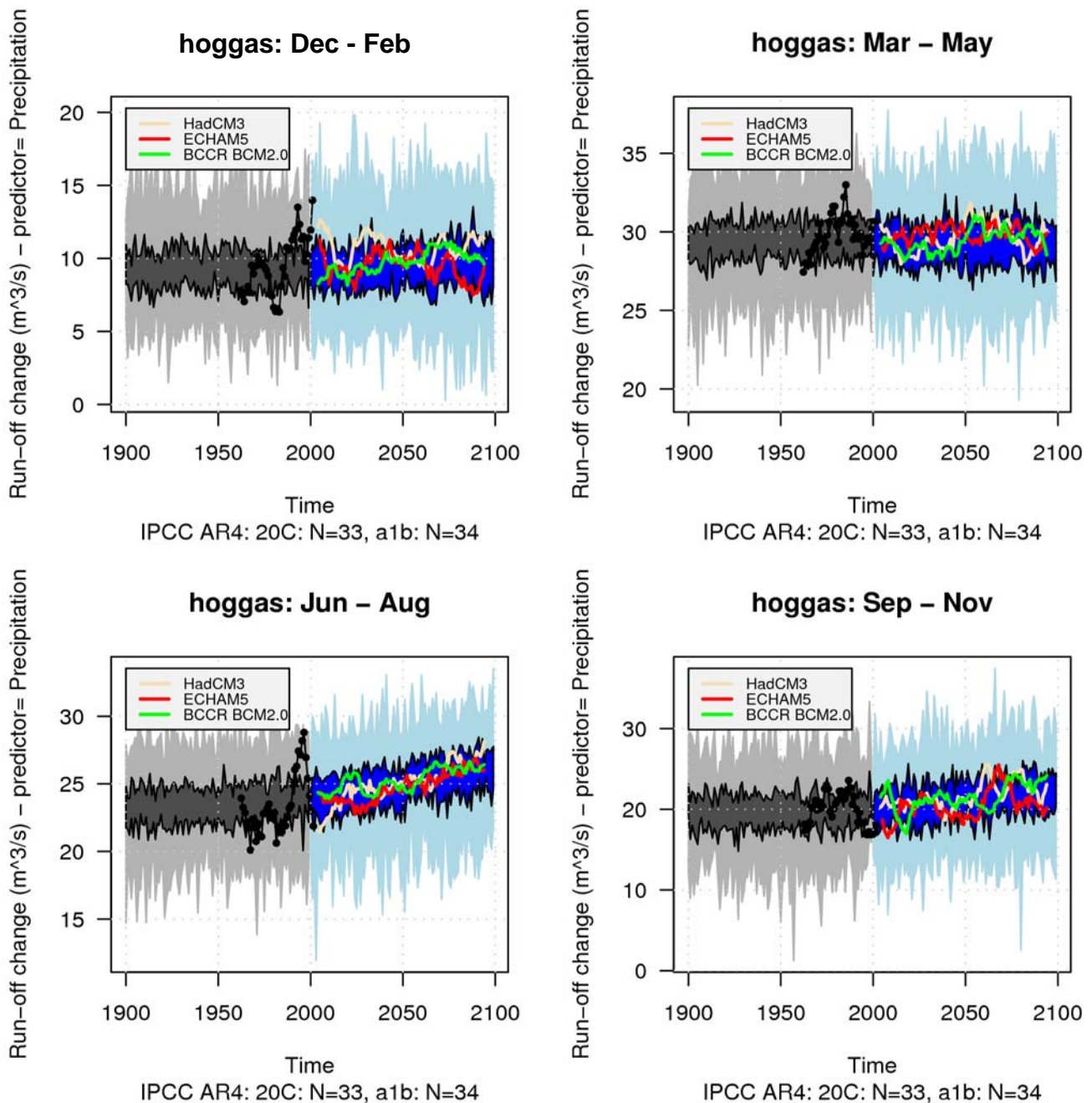
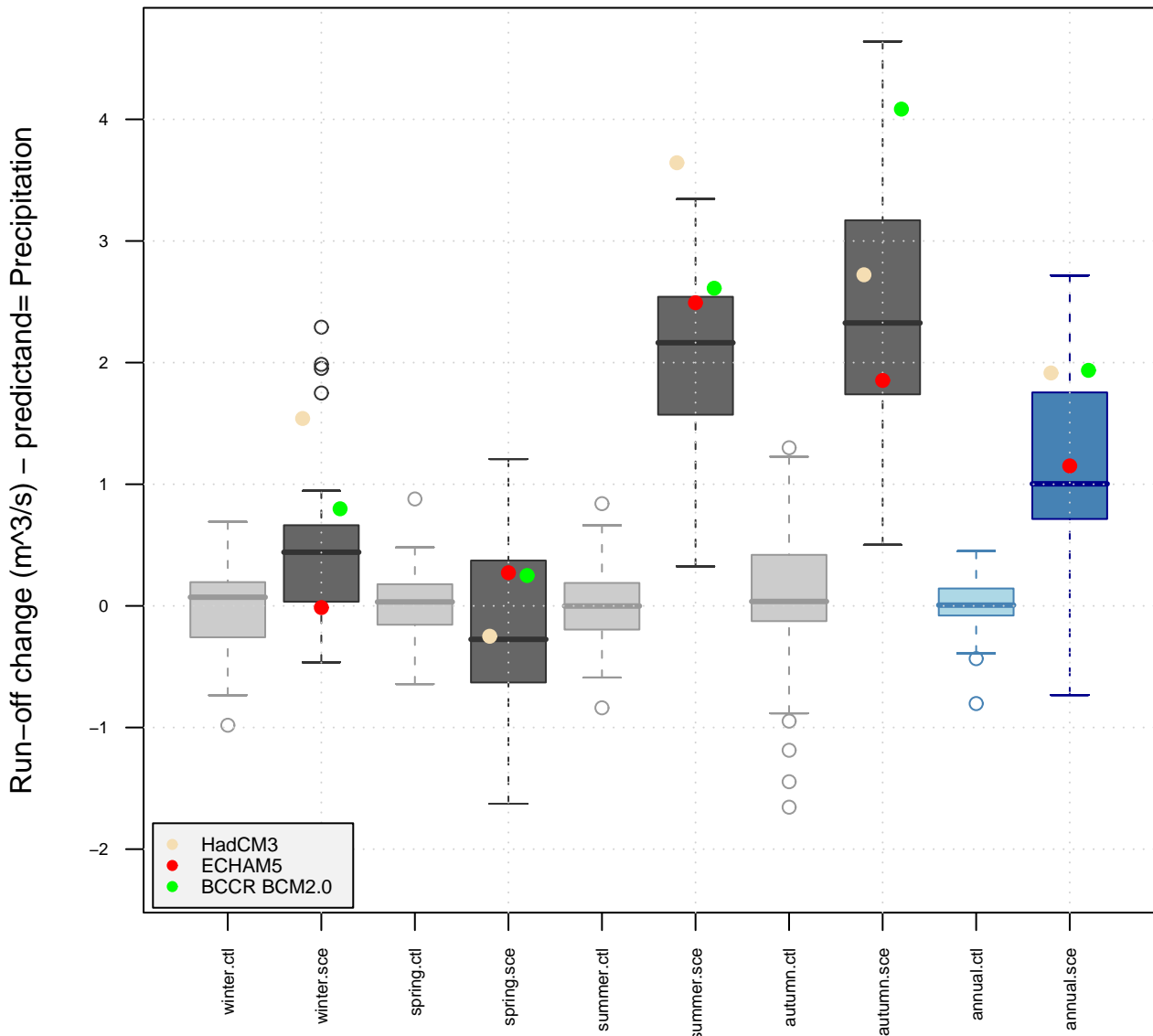


Figure 4.6.2 The figure shows the spread of the evolution of empirically downscaled runoff with precipitation as a predictor from the 33 GCMs used for the historic period 1958 -2002 and the 34 GCMs for the future period 2000-2100 following the SRES A1b emission scenario. Scenarios are established for four seasons; winter (upper left), spring (upper right), summer (lower left) and autumn (lower right). The historic period represents the control runs. Observed runoff is drawn as a black curve. Three selected GCMs are presented in the figure, HadCM3, ECHAM5 and BCCR.

hoggas



2070--2099 scenario w.r.t. 1961--1990N sce=34 N 20c=33

Figure 4.6.3 The figure shows box plot of the change in runoff obtained by empirically downscaled runoff with precipitation as a predictor from the 33 GCMs used for the historic period 1961-1990 (light grey) (light blue is annual mean) and the 34 GCMs for the future period 2070-2099 following the SRES A1b emission scenario (dark grey) (dark blue is annual mean). Results from three models; HadCM3 (off white), ECHAM5 (red) and BCCR BCM2.0 (green) are specified in the figure. Scenarios are established annually and for four seasons. The boxes mark the 25 and 75 percentiles, and the whiskers extend up to 1.5 times the inter-quantile range (IQR). Data beyond 1.5 IQR from the box are marked as outliers.

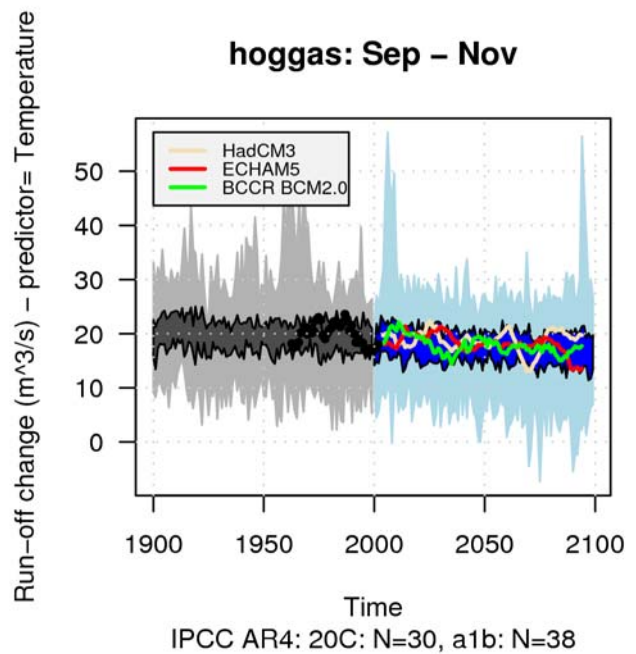
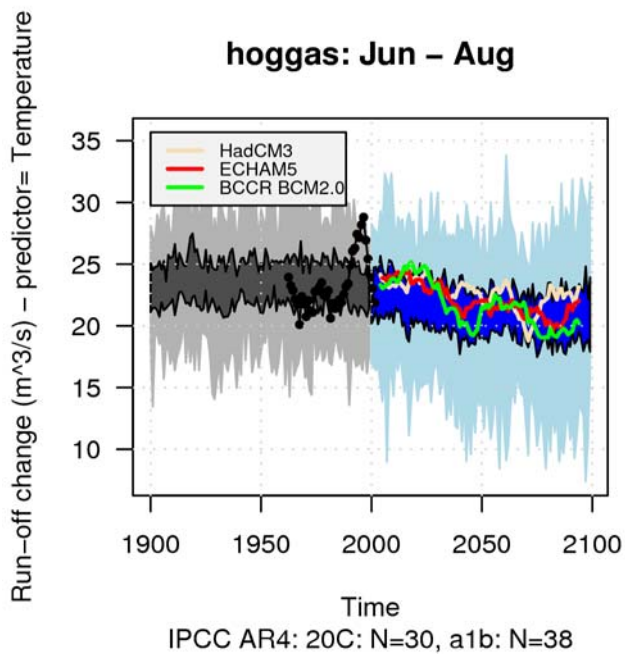
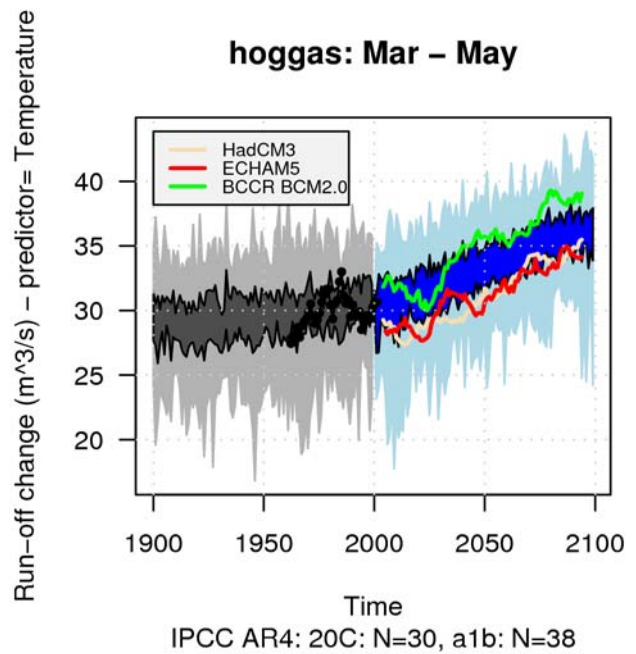
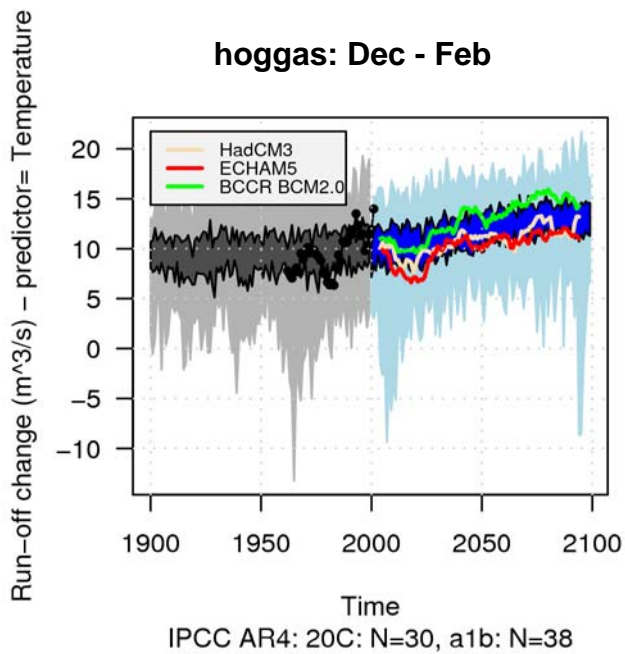
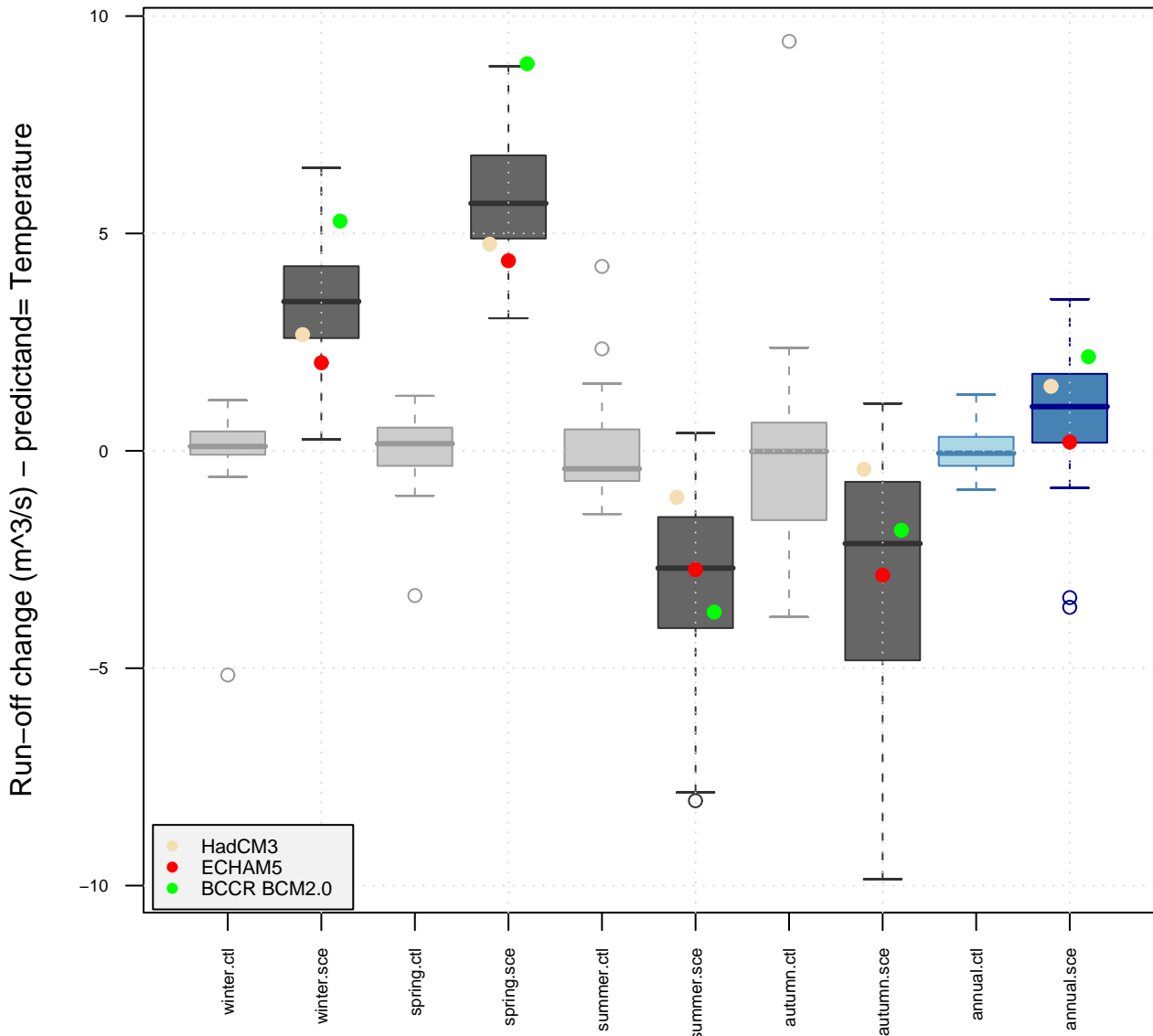


Figure 4.6.4 The figure shows the spread of the evolution of empirically downscaled runoff with temperature as a predictor from the 30 GCMs used for the historic period 1958 -2002 and the 38 GCMs for the future period 2000-2100 following the SRES A1b emission scenario. Scenarios are established for four seasons; winter (upper left), spring (upper right), summer (lower left) and autumn (lower right). The historic period represents the control runs. Observed runoff is drawn as a black curve. Three selected GCMs are presented in the figure, HadCM3, ECHAM5 and BCCR.

hoggas



2070--2099 scenario w.r.t. 1961--1990N sce=38 N 20c=30

Figure 4.6.5 The figure shows box plot of the change in runoff obtained by empirically downscaled runoff with precipitation as a predictor from the 33 GCMs used for the historic period 1961-1990 (light grey) (light blue is annual mean) and the 34 GCMs for the future period 2070-2099 following the SRES A1b emission scenario (dark grey) (dark blue is annual mean). Results from three models; HadCM3 (off white), ECHAM5 (red) and BCCR BCM2.0 (green) are specified in the figure. Scenarios are established annually and for four seasons. The boxes mark the 25 and 75 percentiles, and the whiskers extend up to 1.5 times the inter-quantile range (IQR). Data beyond 1.5 IQR from the box are marked as outliers.

4.7 Nautsundvatn

An indication for how well the empirically downscaled runoff represents the observed runoff series is the coefficient of determination R^2 . A boxplot of R^2 from the regression between the observational part of the common EOFs of ERA40/GCMs and observed runoff is presented in Figure 4.7.1. The spread of the downscaled runoff with precipitation and temperature as predictor for Øvrevatn are presented in Figures 4.7.2 and 4.7.4 respectively. Mean seasonal change in runoff are presented in Figures 4.7.3 and 4.7.5 with precipitation and temperature as predictors respectively.

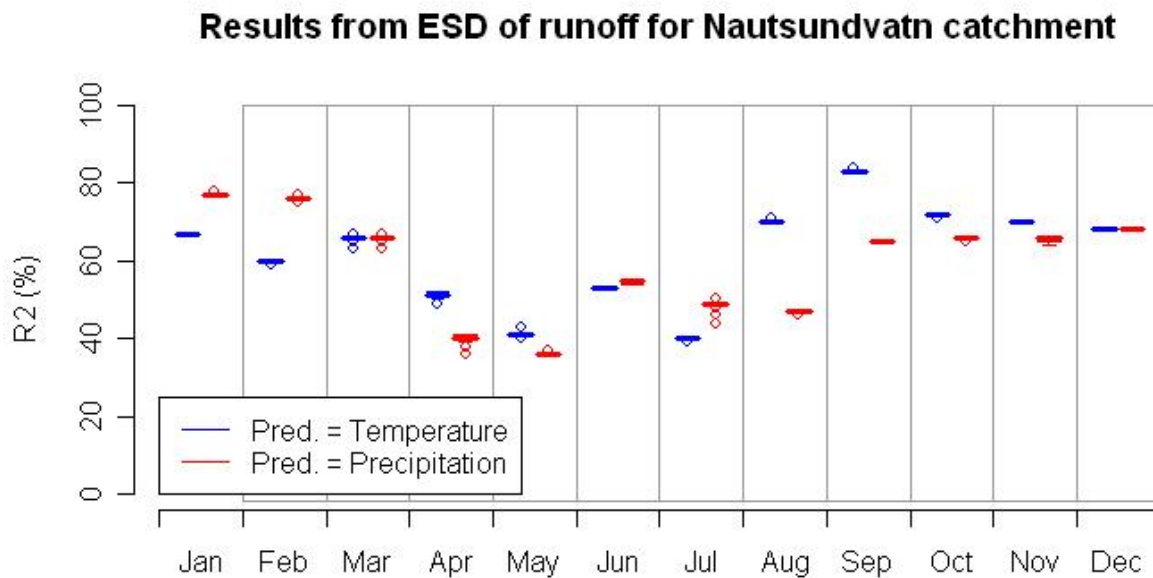


Figure 4.7.1 R^2 from the regression between the observational part of the common EOFs of ERA40/GCMs and observed runoff is presented in a boxplot. 68 GCMs with temperature as predictor (blue) and 67 GCMs with precipitation as predictor (red) are used.

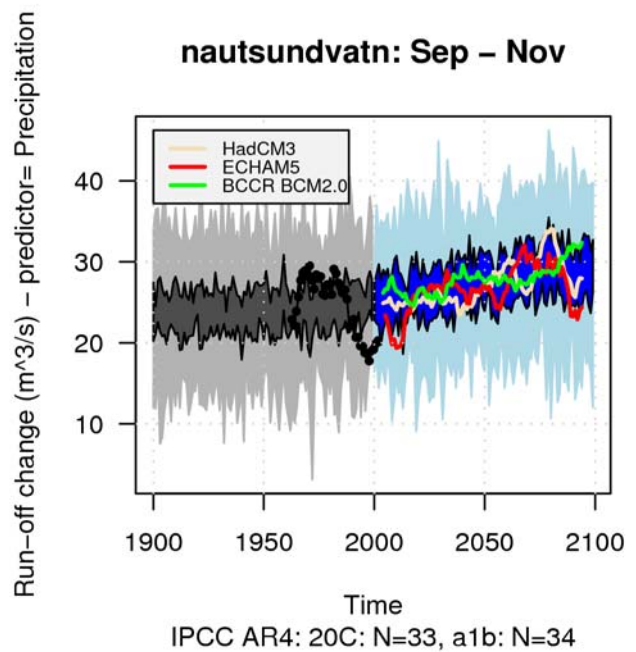
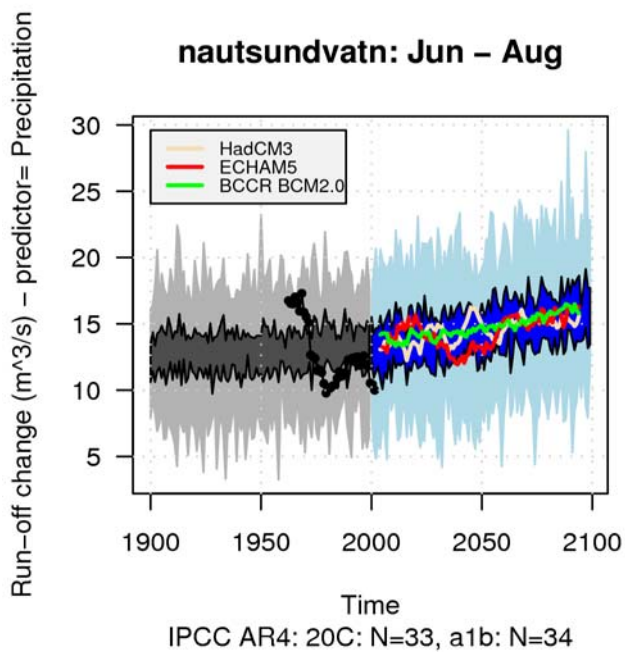
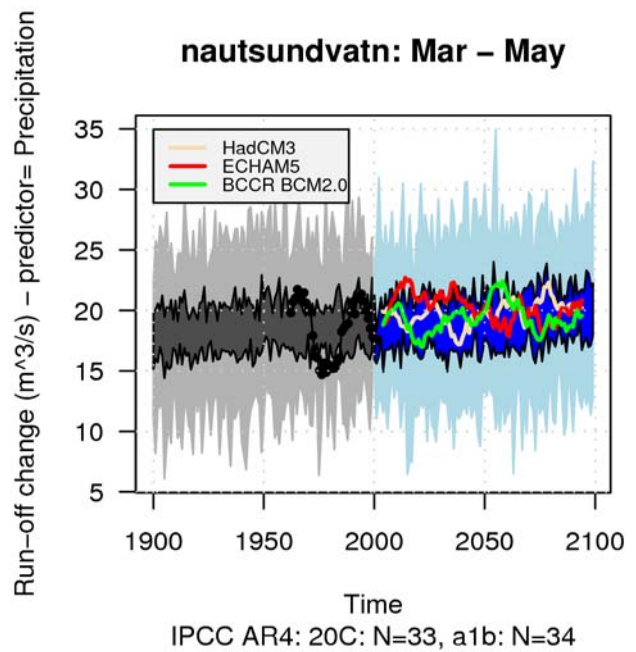
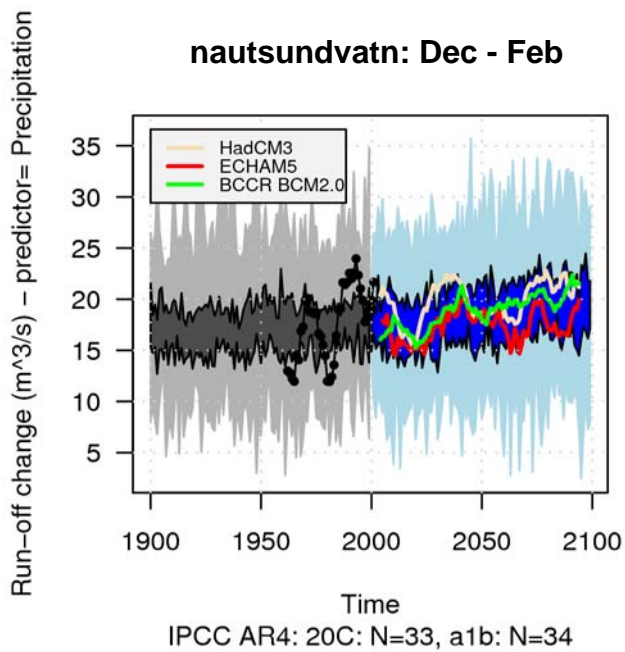
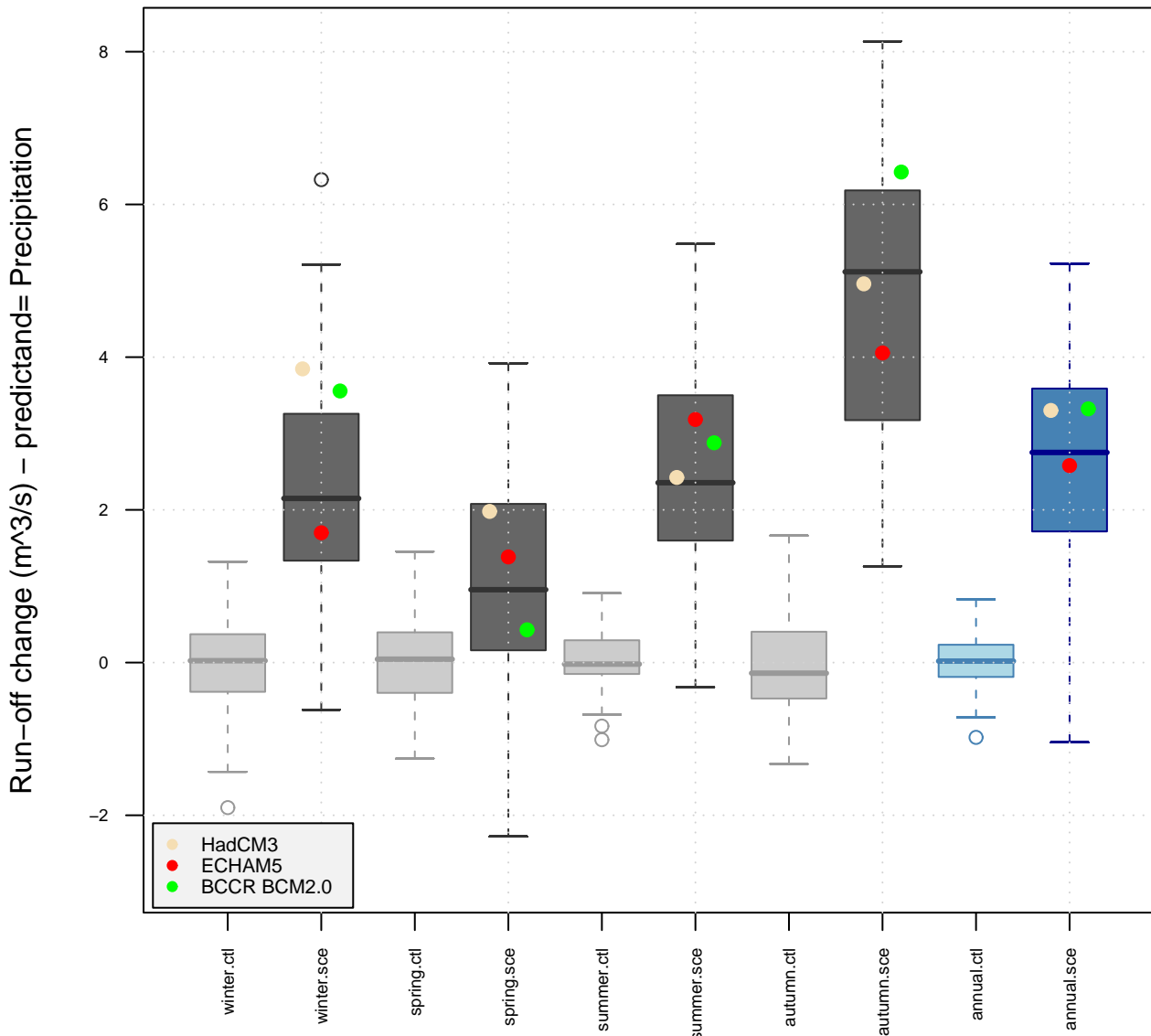


Figure 4.7.2 The figure shows the spread of the evolution of empirically downscaled runoff with precipitation as a predictor from the 33 GCMs used for the historic period 1958 -2002 and the 34 GCMs for the future period 2000-2100 following the SRES A1b emission scenario. Scenarios are established for four seasons; winter (upper left), spring (upper right), summer (lower left) and autumn (lower right). The historic period represents the control runs. Observed runoff is drawn as a black curve. Three selected GCMs are presented in the figure, HadCM3, ECHAM5 and BCCR.

nautsundvatn



2070--2099 scenario w.r.t. 1961--1990N sce=34 N 20c=33

Figure 4.7.3 The figure shows box plot of the change in runoff obtained by empirically downscaled runoff with precipitation as a predictor from the 33 GCMs used for the historic period 1961-1990 (light grey) (light blue is annual mean) and the 34 GCMs for the future period 2070-2099 following the SRES A1b emission scenario (dark grey) (dark blue is annual mean). Results from three models; HadCM3 (off white), ECHAM5 (red) and BCCR BCM2.0 (green) are specified in the figure. Scenarios are established annually and for four seasons. The boxes mark the 25 and 75 percentiles, and the whiskers extend up to 1.5 times the inter-quantile range (IQR). Data beyond 1.5 IQR from the box are marked as outliers.

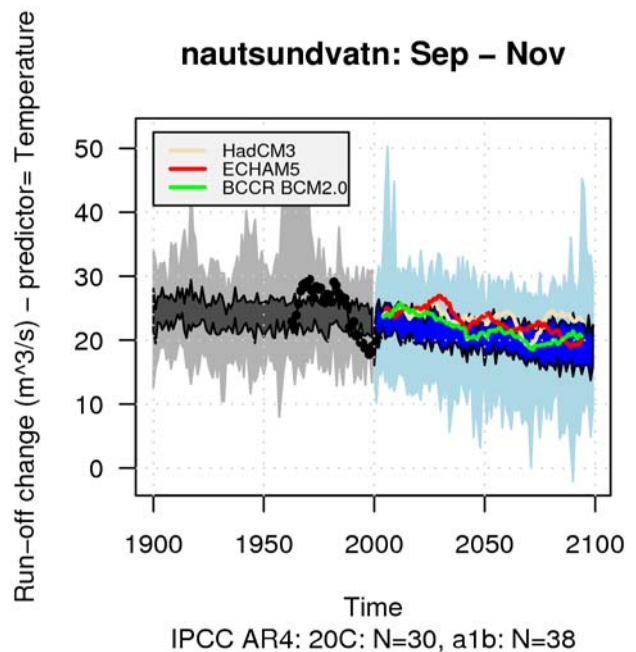
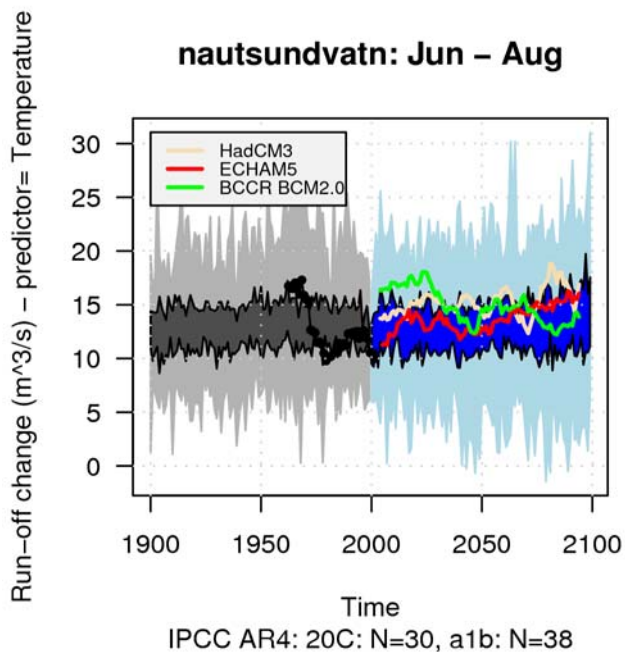
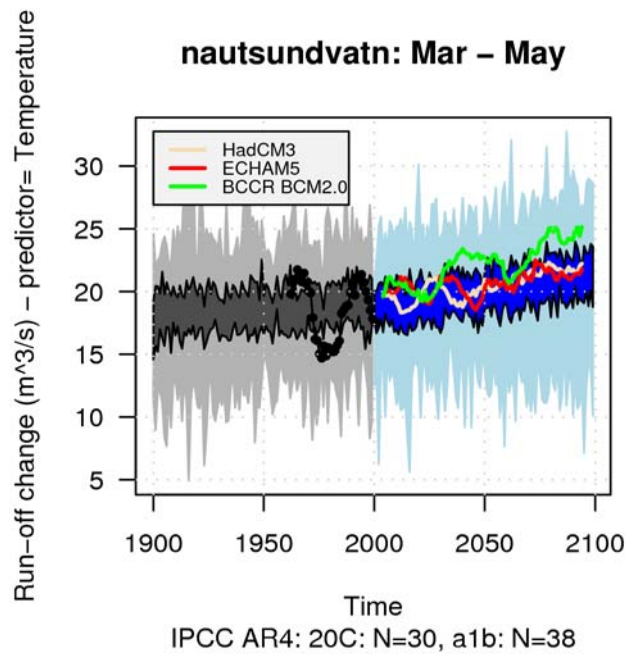
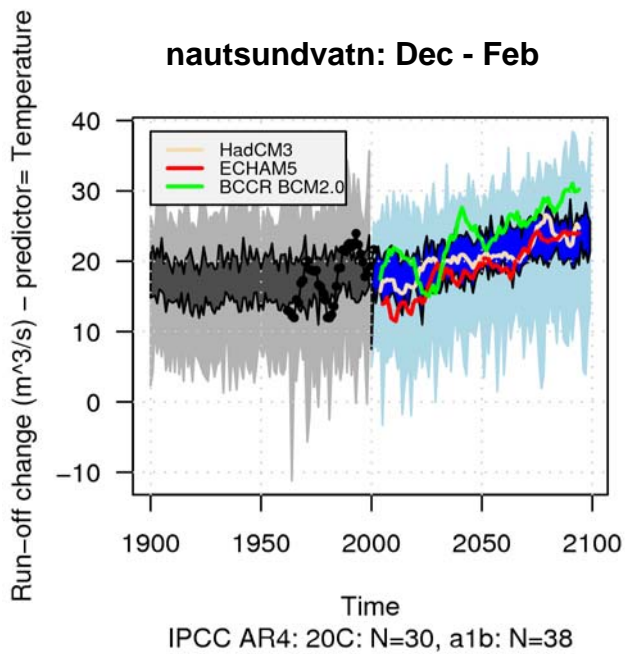
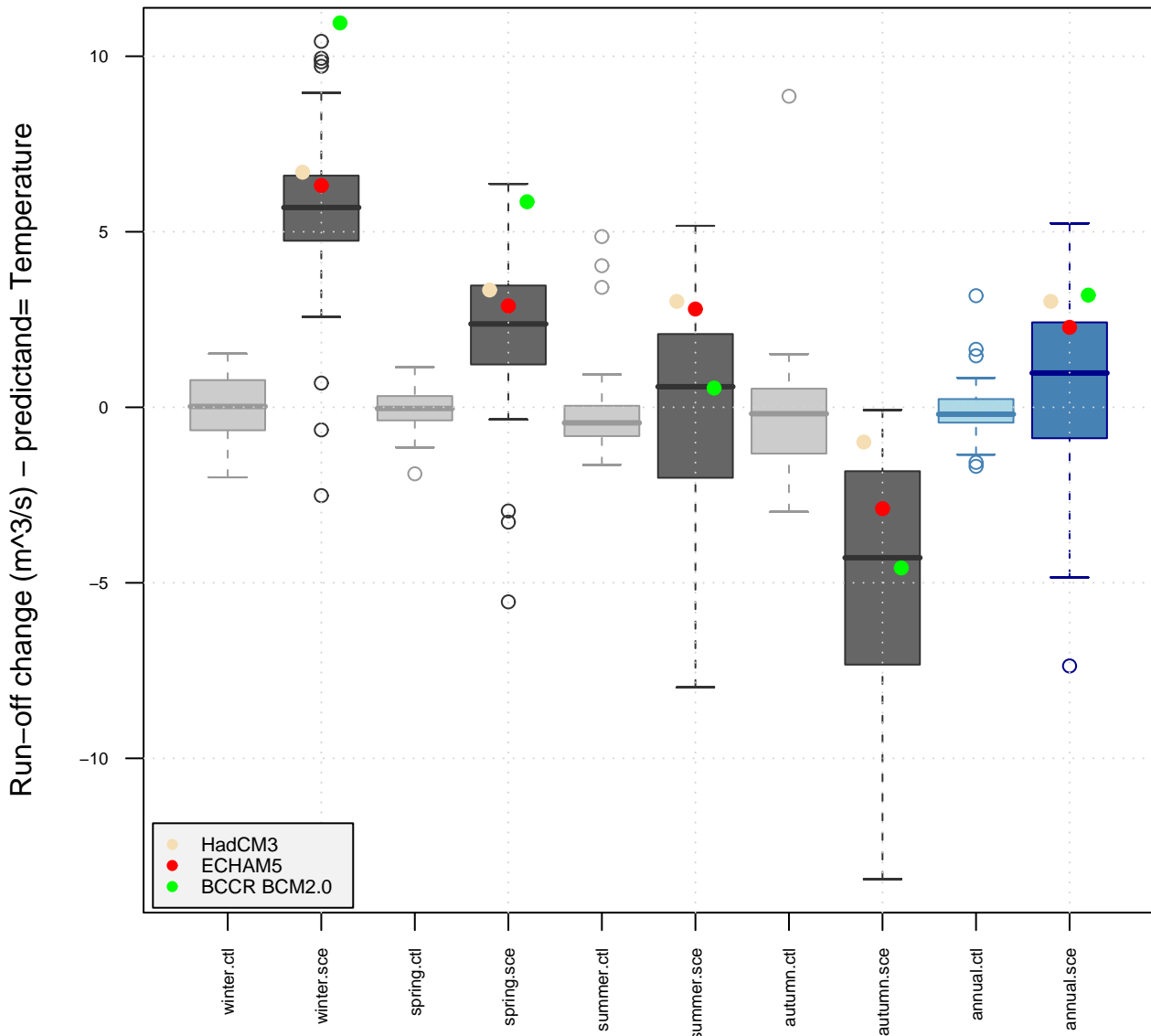


Figure 4.7.4 The figure shows the spread of the evolution of empirically downscaled runoff with temperature as a predictor from the 30 GCMs used for the historic period 1958 -2002 and the 38 GCMs for the future period 2000-2100 following the SRES A1b emission scenario. Scenarios are established for four seasons; winter (upper left), spring (upper right), summer (lower left) and autumn (lower right). The historic period represents the control runs. Observed runoff is drawn as a black curve. Three selected GCMs are presented in the figure, HadCM3, ECHAM5 and BCCR.

nautsundvatn



2070--2099 scenario w.r.t. 1961--1990N sce=38 N 20c=30

Figure 4.7.5 The figure shows box plot of the change in runoff obtained by empirically downscaled runoff with precipitation as a predictor from the 33 GCMs used for the historic period 1961-1990 (light grey) (light blue is annual mean) and the 34 GCMs for the future period 2070-2099 following the SRES A1b emission scenario (dark grey) (dark blue is annual mean). Results from three models; HadCM3 (off white), ECHAM5 (red) and BCCR BCM2.0 (green) are specified in the figure. Scenarios are established annually and for four seasons. The boxes mark the 25 and 75 percentiles, and the whiskers extend up to 1.5 times the inter-quantile range (IQR). Data beyond 1.5 IQR from the box are marked as outliers.

5 Do we find good empirical relations between the predictors and runoff?

Runoff reflects the response in a catchment and its characteristics such as the size, the degree of saturation, evapotranspiration, season of the year etc. It is not to be expected that empirically relations between precipitation or temperature may describe the complete behaviour. Precipitation is expected to capture small, fast responding coastal catchments as well as autumn runoff due to large amounts of rainfall (eastern parts of the country). Temperature is expected to capture the runoff characteristics due to snow melt in inland catchments.

Seven catchments are empirically downscaled using large scale fields of precipitation and temperature as predictor respectively (Section 4). The catchments represent coastal regions exposed for mild and wet westerly winds leading to autumn, winter and spring floods (Røykenes, Dalsbøvatn and Nautsundvatn), inland and northern catchments mainly influenced by large amounts of snow with a marked spring flood (Atnasjø and Øvrevatn). Two catchments are influenced both by spring flood due to snow melt and autumn precipitation (Austenå and Høggås Bru). The catchments are described in Section 2.

The strength of the relationship between the predictor and the predictands is reflected in the R^2 -statistics from the regression analysis. R^2 from the regression between the observational part of the common EOFs of ERA40/GCMs and observed runoff for each model run are established for the catchments studied (Figures 4.1.1, 4.2.1, 4.3.1, 4.4.1, 4.5.1, 4.6.1, 4.7.1 for Øvrevatn, Atnasjø, Røykenes, Austenå, Dalsbøvatn, Høggås bru and Nautsundvant respectively). The R^2 -statistics vary with season and location, but in general they suggest a relationship of moderate strength between the predictors and the predictands.

Øvrevatn and Atnasjø (Sections 4.1 and 4.2 respectively) show highest R^2 with precipitation as predictor. The correlation is low suggesting weak relation. Øvrevatn shows higher R^2 in April, May and August (~60%). In Atnasjø no relations are found between runoff and the predictors in December, it is low in January and February as well. These catchments are dominated cold and stable winter conditions with low runoff. Increase in runoff may be caused by occasional periods with mild weather, even in combination with local increase in runoff due to backwater caused by ice dams. Snowfall on frozen bogs and lakes with ice may also lead to temporary small peaks in runoff.

It is possible that these conditions may lead to weak correlation with precipitation in winter as shown in Figures 4.1.1 and 4.2.1. Slightly better agreement in April and May with temperature as predictor is due to snow melting. If snowmelt occurs in combination with rainfall, the skill is higher for precipitation predictor. Atnasjø is located in a region with infrequent large precipitation episodes due to atmospheric circulation. It is therefore not feasible to use empirical downscaling of runoff directly during winter for Atnasjø and Øvrevatn (upper left in Figures 4.2.2 and 4.2.4). Precipitation is found to be more skilful as a predictor than temperature (Figures 4.1.1 and 4.2.1).

Runoff in Øvrevatn with precipitation as predictor leads to an increase during summer, less pronounced increase in autumn, and no change is found for the rest of the year (Figures 4.1.2 and 4.1.3). For Atnasjø a reduction in runoff is found during summer, no change is found in autumn, while a weaker reduction is predicted during spring (Figures 4.2.2 and 4.2.3). Due to the limitations of ESD, it is not expected that these estimates for Atnasjø and Øvrevatn, representing catchments with a marked spring flood, will provide the complete picture.

Austenå and Høggås Bru (Sections 4.4 and 4.6 respectively) show similar R^2 estimates both for temperature and precipitation as predictor except for April when precipitation gives strongest relation to runoff (Figures 4.4.1 and 4.6.1). The relations are best in March, April and October for Austenå (~60%). For Høggås Bru there is found high R^2 scores in February, September and November as well (~60%). Høggås bru is located at the bottom of the Trondheimsfjord, but is exposed to weather systems from the west. Most of the catchment is at low altitudes, and the precipitation can therefore fall as rain even in

winter. Winter rainfall floods are not uncommon, since mild air masses can penetrate from the Norwegian Sea. ESD is therefore more skillful in Høggås Bru than in Austenå.

Best agreement (in %) is found in autumn when the river runoff is dominated by atmospheric circulation. For the summer months and December-January, the statistical relations are weak (<50%). A problem is that for precipitation and temperature as predictors, similar R^2 estimates are obtained, but the predicted trends for the future for autumn have opposite sign (Figures 4.4.2 and 4.4.3 vs. 4.4.4 and 4.4.5). Scenarios of river runoff for Austenå obtained with dynamically downscaled temperature and precipitation in Roald et al. (2006) show similar results, increase in winter runoff, decrease in spring and summer runoff. Runoff in autumn however shows opposite sign based on the two downscaling methods. The projected changes in the autumn runoff are consistent with the results in other catchments in the same region based on dynamical downscaling. The autumn runoff is reduced using the high emission scenario and increased using the moderate scenario.

The conclusion, however, is the same as for Øvrevatn and Atnasjø; empirical downscaling of river runoff is not feasible for river runoff dominated by snowmelt. But, ESD may be feasible for catchments dominated by atmospheric circulation (precipitation). Austenå is located in the south, but extends far inland, which results in a regular snow cover in the upper parts of the catchment. The reason why there is a close link between precipitation and runoff in March-April is the timing of snowmelt especially during rainfall.

Røykenes, Dalsbøvatn and Nautsundvatn (Sections 4.3, 4.5 and 4.7 respectively) show good skill (>60%) for the months September to March. The summer months June until August show weaker relations (<60%). These catchments are located at the western coast and do not extend to high altitudes. Most of the winter precipitation falls as rain. Snow on the ground is rare and tends to melt quickly. Around 50-60 % of the larger rainfall events are linked to weather systems from southwest to northwest, often with anti-cyclonic circulation over Great Britain or the northern European Mainland (Roald, 2008). This is captured by the ESD analyses. Scenarios based on dynamical downscaling for the Viksvatn catchment in River Gaular near Nautsundvatn show similar changes in most of the seasons to the scenarios for Nautsundvatn (Roald et al., 2006). The catchment is, however, further inland and extends to higher altitudes. Small glaciers are present in the upper part of the Viksvatn catchment. The snow in the winter season is therefore likely to result in a lower agreement between the runoff and the ESD analyses.

Even though the relation between predictors and runoff are both relatively strong, there is a problem that the projections for the future lead to opposite directions in autumn (e.g. lower right in Figures 4.3.2 and 4.3.3 vs. 4.3.4 and 4.3.5, 4.5.2 and 4.3.3 vs. 4.5.4 and 4.3.5, and 4.7.2 and 4.7.3 vs. 4.7.4 and 4.7.5).

The current study does not include catchments exposed to maritime air further inland. These catchments are characterised by larger differences in elevation. The precipitation will therefore fall more frequently as snow in the upper part of the catchments. The link between winter precipitation and runoff would be weaker in these catchments. Increasing winter temperatures will result in more severe winter floods in these catchments as the transition level from snow to rainfall increases and would increase the agreement.

The results discussed above have exhibited strong statistical relationship between predictors and river runoff for small and medium-small catchments dominated by rainfall floods through out the year. A problem is that even though the R^2 for different predictors are similar, the trends are of opposite sense. The conclusion is then that different factors have different counteracting effect on river runoff, and that the net effect is determined by the balance between these two factors. It might be of interest to develop complex relations that involves both predictors. Analyses should explore relationships between weather type classification based on atmospheric circulation and runoff. Established connections can then be used to compute runoff scenarios. ESD appears not to be feasible for describing runoff directly in catchments dominated by large amounts of snow storage.

Acknowledgement

The authors would like to thank Astrid Voksø, Norwegian Water Resources and Energy Directorate (NVE), for providing digital geographical data of the watersheds studied.

References

- Benestad, R.E., E.J. Førland and I. Hanssen-Bauer, 2007, On Models for empirical-statistical downscaling of precipitation *Int. J. Clim.*, **27**:: 649-665, DOI: 10.1002/joc.1421
- Benestad, R.E., 2005, Climate change scenarios for northern Europe from multi-model IPCC AR4 climate simulations *GRL*,**32** doi:10.1029/2005GL023401 No. 17, L17704
- Benestad, R.E., 2004, Empirical-Statistical Downscaling in Climate Modelling *EOS* Volume 85, Number 42, October 19, p. 417
- Benestad, R.E., 2001, A comparison between two empirical downscaling strategies, *Int. J. Climatology*,**Vol 21**, Issue 13, pp.1645-1668. [DOI 10.1002/joc.703]
- Bengtsson, L. K.I. Hodges and S. Hagemann, 2004, Sensitivity of the ERA40 reanalysis to the observing system: determination of the global atmospheric circulation from reduced observations, *Tellus*,**56A**,456-471
- Bergström, S., 1995, The HBV model. In: Singh, V.P. (Ed.), *Computer Models of Watershead Hydrology*. Water Resources Publications, Highlands Ranch, 443-476.
- Engen-Skaugen T., 2007, Refinement of dynamically downscaled precipitation and temperature scenarios. *Climate Change*, DOI 10.1007/s10584-007-9251-6.
- Førland E., Det norske meteorologiske institutt Årsnedbør 1:2 mill. Nasjonalatlas for Norge, kartblad 3.1.1, Statens kartverk.
- Gerstengarbe, F.-W. and Werner, P.C. (2005). Katalog der Grosswetterlagen Europas (1881-2004) nach Paul Hess und Helmut Brezowsky 6., Verbesserte und Ergänzte Auflage. PIK Report No.100, Potsdam, Germany.
- Hisdal, H., Barthelmie, R., Lindström, G., Kolciva, T., Kriauciuniene, J. and Reihan, A. (2007) 5 Statistical analysis. In: Jes Fenger (ed) *Impacts of Climate Change on Renewable Energy Sources*. Norden. ISBN 978-92-893-1465-7.
- Hulme, M. and Barrow, E. (1997). *Climate of the British Isles – present, past and future*. Routledge, London and New York.
- IPCC, 2000, Special report on emission scenarios. A special report of working group III of the intergovernmental Panel on Climate Change. In: Nakicenovic N, Alcamo J, Davis G, de Vries B, Fenhann J, Gaffin S, Gregory K, Gru`bler A, Young Jung T, Kram T, La Rover EL, Michaelis L, Mori S, Morita T, Pepper W, Pitcher H, Price L, Rihai K, Roehrl A, Rogner HH, Sankovski A, Schlesinger M, Shukla P, Smith S, Swart R, van Rooijen S, Victor N, Dadi Z (eds)]. Cambridge University Press, Cambridge
- Meehl G.A., Stocker T. F., Collins, W.D., Friedlingstein P., Gaye, A.T., Gregory, J.:.;, Kitoh, A., Knutti, R., Murphy J.M., Noda, A., Raper S.C.B., Watterson, I.G., Weaver A.J. and Zhao, Z.-C., 2007, *Global Climate Projections*, In *Climate Change 2007: The physical Science Basis. Contribution of Working Group I to the Fourth Assessment report of the Intergovernmental Panel on Climate Change* [Solomon, S., D. Qin, M. Manning, Z. Chen, M. Marquis, K.B. Averyt, M. Tignor and H.L. Miller (eds.)] Cambridge University Press, Cambridge, United Kingdom and New York, NY, USA.
- Roald, L.A., 2008, Large rainfall floods and weather patterns. Norwegian Water Resources and Energy Directorate (NVE), Conculancy Report (in preparation).

- Roald, L., Beldring S., Engen-Skaugen, Førland E.J. and Benestad, R., 2006, Climate change impacts on streamflow in Norway, NVE report No 1/06
- Simmons, A.J. and Gibson, J.K., 2000, The ERA-40 Project Plan, ECMWF, ERA-40 Project Report Series,1, www.ecmwf.int.
- Sælthun, N.R., 1996, The Nordic HBV Model. Norwegian Water Resources and Enerfy Administration, Publication 7, Oslo, 26 pp.
- Tveito, O.E. and Roald, L.A., 2005, Relations between long-term variations in seasonal runoff and large scale atmospheric circulation patterns, met.no report 07, 2005 – climate
- Østmo, A. ,1985, Storofsen. Oversiktsregisteret. Infotrykk, Ski,56 pp

Appendix A

A complete list showing which global climate model runs that is used in the analyses. C20 means 20th century, sresa1b means 20th century following the SRES emission scenario A1b. 101 and 601 are predictors used, daily mean temperature [°C] and daily precipitation sums [mm/day] respectively.

GCM	Period	101	601
BCC.cm1	c20	run1	run1
BCC.cm1	c20	run2	run2
BCCR.bcm2.0	c20	run1	run1
BCCR.bcm2.0	sresa1b	run1	run1
CCCMA.CGCM3.1	c20	run1	run1
CCCMA.CGCM3.1	sresa1b	run1	run1
CNRM.cm3	c20	run1	run1
CNRM.cm3	sresa1b	run1	run1
CSIRO.mk3.0	c20	run1	run1
CSIRO.mk3.0	sresa1b	NA	run1
GFDL.cm2.0	c20	run1	run1
GFDL.cm2.0	sresa1b	run1	run1
GFDL.cm2.1	c20	run1	run1
GFDL.cm2.1	c20	run2	run2
GFDL.cm2.1	c20	run3	run3
GFDL.cm2.1	sresa1b	run1	run1
GISS.aom	c20	run2	run2
GISS.aom	c20	NA	run1
GISS.aom	sresa1b	run1	run1
GISS.aom	sresa1b	run2	run2
GISS.modell_e.h	c20	run1	run1
GISS.modell_e.h	c20	run2	NA
GISS.modell_e.h	c20	run3	run3
GISS.modell_e.h	c20	run4	run4
GISS.modell_e.h	c20	run5	run5
GISS.modell_e.h	sresa1b	run1	run1
GISS.modell_e.h	sresa1b	run2	run2
GISS.modell_e.h	sresa1b	run3	run3
GISS.modell_e.r	sresa1b	run1	NA
GISS.modell_e.r	sresa1b	run2	run2
GISS.modell_e.r	sresa1b	run3	NA
GISS.modell_e.r	sresa1b	run4	run4
GISS.modell_e.r	sresa1b	run5	NA
INMCN3.0	c20	run1	run1
INMCN3.0	sresa1b	run1	run1
IPSL.cm4	c20	run1	run1

IPSL.cm4	sresa1b	run1	run1
MIROC3.2.hires	c20	NA	run1
MIROC3.2.hires	sresa1b	run1	NA
MIROC3.2.medres	sresa1b	run2	run2
MIROC3.2.medres	sresa1b	run3	run3
MIUB.echo.g	sresa1b	run1	run1
MIUB.echo.g	sresa1b	run3	run3
MPI.ECHAM5	c20	run1	run1
MPI.ECHAM5	c20	run2	run2
MPI.ECHAM5	c20	run3	run3
MPI.ECHAM5	sresa1b	run1	run1
MPI.ECHAM5	sresa1b	run2	NA
MPI.ECHAM5	sresa1b	run3	run3
MRI.cgcm2.3.2a	sresa1b	run1	run1
MRI.cgcm2.3.2a	sresa1b	run2	run2
MRI.cgcm2.3.2a	sresa1b	run3	run3
MRI.cgcm2.3.2a	sresa1b	run4	run4
MRI.cgcm2.3.2a	sresa1b	run5	run5
NCAR.cesm3.0	c20	run1	run1
NCAR.cesm3.0	c20	run3	run3
NCAR.cesm3.0	c20	NA	run5
NCAR.cesm3.0	c20	run6	run6
NCAR.cesm3.0	c20	NA	run7
NCAR.cesm3.0	c20	run9	run9
NCAR.cesm3.0	sresa1b	run1	run1
NCAR.cesm3.0	sresa1b	run2	run2
NCAR.cesm3.0	sresa1b	run3	run3
NCAR.pcm1	c20	run2	run2
NCAR.pcm1	c20	run3	run3
NCAR.pcm1	c20	run4	run4
NCAR.pcm1	sresa1b	run1	run1
NCAR.pcm1	sresa1b	run2	run2
NCAR.pcm1	sresa1b	run3	run3
UKMO.hadcm3	c20	run1	run1
UKMO.hadcm3	c20	run2	run2
UKMO.hadcm3	sresa1b	run1	run1
UKMO.hadgem1	sresa1b	run1	run1